This is for you Amma and Appa..
For all the innumerable sacrifices, unconditional love and endless support..

Abstract

The growing population of the world places an enormous demand for energy in some form or the other. Essentially, this means that the struggle to hunt and retrieve fossil fuels has to continue for a smooth functioning of the world. Since early 1900's when drilling for oil and gas started moving away from shores to some remote locations that we are at today, the size and complexity of machinery and the interconnected systems have grown exponentially. Despite investing enormous time, effort and money into implementing technically advanced and innovative barrier systems to prevent Hydrocarbon (HC) leaks on offshore installations in the Norwegian Continental Shelf (NCS), the statistics still stands far from the target zero. Hence, the efforts towards minimizing the number of leaks can never be ceased due to the catastrophic nature of its potential consequences to humans, environment, asset or the reputation of a firm.

This master's thesis features one such effort to visualize the effectiveness of some barrier functions proposed in Modelling Instantaneous Risk for Major Accident Prevention (MIRMAP) report. Some of the most critical barrier systems are incorporated into the chosen generic module, which is then subjected to numerous gas leak simulations using the latest version of the software, Kameleon FireEx - Risk and Barrier Management (KFX-RBM), a Computational Fluid Dynamics (CFD) based simulation tool. A base case scenario is set-up using the chosen module with a 100% functional gas detection system, Emergency Shutdown (ESD) system, with no temporary weather cladding attached and closed fire-proof doors. This set-up is subjected to simulation with six different leak rates, four different wind speeds and two different wind directions. The results of this being a base for comparison, simulations are carried out with partially isolated gas detection system, presuming on-going hot works in the near vicinity with a temporary weather cladding and with fire proof doors left in open position. The variations in the total ignition probability of the module compared to base case would be the main objective of this thesis.

As additional objectives, since the barrier systems could be directly or indirectly influenced by humans, an attempt is made by simulating the base case with a practically acceptable delay in manual activation of shutdown. Furthermore, to reduce the simulation time, numerous simulations are run to arrive at the optimal grid resolution and courant number with the quality of results remaining undiminished.

The case with delayed shutdown due to manual activation of ESD depicted the highest influence to the complementary cumulative frequencies, followed by the case simulated with a temporary weather cladding erected on one of the open ends of the module, with second highest influence. The comparison of the two base case simulations with different leak scenarios (direction and location), revealed that the release point and release direction can significantly influence the probabilities of ignition, either positively or negatively. The simulations that were carried out to optimize the grid resolution resulted in a significant reduction of simulation time with a grid resolution of 125000, while the quality of the results were undiminished. A further analysis by extracting the highest and the least release rates separately resulted in an insight that the grid resolution is a function of release rate.

Preface

This thesis marks the end of a remarkable journey of my masters degree at the Institute of Marine Technology (IMT), Norwegian University of Science and Technology (NTNU). Needless to say, the knowledge that I have acquired through various courses in my study program and through some people-turned-friends whom I gladly met during my stay in Norway, has had a major influence in shaping me to be the person that I am today. This thesis work has been performed in collaboration with Safetec Nordic AS, Trondheim, Norway.

First and foremost, I would like to thank my supervisor at NTNU, Jan Erik Vinnem, for letting me pursue this study as my thesis. His utmost patience while I was plagued with unexpected software-related delays and his thorough guidance regarding the thesis structure and feedback till the final day of submission is highly appreciated. To my supervisor at Safetec, Ingar Fossan, for educating me about this topic since 2018, equipping me with the latest advancements at the industrial frontier and for constantly communicating the importance of this thesis work. The amount of valuable time that he spent explaining deeper insights, addressing numerous questions and for fixing issues related to the software tool is immensely appreciated. This thesis work would have continued to remain as a conceptual idea had it not been for his support.

Secondly, I would also like to thank Safetec Nordic AS for providing me with this wonderful opportunity to pursue my thesis with them, and for facilitating me thoroughly during my stay at their office. I would like to extend my thanks to Rune Natten Kleiveland, Nils Inge Lilleheie and others from DNVGL, Peter Ellevseth and Torleif Veen from Safetec Nordic AS for facilitating me with the software and for their continuous and prompt support in fixing the software and server-related problems.

I would also like to express my sincere gratitude to Sruti Subramanian and Venkatesan Arumugam Elumalai, for their constant support and words of encouragement which ensured that I gave the best that I could.

Finally, my heartfelt thanks to my wonderful family and friends for the lasting belief and faith they have in me, which at times seem to surpass the faith I have upon myself. Last but not least, my sincere thanks to NTNU for this incredible opportunity, the experience of which has been nothing less than life-changing.

Never stop fighting until you arrive at your destined place - that is, the unique you.
Have an aim in life, continuously acquire knowledge, work hard and
have perseverance to realise the great life.
-A.P.J. Abdul Kalam

Trondheim, November 28, 2019

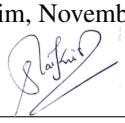

Saikrishna Govindarajan

Table of Contents

List of Tables

List of Figures

Nomenclature

Latin symbols

g	Acceleration due to gravity
E	Kinetic energy
K_r	Residual kinetic energy
P_r	Rate of production of kinetic energy
S_ϕ	Rate of increase of ϕ due to sources
R_e	Reynolds number
k	Turbulent kinetic energy
$\widetilde{Y}_{pr}$	Product mass fraction
n_0	The rate of spontaneous formation of radical nuclei
n	Concentration of radical nuclei
f	Linear branching coefficient
N	Concentration of soot particles
C_f	Mass concentration of fuel
g	Linear termination coefficient
T	Absolute temperature
R	Universal gas constant
a_0	Model constant in EDC
g	Linear termination coefficient

U	Velocity
$u'^{(t)}$	Fluctuating part of velocity
P	Pressure
C_μ	Model constant in k-ε
$C_{1\varepsilon}$	Model constant in k-ε
$C_{2\varepsilon}$	Model constant in k-ε
s	Seconds

Greek symbols

ρ	Density
τ_{ij}	Stress tensor
ψ	Potential energy per unit mass
μ	Coefficient of viscosity
ε_f	Viscous dissipation
ε	Rate of dissipation of turbulent kinetic energy
σ_k	Prandtl number
σ_ε	Prandtl number
ν	Kinematic viscosity
$\widetilde{\dot{\omega}_{fu}}$	Reaction rate for fuel
μ_t	Eddy viscous term

Other symbols

$'$	Fluctuation from mean value
$\dot{\omega}$	Time derivative of ω / unit time
$\overline{E}$	Reynolds averaged quantity
$\widetilde{Y}$	Favre averaged quantity
s	Soot
x, y, z	x-, y-, z-directions

Abbreviations

BORA	=	Barrier and Operational Risk Analysis
CAD	=	Computer Aided Design
CCR	=	Central Control Room
CFD	=	Computational Fluid dynamics
CODAM	=	Corrosion and Damage database
CONCAWE	=	Conservation of Clean Air and Water Europe
DFU	=	Defined hazard and accident condition
EDC	=	Eddy dissipation concept
ESD	=	Emergency Shutdown
ESDV	=	Emergency Shutdown Valve
HC	=	Hydrocarbon
HCR	=	Hydrocarbon Release
HSE	=	Health, Safety and Environment
HVAC	=	Heat Ventilation and Air conditioning
IOGP	=	International Association of Oil and Gas producers
KBB	=	Knowledge-Based Behaviour
KFX	=	Kameleon FireEX furcifer
KFX-RBM	=	Kameleon FireEx - Risk and Barrier Management
KPI	=	Key Performance Indicator
LEL	=	Lower Explosive Limit
LOPC	=	Loss of Primary Containment
MISOF	=	Modelling of Ignition Sources on Offshore oil and gas Facilities
MIRMAP	=	Modelling of Instantaneous Risk for Major Accident Prevention
MTO	=	Man, Technology and Organization
NCS	=	Norwegian Continental Shelf
OLF	=	Norwegian Oil Industry Association
O&M	=	Operations and Maintenance
PDE	=	Partial Differential Equations
P&ID	=	Process and Instrumentation Drawing
PARLOC	=	Pipeline and Riser Loss of Containment report
PLOFAM	=	Process Leak for Offshore installations Frequency Assessment Model
PSA	=	Petroleum Safety Authority [Norway]
PSE	=	Process Safety Event
QRA	=	Quantitative Risk Assessment
RBB	=	Rule-Based Behaviour
RISP	=	Risk Informed decision Support in development Projects
RNNP	=	Trends in Risk level in Petroleum activity
SBB	=	Skill-Based Behaviour
SD	=	Shutdown
UEL	=	Upper Explosive Limit
UKCS	=	United Kingdom Continental Shelf
WOAD	=	World Offshore Accident Database

Chapter 1

Introduction and background

This chapter presents a brief introduction in terms of world's necessity to consistently produce hydrocarbons, which brings along numerous risks. In addition, a brief note on the background information that forms the basis for this thesis is also described. To conclude this chapter, the objectives of this thesis work is listed down followed by a description of report structure.

1.1 Introduction

"The global population in 2050 will be around 9.77 billion people, which is 2 billion more than what the current population is today."

-World Population Review

With growing population, life on earth seems literally impossible without depending on energy in some form or the other [5]. Fossil fuels being the natural energy nucleus, the hunt and retrieval of the same could never be ceased considering the rate at which the world is advancing, as shown in Figure 1.2. Hydrocarbons are a primary energy source for the current advanced civilizations, predominantly as combustible fuels.

To accommodate the exponentially cruising energy needs, the search for hydrocarbons expanded from onshore to offshore locations and furthermore, from shallow to deep and ultra-deep waters. Over the years, this is being achieved through oil and gas exploration, drilling and production, by means of highly sophisticated and advanced drilling ships/rigs, production platforms, processing facilities and transportation, etc. On-board the offshore installations, the amount of pressure that the offshore production systems have to regulate is humongous. Such high pressure leads to hydrocarbon leaks on-board installations/vessels, which are regarded as one of the major risks in the oil and gas industry globally.

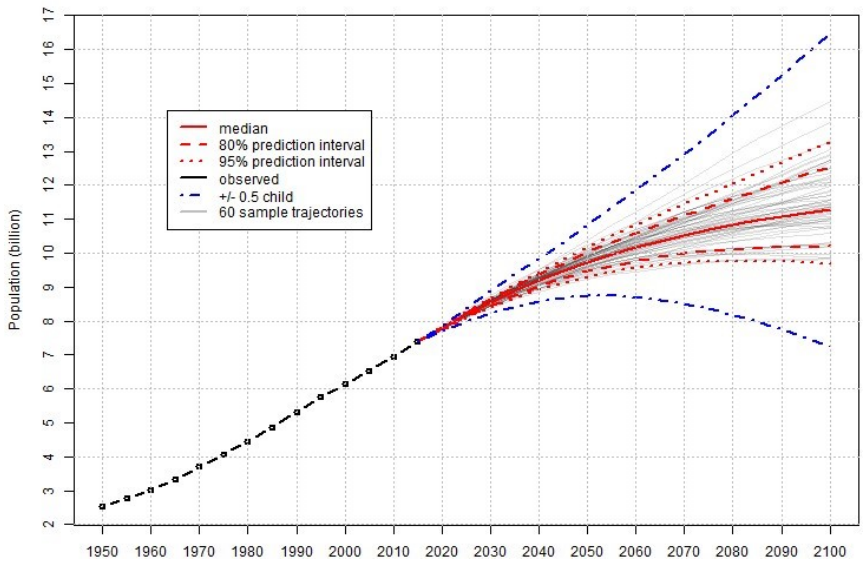

Figure 1.1: World population forecast, Source: United Nations, [5].

1.2 Background

The objective of this section is to present a basis upon which this thesis is built upon. Figure 1.2 depicts that the demand for energy will continue to increase for the next two decades.

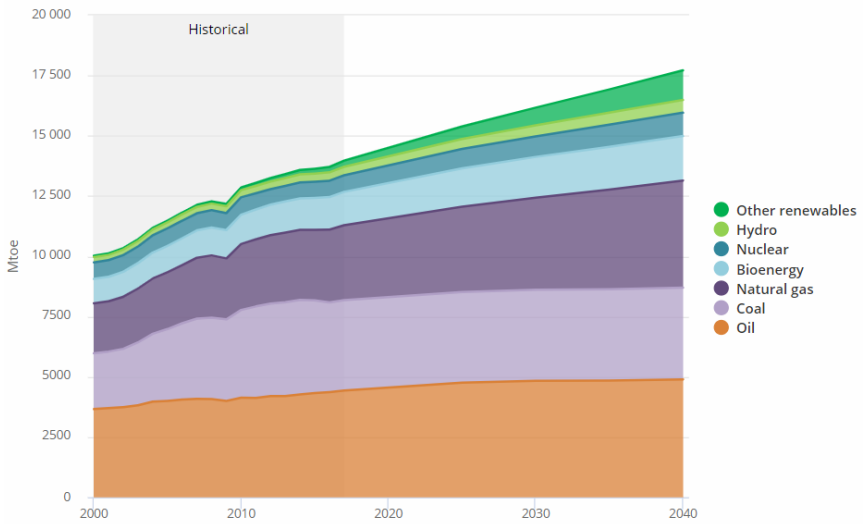

Figure 1.2: World energy demand forecast, Source:International Energy Agency, [1].

"According to the International Energy Agency's World Energy Outlook, the global energy demand will grow by more than a third over the period to 2040" [1].

This is directly proportional to the world's population forecast shown in Figure 1.1. Hence, todays world is striving to increase energy production exponentially to counter the demands of the generations to come. As a counter measure, Figure 1.3 depicts a comparison between fuel production and consumption forecast. The graph shows that the demand for oil is not only increasing but the consumption is catching up consistently as a result of growing global population [6].

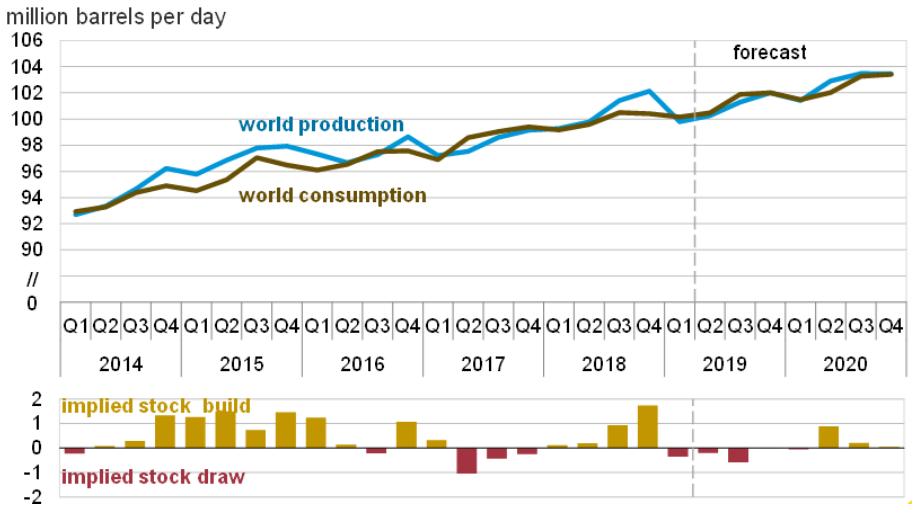

Figure 1.3: World fuel production and consumption forecast, Source: Energy Information Administration, [6].

Figure 1.4 presents the historic, present and future forecast of production distributed based on resource category, [22]. This depicts that the number of vessels and/or offshore installations performing exploration drilling, production, processing and storage would increase constantly. This in turn means that the safety of humans, environment and assets has to be maintained at the highest possible level at all times.

Among 184 rigs, floatels and ship shaped installations operating in North sea, 106 installations are managed by Norwegian operators as shown in Figure 10.2, attached to the Appendix B [26]. With numerous high pressure systems that makes up every offshore production facility, counter measures to prevent any leaks in the systems demand nothing less than extremely consistent and innovative efforts both in the research and industrial frontiers.

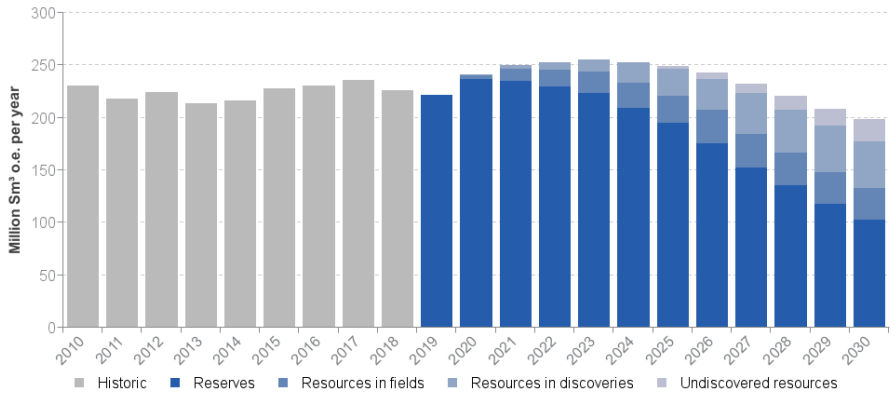

Figure 1.4: Norwegian production history and forecast. Source: Norwegian Petroleum, [22].

1.3 Objectives

The main objective of this thesis is to quantify the performance of the barriers controlling fire and explosion risks using advanced risk analysis methods. In order to achieve the main objectives, the following sub-objectives are to be fulfilled

- Analyse and identify which of the barrier elements presented in MIRMAP study has the highest influence on increasing fire and explosion risks.
- To run base case simulations with the chosen geometrical model with different release point and release direction. Comparing the results of the same to identify the influence of release point and direction on the probabilities of ignition.
- As a sub-study, to analyse and identify the "optimal grid resolution" suitable for the module in question. In addition, to understand its influence on small and large releases. This is targeted to answer the question, "Would it be possible to reduce simulation time without hampering the quality of results?"
- Using the same model to investigate the effects of various scenarios such as delayed Emergency Shutdown (ESD) due to manual activation, partial failure of gas detection, erecting temporary weather cladding and hot-works, on the overall ignition and explosion probabilities of the module.

The study would improve the understanding of the relative importance of barriers affecting fire and explosion risk, which could be used as input for other modelling approaches, such as factor models and the on-going RISP projects in industry aiming to establish simplified quantitative models. Finally, this study would be beneficial to the owners of the software since it is an opportunity to identify and fix some critical bugs, thereby contributing to the robustness of the software.

1.4 Structure of the report

Chapter 2 describes some of the major risks in the Oil and Gas (O&G) industry including the Hydrocarbon (HC) leaks, the causal factors and a typical Man-Technology-Organization (MTO) chart depicting the deviations in an HC leak accident. Chapter 3 introduces the software, KFX, explains some of its underlying theories, numerical methods and user interface. In addition, the geometrical model used in this study is introduced. Chapter 4 presents generic input parameters necessary for gas dispersion simulations, method to set up a case for simulation and the results of the base case simulations. Chapter 5 presents the results of a sub-study, "optimal grid resolution" and the inferences gained from it. In Chapter 6, results of various simulations that were carried out to study sensitivities by inducing parametric variations are presented. Chapters 7 presents critical findings and compares key results. Chapter 8 presents discussions and challenges while Chapter 9 outlines conclusions and briefly describes some potential future work.

Chapter 2

Literature Review

This chapter lays a foundation for this work by providing readers with a brief insight into generic risks in offshore oil and gas industry that every major oil and gas company would have encountered in one way or the other. Also briefly explained are some operational risks in oil and gas industry, major hazard statistics, Norwegian Hydrocarbon (HC) leak statistics and the methodology that had been created and adopted by Norwegian oil and gas industry to counter the threat of hydrocarbon leaks.

2.1 Risks in Oil and Gas industry

The oil and gas industry is plagued with numerous risks right from its design phase to construction, installation, operation and decommissioning phases. The combination of aspects such as the size, quantity and complexity of systems, machineries and their interaction, the location, the enormity of forces to combat etc., makes offshore installations and floating production units highly vulnerable to a wide spectrum of risks.

According to International Association of Oil and Gas Producers (IOGP), the process safety which corresponds to operational safety is a *"disciplined framework for managing the integrity of operating systems and processes that handle hazardous substances. It relies on good design principles, engineering and operating and maintenance practices. It deals with the prevention and control of events that have the potential to release hazardous materials and energy"* [18].

The Norwegian Oil and Gas Association has summarized some of the typical risks in the offshore oil and gas industry, as shown in Table 2.1 [20]. There are numerous examples from the past when such risks remained either unidentified or overseen through different phases of design, construction and operation of installations. On some rather unfortunate instances, the accidental events that emerged out of such unidentified risks have left the industry with irreparable scars in the form of catastrophic consequences. But on the contrary, those accidents acted as catalysts in setting out the Norwegian oil and gas industry in quest for the better.

No	Description
1	Non-ignited hydrocarbon leaks
2	Ignited hydrocarbon leaks
3	Well kicks/loss of well control
4	Fire/explosion in other areas, flammable liquids
5	Vessel on collision course
6	Drifting object
7	Collision with field-related vessel/installation/shuttle tanker
8	Structural damage to platform/stability/anchoring/positioning failure
9	Leaking from subsea production systems/pipelines/risers/flowlines/ loading buoys/loading hoses
10	Damage to subsea production equipment/pipeline systems/diving equipment caused by fishing gear
11	Evacuation (precautionary/emergency evacuation)
12	Helicopter crash/emergency landing on/near installation

Table 2.1: Overview of major hazards precursor event categories, [12].

Some noteworthy accidents that shaped up the industry globally are as follows. Alexander L. Kielland capsize, Ocean Ranger capsize, Sleipner GBS capsize, P36 capsize, Mumbai High north riser rupture, Piper Alpha explosion and fire, Usumacinta blowout, Sao Mateus explosion and fire, Mocando blowout, Deepsea driller capsize, Ekofisk B blowout, Ekofisk B blowout, Norne shuttle tanker collision, Gryphon Alpha multiple anchor line failure, Snorre Alpha subsea gas blowout, Glomar Jawa sea capsize etc., [29].

Such accidents and other dangerous near misses leave behind enormous amount of vital information that could be used to prevent such occurrences in future. In Norway, there are number of databases that collect data in view of putting them to best use. Some of the databases are mentioned in Table 2.2.

Accidental event	Data sources
Process leaks	Petroleum Safety Authority of Norway, Trends in risk level in petroleum activity (RNNP)
Blowout	Sintef blowout database, kick statistics from RNNP
Riser/ flowline / pipeline leaks	Pipeline and Riser Loss of Containment report (PARLOC), Corrosion and Damage database (CODAM), Conservation of Clean Air and Water Europe (CONCAWE).
Marine system failures	RNNP, World Offshore Accident Database (WOAD) and HSE reports
Structural failures and impacts	RNNP, WOAD, HSE reports
Dropped objects	CODAM, RNNP, HSE reports

Table 2.2: Data sources for accidents and near misses [14].

One way to make the best use of such accumulated data is to analyze them with any risk assessment techniques or case studies and arrive at a risk picture, which in turn could

be used to improve the design or develop barrier strategies. In this section, one such data collection by Petroleum Safety Authority of Norway (PSA) is presented. PSA gathers data through one for its projects which monitors the "Trends in Risk Levels in Petroleum Activity (RNNP)" in the Norwegian Continental shelf (NCS).

2.1.1 RNNP

"The Trends in Risk Level in Petroleum Activity (RNNP)" was initiated between 1999 and 2000, with an aim to track the fluctuations of trends in the risk levels posed by various Defined hazard and accident condition (DFUs) in the Norwegian Continental Shelf. One of the major reasons for its success could be attributed to the equal involvement of companies, unions and governmental agencies by contributing to a shared understanding of risks and promoting risk-free culture. The main focus of RNNP is on personal risks and environmental factors. For the risks associated with major hazards on the installations, the following types of indicators have been developed through RNNP, [14].

- Indicators based on the occurrences of incidents and near-misses (i.e precursor events).
- Indicators based on performance of barriers that are installed in order to protect against these hazards and their consequence potential.

The categories presented in Table 2.1 shows an overview of some of the DFUs related to major accidents. Data for DFUs are being collected through various methods and being quality assured before being fed into the database. Figure 2.1 presents the number of DFUs registered in NCS since 2000. There is a significant declining trend in the number of DFUs from 119 in 2002 to 30 in 2018. This is due to the combined efforts from authorities, companies and research institutions.

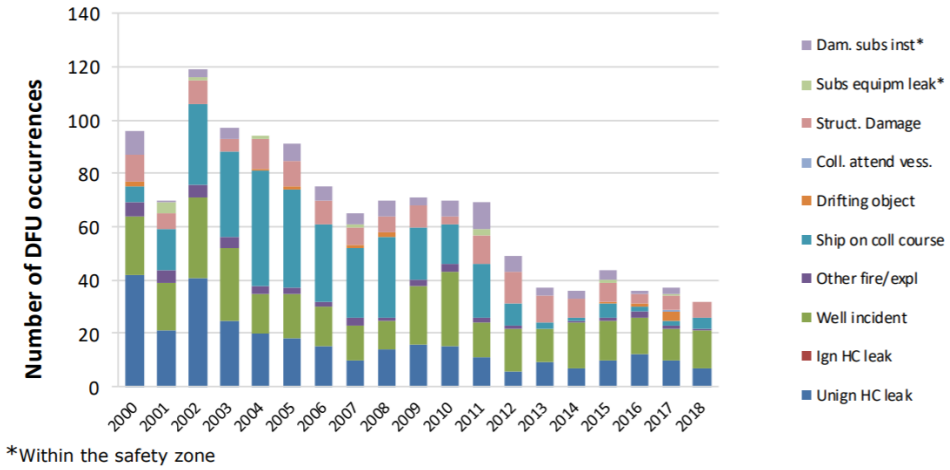

Figure 2.1: DFUs reported from 2000 to 2018 for 10 major accident categories[14]

According to the "Safety performance indicators" report published by International Association of Oil and Gas Producers (IOGP) [17], the accidental events are classified based on a four-tier framework of Key-Performance Indicators (KPIs) among which, Tiers 1 and 2 are predominantly related to Loss of Primary Containment (LOPC) and are referred to as a Process Safety Event (PSE). The Tier 1 and Tier 2 record events with greater consequence within the four-tier approach.

Although the data presented in Figure 2.2 is based on the data from participating companies, it could still be relevant to study the number of high-consequence events occurring. Among all the DFUs, the HC leaks are considered to be the biggest threat solely due to the catastrophic consequences it could bring about. This leads to the next section which presents an overview of HC leak statistics and the importance of minimizing HC leaks.

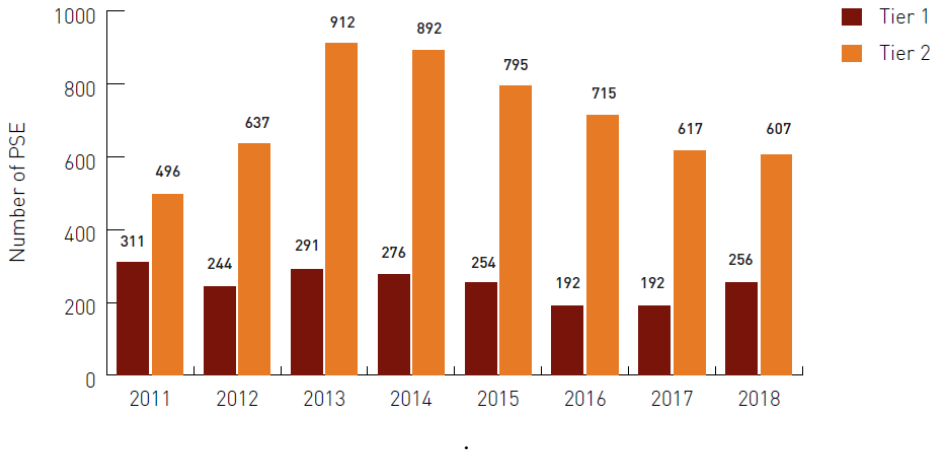

Figure 2.2: Total number of PSE -Tier 1 and Tier 2, [17]

2.2 Hydrocarbon (HC) leaks

In terms of occurrences and consequence, the HC leaks are considered as one of the most critical risk for major accidents in the offshore industry worldwide. There are several databases that are collecting facts on HC leaks in views of putting such data to best use in the form of risk assessments. In Norway, the Petroleum Safety Authority, through a project titled "Trends in Risk levels in Petroleum Activity (RNNP)", has been maintaining trust worthy records pertaining to the number of occurrences of HC leaks each year since 2000 [16]. This data has been widely utilized in several studies in Norway in view of improving the health, safety and environmental conditions in the offshore industry with respect to HC leaks.

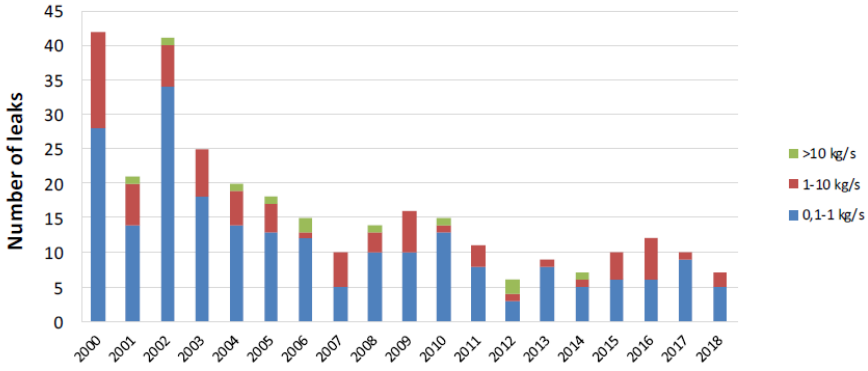

Figure 2.3: Number of HC leaks exceeding 0.1 kg/s, [14].

Figure 2.3 shows the number of hydrocarbon leaks greater than 0.1 kg/s in the period 2000 - 2018. The HC leaks could be of any type hydrocarbon such as gas, two-phase or stabilized oil or condensate according to Norwegian classification [14].

Be it any form of leak, the consequences of major HC leak could be catastrophic. One of the biggest example that shook the industry is the Piper Alpha disaster, wherein a gas leak ended up claiming 165 lives in UK in 1988. Ever since then, the Norwegian Government has taken measures to involve companies, governmental agencies and research institutions to explore steps to prevent such gas leaks. Extensive studies have been carried out between 2008 and 2014, wherein there were 78 leaks with a leak rate of > 0.1 kg/s, [30].

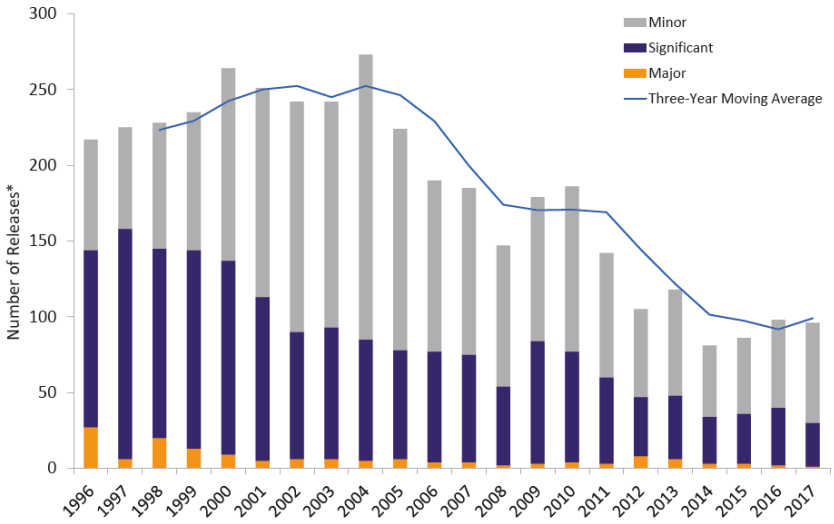

Figure 2.4: Number of HCRs occurring offshore, [19].

In comparison, in the UK, similar statistics are recorded and presented in the form of Health and Safety report which is published every year. The report presents the hydrocarbon releases (HCRs) in the United Kingdom Continental Shelf (UKCS), that are reportable in accordance to EU regulations. Figure 2.4 shows that the number of reportable leaks in the UK has also seen some significant decline in numbers from 260 in 2000 to just under a 100 in 2017, with almost no major leaks.

The declining trend in the number of HC leaks in Norway and UK as presented in the Figures 2.3 and 2.4 respectively, is a major evidence that the efforts have been consistent and focused to minimize the HC leak events over the years. Although one could argue that the numbers illustrate a significant achievement, even one undesired major leak could lead to irreparable losses, as was the case with several noteworthy accidents presented in Section 2.1.

2.3 Causal factors

The initiating events for HC leaks could be a single event or a combination of events. The initiating event could also represent the hazardous event and will in all cases requires actions from system safety functions, [24]. The Barrier and Operational Risk Analysis (BORA) is a project carried out between 2003 and 2006 to study the barrier situation in detail when operational activities are carried out. An overview of initiating events presented in BORA is shown in Table 2.3 [31].

Initiating event type	Initiating events
Technical degradation of system	Degradation of valve sealing, Degradation of flange gasket, Loss of bolt tensioning, Fatigue, Internal corrosion, External corrosion, Erosion, Other causes.
Human intervention introducing latent error	Incorrect blinding/isolation, Incorrect fitting of flanges or bolts during maintenance, Valve(s) in incorrect position after maintenance, Erroneous choice or installations of sealing device, Maloperation of valve(s) during manual operation*, Maloperation of temporary hoses.
Human intervention causing immediate release	Break-down of isolation system during maintenance, Maloperation of valve(s) during manual operation*, Work on wrong equipment, not known to be pressurised.
Process disturbance	Overpressure, Overflow/Overfilling.
Inherent design errors	Design related failures.
External events	Impart from falling objects, Impact from bumping/ collision.
*May lead to either introduction of latent error or immediate release.	

Table 2.3: An overview of initiating events of HC leaks presented in BORA [31].

A study considering 110 leaks over a 10 year period from 2008 to 2017 was carried out, wherein there were 86 causes identified to have contributed to 11 major accidents were

analysed. These accidents had catastrophic damage potential to humans, environment, assets or the reputation of the firm. Figure 2.5 shows of the contribution of from technical, operational and organizational factors that were directly or indirectly responsible for the occurrence of major HC leaks [25]. Since the Human-Organizational aspects had a major contribution of 69%, they were further broken down into sub aspects to identify the root causes of the accidents.

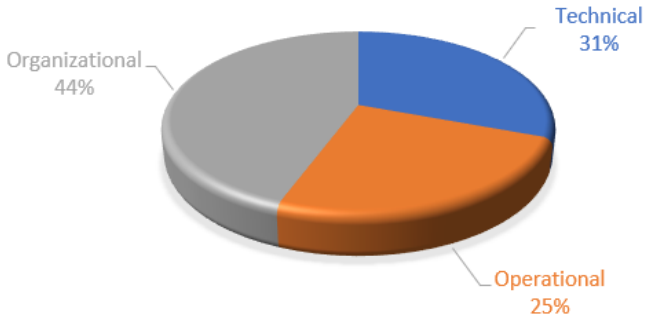

Figure 2.5: Classification of causal factors, [25].

The 25% of the human contribution to the major leaks were further classified into psychological aspects which in turn were influenced by inexperience, incompetence and negligence [25]. This is further explained as follows

- *Inexperience*: Operators with sufficient training but are relatively inexperienced in handling complex safety-critical systems (e.g., operators who are less than six months into the job).

- *Incompetence*: Operators with sufficient training and experience but not at the current operation/system that they are tasked to handle. Typically happens when operators are switched between different installations.

- *Negligence*: Operators with sufficient training, skills and experience, but have a tendency to overlook things (e.g., due to overconfidence).

The results show that among the human aspects considered, the tendency to overlook some critical aspects, especially among the experienced persons seem to dominate with 73% contribution. The study concluded that the aspects of inexperience, incompetence and negligence shown in Figure 2.6, could have major influence on the behavioral aspects namely skill, rule and knowledge based behaviours, explained as follows:

- *Skill-based behaviour (SBB)* represents performance during activities which takes place without conscious control. The types of errors that can occur here are the slips and lapses of the skilled person performing a familiar task.

- *Rule-based behaviour (RBB)* typically occurs in a familiar situation and involves stored rules or procedures. The general types of errors here is the tendency to use familiar solutions even when these are not the most efficient. (e.g., shortcuts).
- *Knowledge-based behaviour (KBB)* occurs in unfamiliar circumstances. Mistakes here generally consists of misdiagnosis and miscalculations.

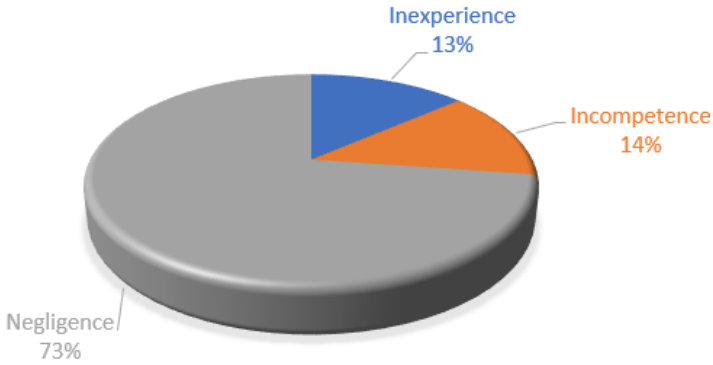

Figure 2.6: Classification of human factors [25].

Similarly, breaking down the 44% of organizational factors into sub categories, deficient risk assessments, lack of involvement from the management and deficient competence management seem to contribute 58% to the root causes as shown in Figure 2.7. The authors state that most lapses in risk assessments are results of poor understanding of the systems functions either by the land-based staff who assist in conducting Risk Assessments (RA) or "this-would-be-enough" attitude of some operators [25].

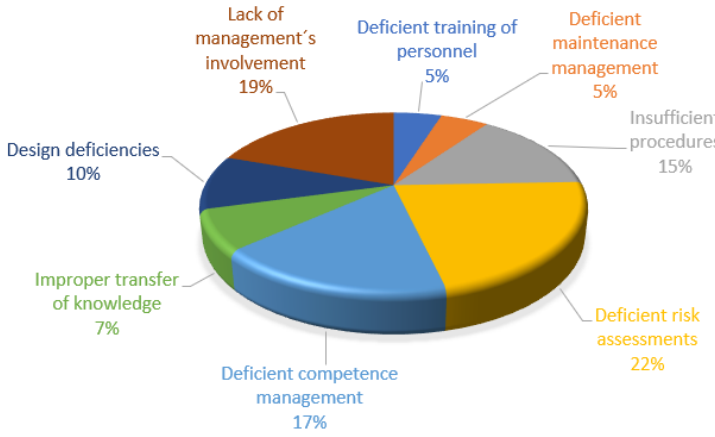

Figure 2.7: Classification of organizational factors [25].

2.4 Man-Technology-Organization (MTO)

Typically, any consequence/s of a major accident would have contributions from technical, organizational and operational factors contributing to the root causes of the accident. In order to identify this, one of the most widely used techniques is the MTO analysis which aids not only to identify the individual contributions from technical, operational and organizational factors but also to identify the deviations from the ideal coarse of events.

To further understand the MTO analysis, it would be relevant to pick a case that is available in the public domain and study how the contributions from M-T-O factors have shaped the consequences of that particular accident. The following section gives a short summary on the HC leak that occurred on Heimdal Main Platform (HMP) in 2012 in NCS.

2.4.1 Summary of the accident

An oil leak in one of the Emergency Shutdown Valves (ESDV) in the module M40 of by then, Statoil's Heimdal main platform forced a partial production shutdown and depressurization. Preparations for testing the ESDVs included blowdown of a bleed-off pipeline to the flare. En route to flare, this pipeline consists of a main control valve (HCV20021) which is a seat valve with actuator and is remotely operated from central control room (CCR), three manual shut-off valves among which NC1 and NC3 are ball valves and NC2 is a seat valve as shown in Figure 2.8. NC1 and NC2 are located upstream of the HCV whilst NC3 is situated downstream.

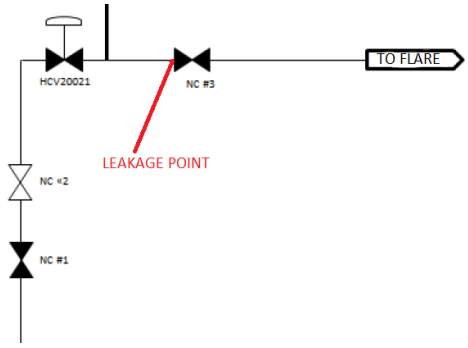

Figure 2.8: Blowdown line to flare [15].

The NC3 which functioned as the final technical barrier to the flare was in closed position. As the remotely operated valve HCV20021 was opened from the control room, gas at 129 bar impacted NC3 with a design pressure rating of 16 bar, causing the gasket between the valve and the pipe flange to fail. The gas pressure blew off the cladding and insulation covering the manual valve and the gas leaked into module M40 at 12:40 hrs on Saturday 25^th May 2012.

One operator was working in the module at the time, but was not exposed to flying debris or any health effects from the leaking gas. Following immediate notification from the process operator, the CCR operator shut off the HCV, which eventually ceased at 12:45

hrs. Gas was detected in several of the surrounding modules M30, M50 and M60 which initiated the deluge system.

Evacuation alarm was activated immediately and personnel mustered at the life boats and the affected areas were free of gas after about 30 minutes, though gas remained in one segment of the transit system. A total volume of 3500 kg of gas leaked over 252 seconds at an initial leak rate of 16.9 kg/s. Emergency response operations were carried out by depressurizing via other valves around the leak site and the emergency situation concluded at 16:10 hrs [7] [15].

The following observations surfaced to conclude the report:

- Risks pertaining the planned job were not identified, discussed and communicated clearly between the planning team, which involved Operations and Maintenance (O&M) lead, process operator plus 2 trainees and Central Control Room (CCR) operator.
- The operator who performed the opening of manual valves was not involved in job planning.
- The procedure did not describe which valves to open and in what sequence.
- Process and Instrumentation Drawings (P&IDs) were obsolete and misguiding.

The MTO interactions are presented in the form of a Venn diagram as shown in Figure 2.9. It is evident that the major influencing factors are the M-O interactions, which ended up as the biggest contributor. A complete MTO-analysis worksheet is attached to Appendix A, Figure 10.1.

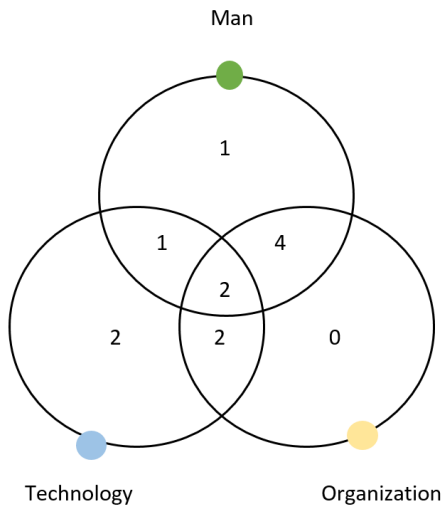

Figure 2.9: Venn diagram - MTO interactions

2.5 An overview of MIRMAP

Modelling Instantaneous Risk for Major Accident Prevention (MIRMAP) is a four-year research project started in 2013 by Norwegian University of Science and Technology (NTNU), NTNU Studio Apertura, Preventor and Safetec Nordic AS. The aim of MIRMAP is to develop a model for instantaneous operational decision support unlike the quantitative risk analysis (QRA) which presents the average risk level for a facility over a year. The method focuses on modelling risks associated with activities and it is simplified to avoid time consuming consequence calculations. The results would enable the decision makers to prioritize, plan and schedule activities with better knowledge about the instantaneous risk pictures.

The QRA performed during the design phase of the project would have assumptions for the average level of work activities per day and the risk would have been calculated based on the assumption. Whereas in reality, the operational risks might change on daily basis which is unaccounted for in the initial QRA. The MIRMAP methodology is to capture such changes in the risk picture based on the actual level of work activities on the installation, eventually serving as a better decision-making tool.

Simply put, the modelling objective in the MIRMAP report is defined as "major accident risk due to hydrocarbon leaks (what) from offshore oil/gas installations (where) to provide an updated risk picture on a daily basis (why)" [13].

In view of developing a generic risk model, the authors have identified four main barrier functions as follows:

1. *Prevent Release* - Avoidance and control of hydrocarbon leakages.

2. *Limit Release Size* - Detection, stoppage and/or reduction of leak size.

3. *Prevent Ignition* - Prevent and avoid creation of uncontrolled ignition sources.

4. *Prevent Escalation* - Limit consequences of explosion, reduce heat loads and fire sizes and avoid intensification of an ignited hydrocarbon leak.

In order to be reasonably practicable, the simulation cases for the current study follows the aforementioned barrier functions. Majority of the HC leaks in NCS have occurred in modules that were already isolated for some planned activities. This shows that the risks for personnel within the module is extremely higher than a person who is at a far off location on the installation. Therefore, the risk picture within modules is of more importance compared to that of the entire installation. Hence the simulation cases in this study are confined to a module which will be introduced in Chapter 3.

Considering the historical cases and the current practical issues that are prevailing onboard the installations in NCS, the cases chosen for simulations are presented in Table 2.4.

Barrier function	Barrier sub-function	Barrier system	Base case	Sensitivity case
Prevent release	Containment	Process shut down	Auto triggering Emergency Shutdown Valve (ESDV)	Delays in shutdown time (Human intervention)
Limit release size	Detect leak	Gas detection	Gas detection system functioning as normal (100% functionality)	Isolate gas detection partially (60% functionality)
Prevent ignition	Control of ongoing work	Ignition source control (Hot work)	Gas cloud with no ignition	Gas cloud with higher ignition probability due to additional ignition sources
	Prevent gas cloud build-up	Ventilation	No wind-shielding curtain in place	Intend to add porous wind- shielding curtain on one of the open end (Typically used during winters to prevent heavy winds)

Table 2.4: Scenarios for simulation.

2.6 Importance of QRA

The offshore risk assessments over the past two decades have been inclining towards strengthening the barriers that eventually reduces the occurrence of accidental events, as shown in Figure 2.10. Among various events, the gas leaks, fires and explosions have been prioritized the most due to their catastrophic consequence potential.

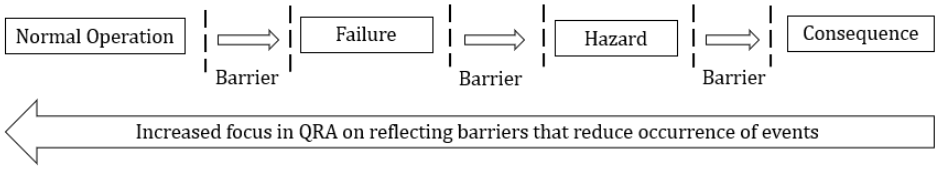

Figure 2.10: Importance of QRA

This demands a thorough understanding of the complex relationship between the barriers in place and the physical phenomena, as the events unfold. Figure 2.11 shows that the damage potential is proportional to time. Therefore, it is vital to optimize the safety design for the stages immediately post the leak initiation. In other words, the ignition probability should be as low as possible after leak detection.

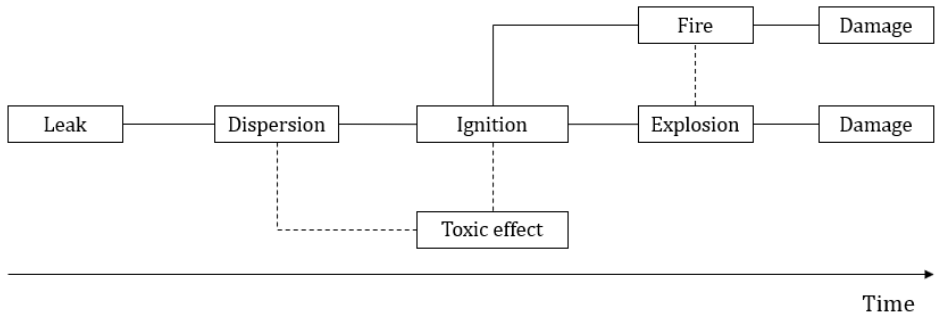

Figure 2.11: Physical phenomena post initiating event

One of the objectives of this thesis work is to study the immediate effects of a gas leak. This includes the effect of gas detection, system isolation and isolation of ignition sources, ESDV activation time and blow down initiation time as shown in Figure 2.12. The transient characteristics of the dispersion process defines the exposure probability of live sources of ignition.

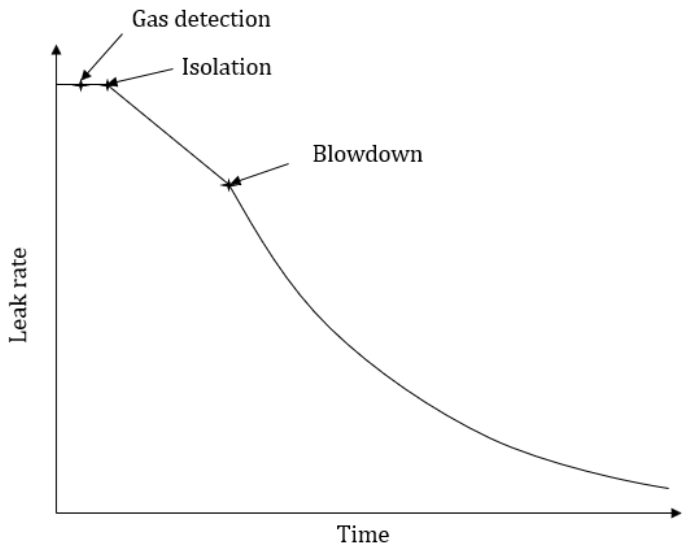

Figure 2.12: Effect of gas detection, ESD and BD.

Eventually, the results of the study that is being carried out in this thesis work will aid as a powerful decision support tool during the design, operational, modification as well as decommissioning stages of an installation. In addition to this, the experience from such studies could serve as a valuable input for other modelling approaches such as factor models or simplified quantitative models.

Chapter 3

Software - KFX

The software used for this project is Kameleon FireEx KFX Furcifer (herein referred as KFX). KFX is one of the leading Computational Fluid Dynamics (CFD) based tools developed by DNV GL CFD solutions AS. The first two sections of this chapter delineates the purpose of KFX, underlying theories and what it could mean to offshore oil and gas industry in terms of risk assessments. The third and fourth sections presents the software's versatile interface, ways to set up simulations and the process of extracting and interpreting simulation results. The last section presents the generic model which has been utilized as the test model of this project work.

KFX was developed for three dimensional transient flare, fire and gas dispersion simulations. It is also interfaced with finite-element structure response codes for dynamic structural response analysis. KFX also includes detailed Lagrangian models for fire mitigation by water systems namely water mist systems, water curtains, deluge, sprinklers etc. Owing to aforesaid functionalities, KFX is one of the powerful tools for the Offshore Oil and Gas industry, for the sake of post-accident investigations. In addition, KFX also enables pro-active gas leaks and explosion simulations, that could enhance the process safety on-board installations. Other capabilities of KFX would also include, but not limited to:

- Simulation of all kinds of fires such as jet fires, pool fires, two phase spray fires, flares, fire in enclosures, in complex geometries, in still air or windy conditions, etc.
- Fire impact on structures and process equipment.
- Fire temperature, radiation and smoke impact on humans.
- Calculation of explosive gas cloud sizes.
- Gas and fire detection systems.
- HVAC (ventilation simulations).
- Optimization of passive fire protection.

3.1 Background and Theory

This section presents the underlying numerical models that the KFX is built upon. The governing equations that are to be solved for 3D transient fire and gas dispersion simulations are Partial Differential Equations (PDE) describing the transient behaviour of the different field variable in space [2].

3.1.1 General equations

Conservation of Mass

For any compressible fluids, the three-dimensional mass conservation or continuity equation is given by Equation 3.1.1.

$$\frac{\partial \rho}{\partial t} + div(\rho u) = 0 \tag{3.1.1}$$

The first derivative term on the left depicts the rate of change of density and the second gives the net mass flow out of the element across its boundary [28].

Conservation of Momentum

Momentum is defined as the product of mass and velocity of a body in motion. The surface forces are described by the stress tensor $\tau_{ij(x,t)}$, [28]. The potential energy per unit mass associated with gravity is given by ψ, the body force per unit mass is

$$g = -\nabla \psi \tag{3.1.2}$$

where g is the acceleration due to gravity. The momentum equation shown in Equation 3.1.3, causes the fluid to accelerate. The stress tensor τ_{ij} is given by Equation 3.1.4

$$\rho \frac{DU_j}{Dt} = \frac{\partial \tau_{ij}}{\partial x_i} - \rho \frac{\partial \psi}{\partial x_j} \tag{3.1.3}$$

$$\tau_{ij} = -P\delta_{ij} + \mu(\frac{\partial U_i}{\partial x_j} + \frac{\partial U_j}{\partial x_i}) \tag{3.1.4}$$

where P is the pressure, and μ is the coefficient of viscosity. For constant density fluids, the momentum conservation is governed by Navier-Stokes equation, Equation 3.1.5

$$\rho \frac{DU_j}{Dt} = \mu \frac{\partial^2 U_j}{\partial x_i \partial x_i} - \frac{\partial P}{\partial x_j} - \rho \frac{\partial \psi}{\partial x_j} \tag{3.1.5}$$

Conservation of Energy

The energy equation is governed by the first law of thermodynamics which states that the rate of increase of energy of a fluid particle is the sum of net rates of heat added and the work done on fluid particles, [23]. The kinetic energy $\overline{E}(x,t)$ is obtained by filtering the kinetic-energy field $E(x,t) \equiv \frac{1}{2}U.U$, i.e.,

$$\overline{E} \equiv \frac{1}{2}\overline{U.U} \tag{3.1.6}$$

This could be further decomposed as proposed by [23] as

$$\overline{E} = E_f + K_r \tag{3.1.7}$$

where

$$E_f \equiv \frac{1}{2}U.\overline{U} \tag{3.1.8}$$

is the kinetic energy of the filtered velocity field, and K_r is the residual kinetic energy

$$K_r \equiv \frac{1}{2}\overline{U.U} - \frac{1}{2}\overline{U}.\overline{U} = \frac{1}{2}\tau_{ii}^R \tag{3.1.9}$$

The energy conservation equation can be written as

$$\frac{\overline{D}E_f}{\overline{D}t} - \frac{\partial}{\partial x_i}[\overline{U_j}(2\nu\overline{S}_{ij} - \tau_{ij}^r - \frac{\overline{P}}{\rho}\delta_{ij})] = \varepsilon_f - P_r \tag{3.1.10}$$

where ε_f and P_r are defined as

$$\varepsilon_f \equiv 2\nu\overline{S}_{ij}\overline{S}_{ij} \tag{3.1.11}$$

$$P_r = -\tau_{ij}^r\overline{S}_{ij} \tag{3.1.12}$$

where P_r is the rate of production of kinetic energy and ε_f represents the viscous dissipation.

3.1.2 Transport equations

The partial differential equation describing fluid flow are commonly referred to as transport equations. The transport equations are discretized into finite volume difference equations which are particularly suited for conservation of the different variables to be solved. By

introducing a generic variable ϕ, the conservative form of all fluid equations can be written as shown in Equation 3.1.13

$$\frac{\partial(\rho\phi)}{\partial t} + div(\rho\phi u) \;=\; div(\varsigma\ grad\phi) \;+\; S_\phi \tag{3.1.13}$$

In words,

Rate of increase of ϕ of fluid element	Net rate of flow + of ϕ out of fluid element	Rate of increase = of ϕ due to diffusion	Rate of increase + of ϕ due to sources

Equation 3.1.13 is termed as transport equation for property ϕ where ς being the diffusive coefficient [28] [3].

3.1.3 Turbulent flows

At values below the critical Reynolds number Re_{crit}, the flow is smooth, referred as laminar flow and at values above Re_{crit}, the flow is random and chaotic and referred to as turbulent flow. Hence the Reynolds number Re is the factor that decides the type of flow. Equation 3.1.14 presents the Reynolds decomposition where the velocity $u(t)$ is decomposed into a steady part U and a fluctuating part $u^{'(t)}$.

$$u(t) \;=\; U \;+\; u^{'\,(t)} \tag{3.1.14}$$

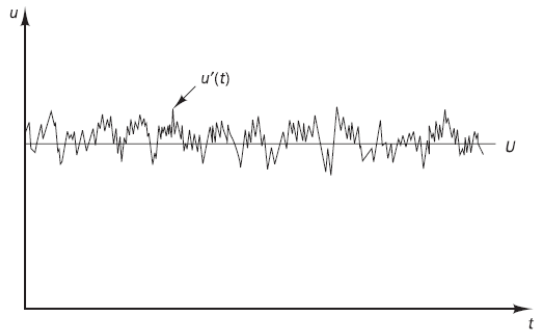

Figure 3.1: Reynolds decomposition [28]

The K-ε turbulence model

The K-ε model is the most widely used turbulent models applied in most commercial CFD codes. The K-ε model has two model equations, one each for K and ε. The following transport equations are used for the standard k-ε model.

$$\frac{\partial(\rho k)}{\partial t} + div\,(\rho k U) = div[\frac{u_t}{\sigma_k} grad\, k] + 2\mu_t S_{ij} \,.\, S_{ij} - \rho\varepsilon \tag{3.1.15}$$

$$\frac{\partial(\rho\varepsilon)}{\partial t} + div\,(\rho\varepsilon U) = div[\frac{u_t}{\sigma_\varepsilon} grad\, \varepsilon] + C_{1\varepsilon}\frac{\varepsilon}{k} 2\mu_t S_{ij} \,.\, S_{ij} - C_{2\varepsilon}\rho\frac{\varepsilon^2}{k} \tag{3.1.16}$$

In word form, the equations could be explained as follows

Rate of change of k or ε	+	Transport of k or ε by convection	=	Transport of k or ε by diffusion	+	Rate of production of k or ε	−	Rate of destruction of k or ε

The above equations have five adjustable constants C_μ, σ_k, σ_ε, $C_{1\varepsilon}$, $C_{2\varepsilon}$ with the following values:

$$C_\mu = 0.09,\ \sigma_k = 1.00,\ \sigma_\varepsilon = 1.30,\ C_{1\varepsilon} = 1.44,\ C_{2\varepsilon} = 1.92 \tag{3.1.17}$$

Prandtl numbers σ_k, σ_ε, connect the diffusivities of k and ε to eddy viscosity term μ_t, [28].

3.1.4 The Eddy Dissipation Concept (EDC)

The concept of EDC model is to incorporate the fine structures in a turbulent reacting flow and it is a modified version of eddy break-up model (EBU). The model could be summarized as follows

The mass fraction of fine structures could be defined as

$$\gamma^* = 4,6\,(\frac{\nu\varepsilon}{k^2})^{\frac{1}{2}} \tag{3.1.18}$$

where ν is the kinematic viscosity, k and ε are the turbulent kinetic energy and dissipation and 4.6 is a model constant [28] [3].

The reaction fraction and the reaction rate could be defined as follows

$$X = \frac{\frac{\widetilde{Y}_{pr}}{(1+s)}}{\widetilde{Y}_{min} + \frac{\widetilde{Y}_{pr}}{(1+s)}} \tag{3.1.19}$$

where $\widetilde{Y}_{pr}$ is the product mass fraction.

$$\widetilde{\dot{\omega}}_{fu} = -\overline{\rho}\frac{\varepsilon}{k} C_{EDC} min(\widetilde{Y}_{fu},\ \frac{\widetilde{Y}_{ox}}{s})(\frac{X}{1 - \gamma * X}) \tag{3.1.20}$$

where C_{EDC} is a model constant with a value of 11.2, [4].

3.1.5 The Eddy Dissipation Soot model

Soot is a mass of carbon particles resulting from incomplete combustion of hydrocarbons. Soot roughly contains eight parts of carbon and one part of hydrogen (soot density is 1.84701 g/cm^3 [21].

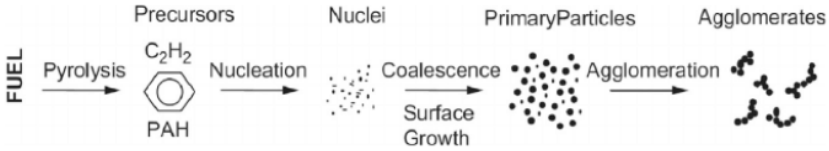

Figure 3.2: Schematic diagram of the soot formation step process from gas phase to solid agglomerated particles in five steps [21].

A description that the nuclei of soot particles are products of a chemical reaction is put forward in [27] and also proposed equations for the rate of formation of nuclei which is expressed by

$$R_{(n,f)} = n_0 + (f - g)n - g_0 \,.\, n \,.\, N \; (part/m^3/s) \tag{3.1.21}$$

where n_0 is the rate of spontaneous formation of radical nuclei from the fuel, *n* is the concentration of radical nuclei, *f* is a linear branching coefficient, *g* is a linear termination coefficient and *N* is the concentration of soot particles (part/m^3). n_0) is expressed by

$$n_0 = a_0 \,.\, C_f \,.exp(\frac{-E}{RT}) \; (part/m^3/s) \tag{3.1.22}$$

where a_0 is a constant, C_f is the mass concentration of fuel (Kg/m^3), *E* is the activation energy, *T* is the absolute temperature and *R* is the universal gas constant, [11].

There are also other sub models that has been utilized in KFX which provide information about source terms of different field variables.

- Pool model - Model of pool spreading including “stair case” model and evaporation model due to flashing, convection and boiling.
- Spray model - Lagrangian model following parcel of droplets with uniform properties.
- Radiation model - The discrete transfer model of Shah and Lockwood, Absorption model etc..
- Wall model for turbulent flow - Dissipation of turbulent kinetic energy adjacent to the wall is found by assuming flat plate theory of turbulent shear force.
- Wall temperature model - Used in radiation model and source term for enthalpy.
- The EDC turbulence combustion model by Magnussen.

3.2 KFX user interface

This section aims to provide users an insight into KFX's user interface, its versatile functionalities, setting up of cases for simulation, selecting which results to log as well as interpreting them.

3.2.1 Getting Started

In windows version, KFX license client is started by clicking KFXstart64 while in Linux version by typing kfxstart on the command line. The newest version KFX Risk and Barrier management can be started by typing kfxrbm in the linux terminal window. The following window shown in Figure 3.3, appears on the screen [2].

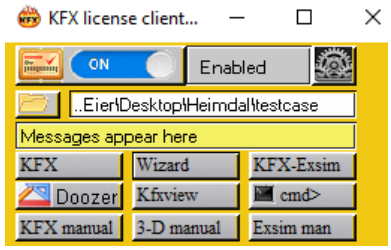

Figure 3.3: KFX licence client with valid license [2].

In addition, a wizard displaying KFX Log messages appears as shown in Figure 3.4, which displays all the messages including license validity and error messages.

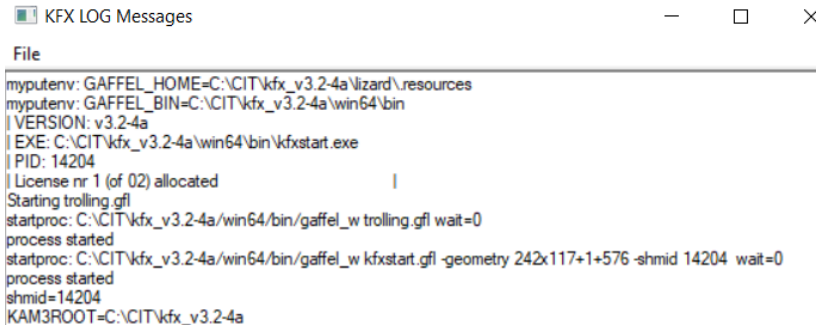

Figure 3.4: KFX licence client messages log [2].

The working directory could be changed by clicking the folder icon on Figure 3.3, which is highly recommended. The nine grey buttons in the lower part of the window are used to start various applications of KFX and the user manuals.

The **KFX** button will open the default KFX user interface as shown in Figure 3.5. The window on the left is the KFX window manager which presents every bit of information required by the user to set up various simulations, choose the desired results to be logged

and also visualize the results as the simulation is running. The window on the right shows the loaded geometrical model in any selected plane incorporated with the chosen grid resolution.

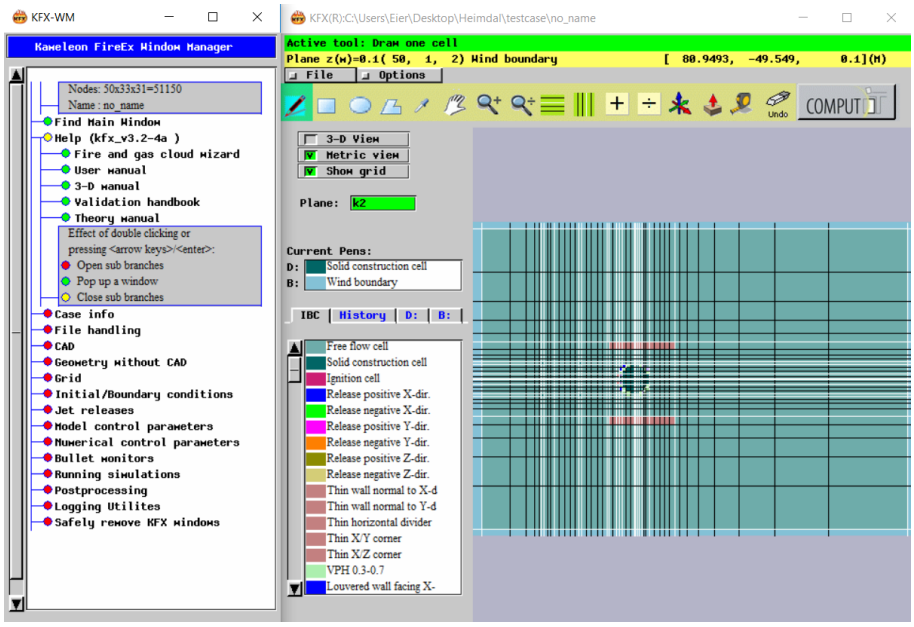

Figure 3.5: Default KFX user interface [2].

The **wizard** button opens up a Fire and Gas cloud simulation wizard. This wizard, simply put, is the easiest and most efficient way to set up a case for running a simulation with optimal input information. As shown in Figure 3.6, this simplistic wizard takes users through different sub-categories namely simulation type, loading or creating geometry file, logging wind and temperature parameters, leak characteristics such as leak rate, hole diameter, reservoir temperature, location of leak etc., composition of fuel, grid data and domain boundaries. The calculate buttons also lets the users calculate the necessary parameters namely Lower Explosive Limit (LEL) and Upper Explosive Limit (UEL), equivalent hole diameter of the leak source, etc.

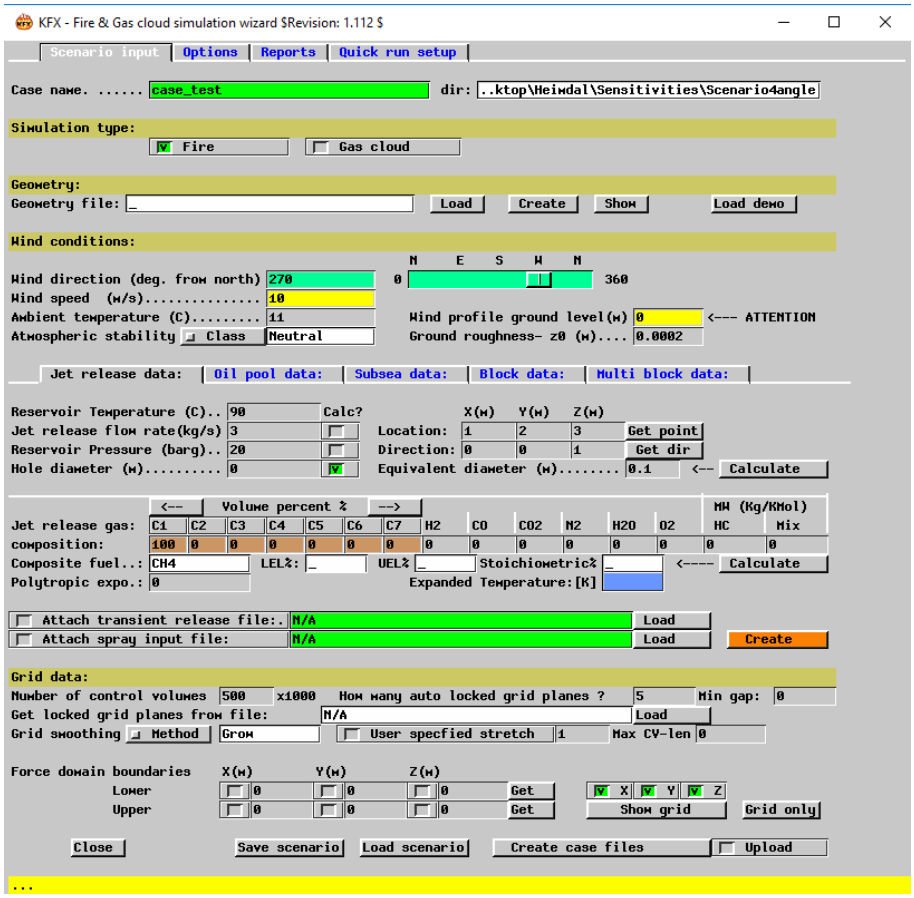

Figure 3.6: KFX Fire and Gas cloud simulation wizard, [2].

The “Options” tab within this wizard presents time scaling and multi block simulation options, which are optional parameters that could define the simulations, as shown in Figure 3.7.

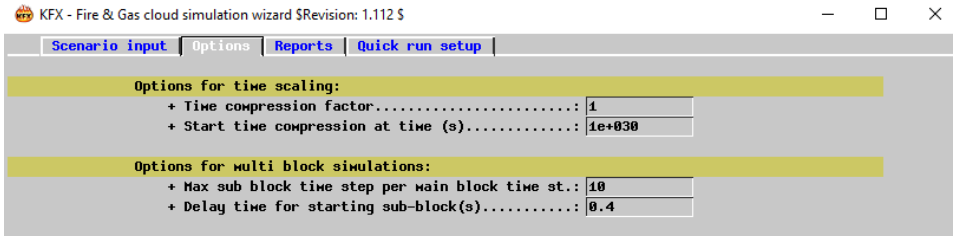

Figure 3.7: KFX Fire and Gas cloud wizard presenting additional options [2].

In the risk and barrier management version of KFX which is KFXRBM, there are some very useful additional input options added to this tab of the Fire and Gas cloud simulation wizard as shown in Figure 3.8. The additional input options enables calculations of transient leak from gas segment or vessel with blow down and Emergency Shut Down (ESD). Some important sensitivities like delays in blow down activation, time taken for ESD valve closure, etc., could be studied from this wizard.

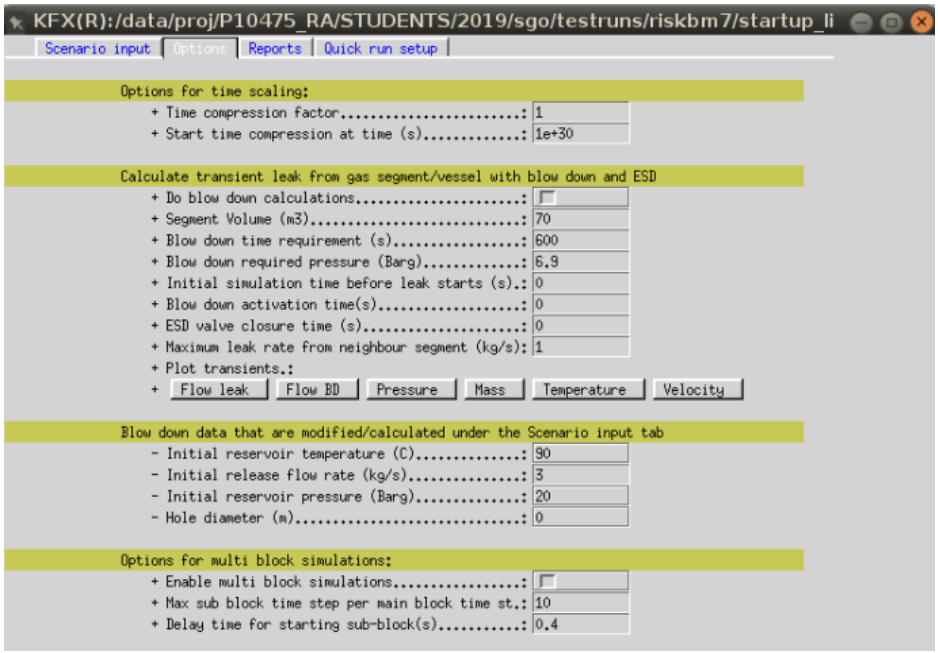

Figure 3.8: KFXRBM Fire and Gas cloud wizard presenting additional options [2].

The “Reports” tab in this wizard presents options that lets the users choose the most interested domain to log results and to select the stop criteria for simulation. The “Quick run setup” tab lets the user choose the various text and visual output files to be logged during the simulation and also to start the simulation. These two tabs are presented in Chapter 4.

The **KFX-Exsim** button opens the user interface for KFX-Exsim, shown in Figure 3.9. The KFX-Exsim explosion simulator can be run from this user interface if the KFX-Exsim license is installed.

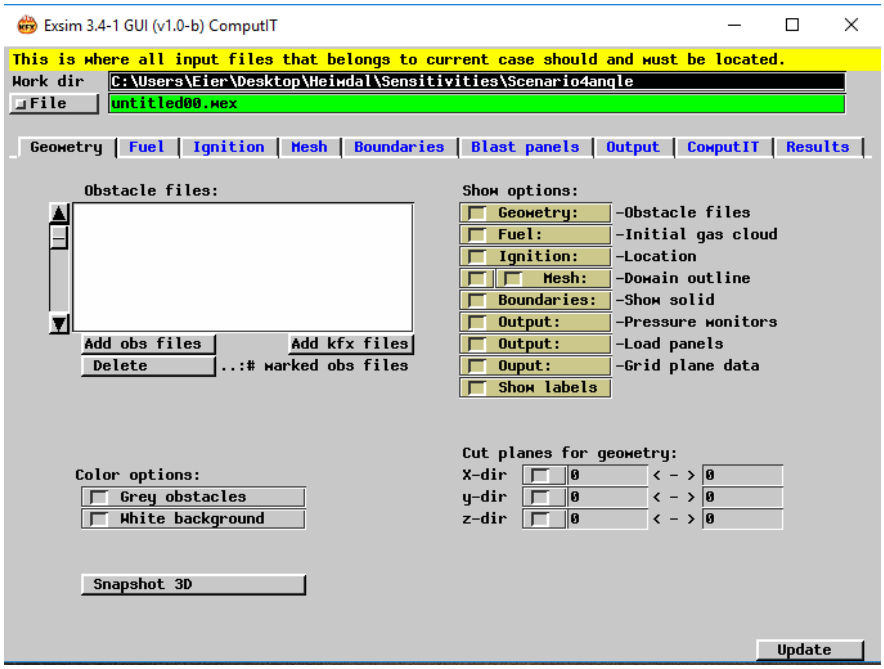

Figure 3.9: KFX Exsim GUI.

The **Doozer** button starts the three dimensional (3D) drawing tool in KFX, as shown in Figure 3.10. Alternatively KFX also allows importing CAD files to create geometrical model files in $.kfx$ format.

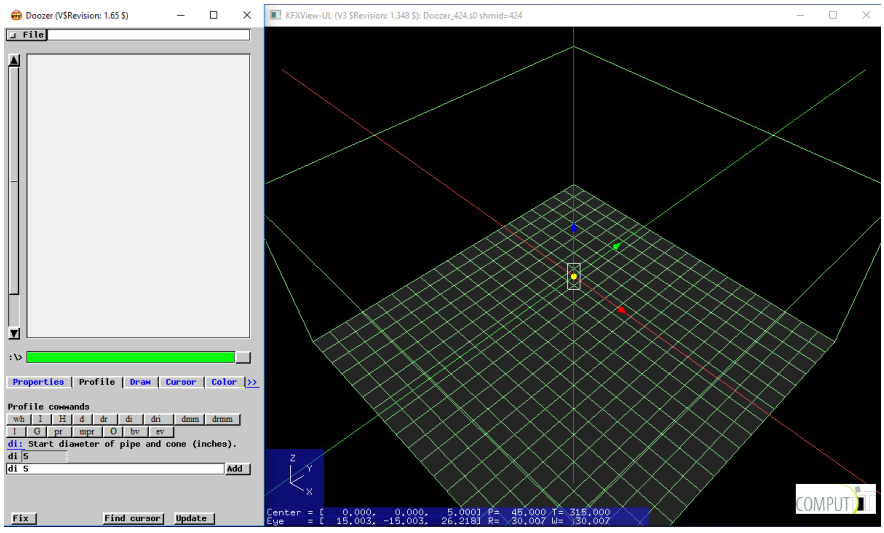

Figure 3.10: KFX Doozer CAD drawing tool [2].

The **Kfxview** button opens the interface for Kfxview, as in Figure 3.11. This interface enables users to load one or several result files along with the geometry file to the wizard. The attached files can be viewed as a 3D visualization by adjusting various contours. The best part of this interface is that it updates the geometrical model with result files simultaneously as the simulation is running.

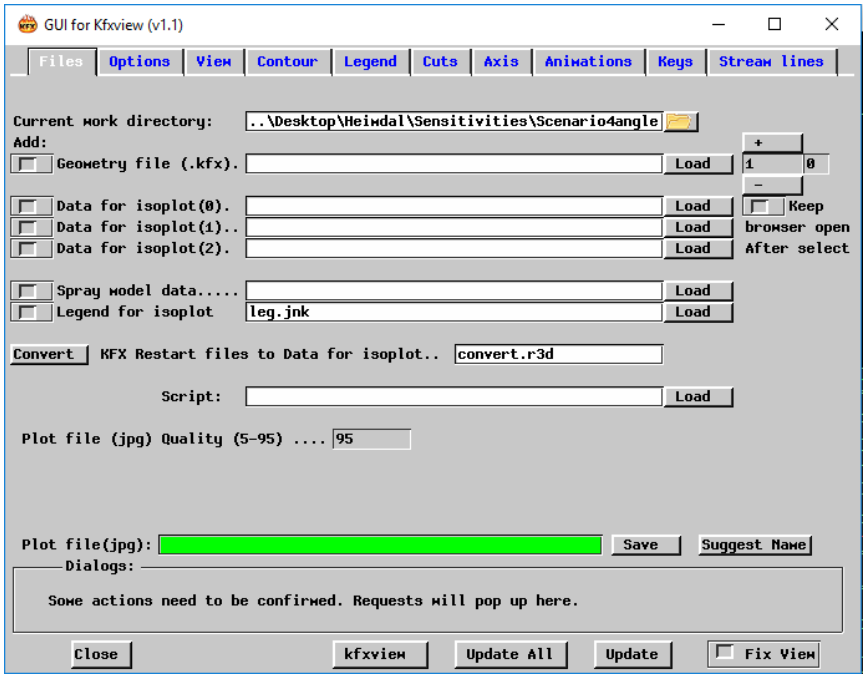

Figure 3.11: KFX View user interface [2].

The **cmd** button will launch a Linux or a Windows terminal window, shown in Figure 3.12, where the users will have access to all KFX command line tools such as *fieldutil*, *bull2flux* and *kfxgrep*. These tools will only be available from a terminal window launched from the KFX license client. The terminal window can also be used to execute any available Linux or Windows commands and applications. The bottom row of buttons opens up the respective user manuals as the name of the button suggests.

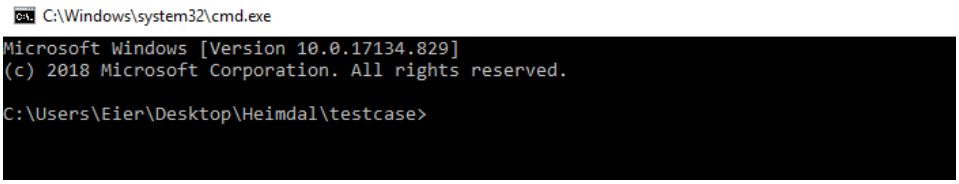

Figure 3.12: KFX Linux terminal window [2].

3.3 Geometrical model

The geometrical model is chosen to be generic and hence it reflects common characteristics exhibited by the most of the installations in the Norwegian Continental Shelf (NCS). The geometrical model is established such that it aids to study the importance of geometrical layout of a module or installation for the estimated fire and explosion risk. For the purpose of this study, one of the generic model established in "Modelling of Ignition Sources for Offshore oil and gas Facilities, (MISOF)" is chosen but with added structural features to make it as practical to a real module as possible [9].

The generic module follows typical size of offshore modules installed at the NCS, ranging from 4,000 to 40,000 gross m^3. The ventilation conditions in terms of openness of peripheral walls represent typical layout found at offshore installations. The main equipment such as piping and structures are built according to typical design [9]. It should be noted that the module studied is this thesis is considered to represent rather unfavorable designs in terms of explosion risk due to poor global ventilation conditions. Therefore, the estimated explosion risk using PLOFAM and MISOF models using KFX is expected to be less for equally sized modules in the North Sea.

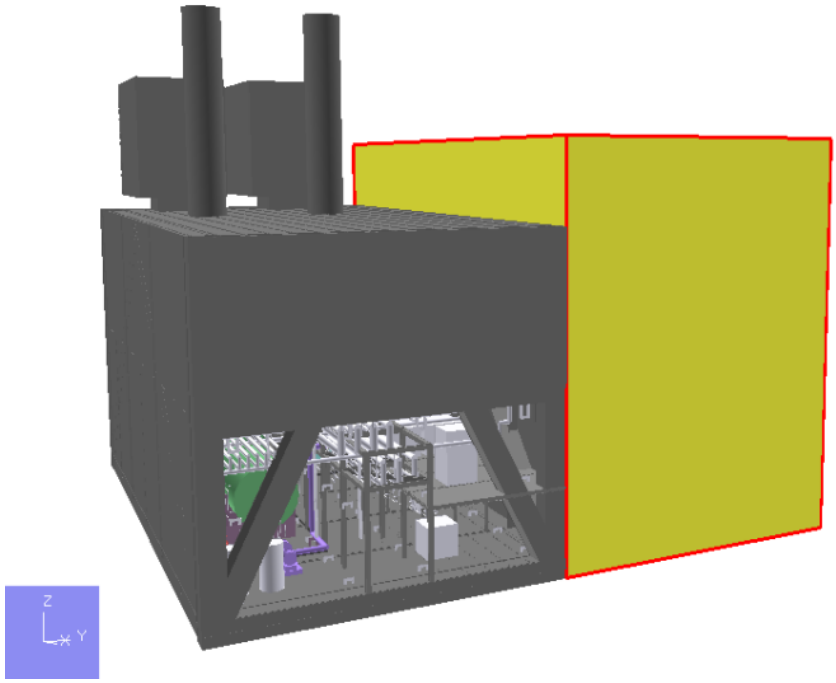

Figure 3.13: Generic geometrical model used in this study

Practically, the module in which work activity is planned would be isolated from the rest of the installation by using isolation valves. Hence any leaks that occur after that would have most of its effect within the isolated module. For instance, personnel exposure at the actual leak site due to local leak is higher than the personnel exposure in a different

location on the installation. This is the reason why choosing small modules over an entire installation for gas/fire dispersion analysis is more reasonably practicable.

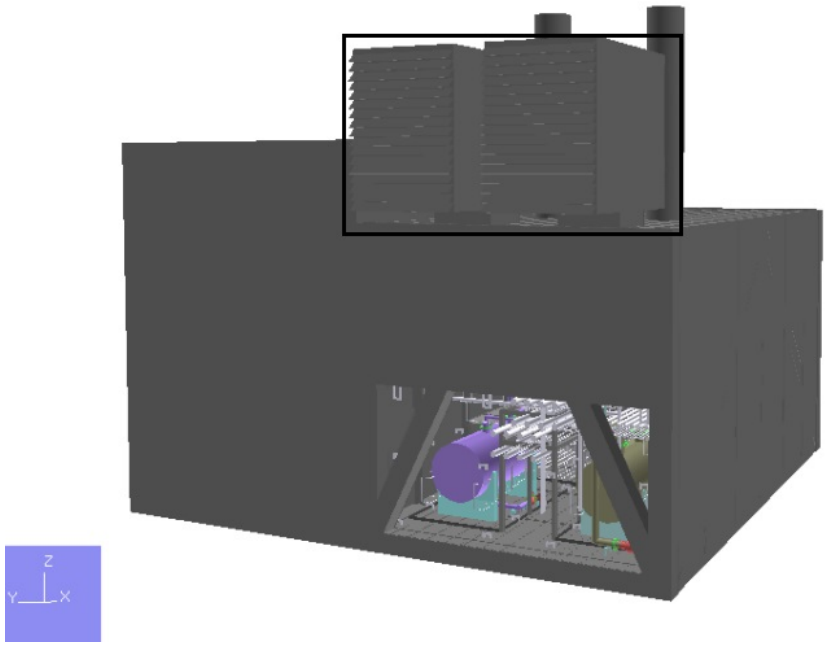

Figure 3.14: Generic geometrical model used in this study

The large solid block seen on the right half in Figure 3.13 and the two turbines on the top right in Figure 3.14 are added features that were not a part of the geometrical model utilized in MISOF study. The east and west walls of the module are open as the positive Y axis points towards North. The module is drawn using KFX and the text file could be converted into different formats.

For the purpose of this study the module has been equipped with 15 Infrared (IR) point type detectors distributed in two levels, with two IR open path line type detectors stretching from the top corner to the bottom corners of East and West open walls diagonally. In addition, the module is also equipped with six ignition sources namely four pumps, one electrical equipment and one classified as generic, to account for hot works, if any.

A file with an extension of ".xml", containing the details of detectors and ignitors is attached to Appendix G, Figures 10.10 and 10.11. It is to be noted that the cited ".xml" file would be used for most of the simulations in this study, unless specified exclusively in the respective sections regarding the changes to the ".xml" file.

Chapter 4

Case study and simulations

This chapter presents some generic and case-specific inputs that are necessary for setting up, executing and extracting results from the simulations. The inputs are based on historic accident statistics and some trends in gas leak accident-parameters in the NCS. Some parameters such as the leak rate, wind speed and wind direction correspond to the typical values from that of the installations in the NCS.

4.1 Generic input parameters

In order to capture the results as accurately as possible, there is a need to have a wide spectre of parametric permutations and combinations. In this way, it would be possible to account for the variations in the smallest worst case scenario to the worst of the worst case scenarios. This would give an overall risk picture that could be used effectively during the design, modification, operation as well as during decommissioning stages of a project, depending on its necessity.

In addition to the generic inputs, each leak scenario will be analysed for six different leak rates, four different wind speeds and two different wind direction. The leak rates start from 0.5 kg/s and multiplies itself by a factor of four till 512 kg/s which would be the largest leak. The wind speeds are chosen as 2, 8, 12 and 18 m/s. The two wind directions are 120 degrees and 315 degrees as they could influence the gas leak through the two open ends of the module. The worst combination of leak rate 512 kg/s and wind speed of 18 m/s is chosen based on one of the accidents that had occurred in the NCS. Therefore every leak scenario would have a combination of six leak rates, first three wind speeds and two wind directions, which makes up 36 cases. In addition, there would be four cases featuring the highest wind speed 18 m/s, which totals to 40 cases per scenario. A summary of the input parameters for the cases that are to be simulated for every leak scenario is presented in Table 4.1.

Leak rates (Kg/s)	Wind speeds (m/s)	Wind direction (degrees)
0.5	2	120
2	8	315
8	12	
32	18 (Rare case)	
128		
512		

Table 4.1: Cases for simulations

4.2 Base case scenario - Pipe failure

In this thesis, the focus is to analyse gas leaks, dispersion and and probability of ignition of the leaked gas. In essence, it focuses on the events occurring before the accidental event in a bow-tie model (i.e the left hand side).

The name "Base case" fundamentally refers to a situation wherein the chosen module is operating in normal circumstances. The normal circumstances in turn means that the barrier systems namely gas detection system and auto triggering emergency shut down systems are functioning normally with 100% functionality and there has been no wind-shielding curtain added to any of the open ends of the module and that any gas leak will be detected immediately without any delays, as shown in Table 2.4.

The chosen scenario is a pipe leak which is located approximately at the centre of the module, shown in Figures 3.13 and 3.14. The coordinates of the gas leak point 15.502, 7.9996, 4.6937 corresponding to X,Y and Z directions respectively will remain the same for base case and sensitivity cases. The fuel composition is decided to be methane and would remain the same throughout this study. Likewise, the parameters such as reservoir temperature (Celsius), reservoir pressure (Barg) and hole diameter (Meters) also would remain the same throughout the course of this study.

Since KFX operates based on the principles of finite volumes, the area of interest would be divided into finite control volumes for the ease of simulations. If the number of control volumes chosen is very less, the rendered results might be inaccurate or rather coarse. On the contrary, a very fine grid resolution would render accurate results but would tremendously increase the simulation time. Hence its always a trade-off when deciding on an optimal grid resolution. A coarser grid resolution, for instance, 50,000 or 75,000, would be suitable when trying to simulate an entire installation for the first time to get an approximation of results. But in cases when one has to simulate a small module or any particular section within a module, a finer resolution could be desirable. For this particular base case, the grid resolution has been chosen to be 200,000. The fire and gas cloud simulation wizard showing the parameters chosen to set up the base case is shown in Figure 4.1.

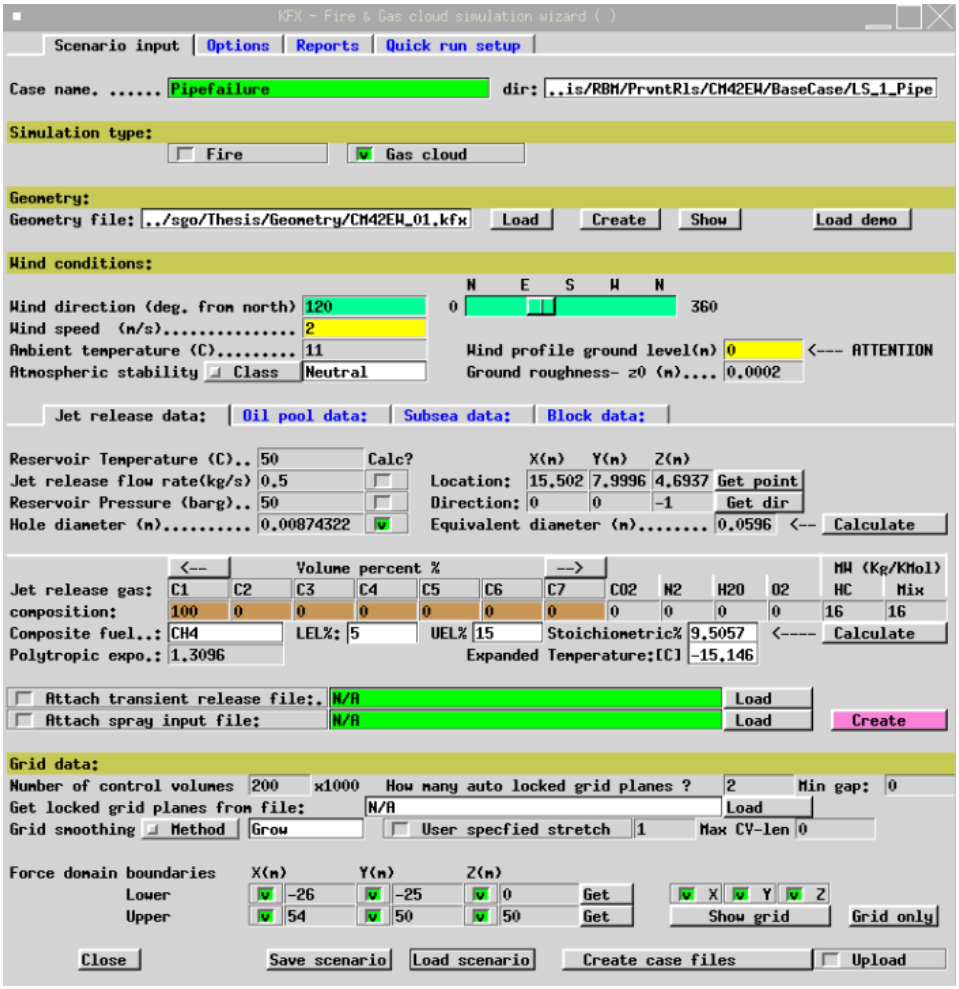

Figure 4.1: Fire and gas cloud simulation wizard for base case set-up

Running a simulation involves creating a scenario file which has an extension of ".scn". The scenario file is created by create case files button in the bottom of the wizard shown in the Figure 4.1. Before creating a scenario file, inputs shall be specified also in the options tab shown in Figure 3.7. The generated scenario file would contain every input specified by the user and more.

In addition to the parameters defined in the fire and gas cloud simulation wizard in Figure 4.1, there are some Risk and Barrier Management (RBM), parameters that are to be defined for the simulations to run. These parameters are defined in such a way that they are aligned with the risk and barrier criteria that the installations are designed for. For example, the installations would have a blow down time requirement and blow down activation time etc. that are to be met. These parameters are explained in detail in the Table 4.4 while the below tables, Table 4.2 and Table 4.3 presents the SCN file parameters.

Parameter	Description	Units	Base case 1_GR2
Case_name	Case name and path to location		/CM42EW_wd120.. ../Pipefailure'
Data_type	Release tab active		'Jet_release_data:'
Tmax	Maximum simulation time	[s]	1,00E+30
Jet_position	Hole location coordinates		(15.5,7.99,4.69)
Jet_direction	Release direction		(0,0,-1)
Res_temperature	Reservoir temperature	[C]	50
Jet_pressure	Jet gauge pressure	[barg]	50
Jet_flowrate	Initial leak rate	[kg/s]	0.5
Jet_gas_components	Released HC vector		('C1')
Jet_gas_composition	Released HC mixture volumetric fraction vector		('100')
Gas_cloud_sim	Simulation type: (0 - Fire) and (1-Gas dispersion)		1
Wind_angle	Clockwise angle from north	[m/s]	120
Wind_10	Wind speed at 10m of altitude	[m/s]	2
Wind_stability	Wind class (Pasquill)		'Neutral'
Wind_Z0	Wind profile at ground level	[m]	0
Ambient_T	Ambient temperature	[C]	11
Wind_roughness	Ground roughness (scale length of the wind profile)	[m]	0.0002
Geometry_file	Path to the geometry file (.kfx extension)		'/data/Geometry/ CM42EW_01.kfx'
Geometry_min	Lower corner coordinates of calculation grid		(-26,-25,0)
Geometry_max	Upper corner coordinates of calculation grid		(54,50,50)
Vol_box_min	Lower corner coordinates of the interested calculation domain		(-1,-0.3,0)
Vol_box_max	Upper corner coordinates of the interested calculation domain		(29,15.7,8)
Stoppro	Criterion to stop simulation when upon the flammable cloud reaching a plateau	[s]	1
Dt_rowcum	Intervals for saving cumulative gas cloud reports	[s]	0.1
Dt_volstop	Stop run criterion based on the size of the cloud	[s]	10000
Time_controls	Time compression factor. The starting time for compression	[s]	(1,1e+30,10,0,0,0,0,0)

Table 4.2: Scenario file parameters - Part 1

Parameter	Description	Base case 1_GR2
Gridpoints	Target number of grid points in calculation domain	200000
Lockedplanes	Number of grid planes locked to the largest parallel surfaces for each direction	2
Spray_file	Spray file attached to the case	'N/A'
Grid_parameters	Data vector for controlling the grid generator	('Grow','N/A',0,1,0,0)
Block_parameters	Data vector for defining a volume with homogeneous grid	(0,0,0,10,10,10, 9999,9999,9999)
Sub_block	Data vector for defining the sub block	(1,4000,1000,0,0, 0,0,0,0)
Pool_parameters	Data vector for controlling the pool formation	('Rectangle',0.01,0, 0.005,373,288,0,1,0,0)
History_points	Text file containing points for history data monitoring	'N/A'
Subsea_parameters	Data vector for controlling sub-sea release	('Gauss',1,1.3,0,0,0,0,0,0)
Rbm	Data vector for the risk and barrier management parameters	('Segment_1',70,790000, 600,0,0,1,1e-005, 0.00235,0,0,1,0,0,0,0)

Table 4.3: Scenario file parameters - Part 2

Parameter	Unit	Rationale
Segment Volume	Cubic meters	The volume of segment / module
Blow down time requirement	Seconds (s)	Time requirement to reach required blow down pressure
Blow down pressure requirement	Barg	The required pressure above ambient to be reached at the specified blow-down time
Initial simulation time before leak starts	Seconds (s)	Time specified to account for steady state ventilation before leak starts
Blow down activation time	Seconds (s)	Time taken for detection until the ESD valves are activated
ESD valve closure time	Seconds (s)	The time it takes from ESD valve activation until it is fully closed
Maximum leak rate from the neighbouring segment	Kilograms per second (kg/s)	The maximum inflow rate from neighbouring segment/s before the ESD is fully activated

Table 4.4: Risk and Barrier Management (RBM) parameters.

The Table 4.5, presents the RBM parameters specified for the base case scenario. The value for immediate ignition probability corresponds to that from MISOF report [9] and the values of other parameters are based on practical real-case scenarios onboard the installations in the NCS.

Parameter	Value	Unit
Segment Volume	100	Cubic meters
Blow down time requirement	900	Seconds
Blow down pressure requirement	790000	Pascal
Initial simulation time before leak starts	0	Seconds
Blow down activation time	2	Seconds
ESD valve closure time	5	Seconds
Maximum in-flow from neighbour segment	20	kg/s
Number of detectors initiating the ESD closure / Blowdown	2	
Immediate ignition probability	0.0023	

Table 4.5: RBM parameters for base case set-up.

The scenario file that has been set-up contains data to run just one case. Hence to account for multiple leak rates, wind speeds and wind directions as shown in Table 4.1, one would imagine that one needs to create the scenario file for each and every combination of leak rate, wind speed and wind direction. This is a time consuming and tedious process of setting up an SCN file containing 40 different cases. Hence, the new version of KFX, i.e., the KFX-RBM, has a feature called power scan that allows the users to create an SCN file containing multiple cases (For example: 200 cases) in a significantly shorter time frame and with less complexity.

4.2.1 Powerscan

Powerscan is a tool for efficient generation of KFX scenarios with parameter variations. It uses a grid generator called *Meshmerize*, and code from the GUI panel in KFX called "Fire & Gas cloud simulation wizard". Powerscan enables the Fire & Gas cloud simulation wizard to save key input for a scenario in a text formatted file that can be edited in a text editor or by some clever scripting. These text files are row/column formatted files where each column has a header containing a keyword that can be interpreted by Powerscan, and each row represents a scenario. Scenario variation can then be made by just copying a scenario line and change only the parameters that are varied for each scenario [2].

For the base case, since there are 40 individual cases to be created, the first case which was created using the fire and gas cloud simulation wizard was copied 39 more times. Since dealing with such numerically complex file could be error-prone, a unique naming system was formulated to avoid any confusions. The naming system also facilitates easy identification of case files which will be dumped categorically in unique folders with the folder names corresponding to the case names upon running a powerscan. Figure 4.2 depicts the naming system of a completed scenario file with an extension ".scn", for the base case of a pipe failure scenario.

```
                    #Case_name                    data_type           tmax
 './CM42EW_bc_ls1_gr2_q0.5_ws02_wd120/Pipefailure' 'Jet_release_data:' 1e+30
'./CM42EW_ls1_gr2_q0.5_ws08_wd120/Pipefailure' 'Jet_release_data:' 1e+30
'./CM42EW_ls1_gr2_q0.5_ws12_wd120/Pipefailure' 'Jet_release_data:' 1e+30
'./CM42EW_ls1_gr2_q0.5_ws02_wd315/Pipefailure' 'Jet_release_data:' 1e+30
'./CM42EW_ls1_gr2_q0.5_ws08_wd315/Pipefailure' 'Jet_release_data:' 1e+30
'./CM42EW_ls1_gr2_q0.5_ws12_wd315/Pipefailure' 'Jet_release_data:' 1e+30
'./CM42EW_ls1_gr2_q02_ws02_wd120/Pipefailure' 'Jet_release_data:' 1e+30
'./CM42EW_ls1_gr2_q02_ws08_wd120/Pipefailure' 'Jet_release_data:' 1e+30
'./CM42EW_ls1_gr2_q02_ws12_wd120/Pipefailure' 'Jet_release_data:' 1e+30
'./CM42EW_ls1_gr2_q02_ws02_wd315/Pipefailure' 'Jet_release_data:' 1e+30
'./CM42EW_ls1_gr2_q02_ws08_wd315/Pipefailure' 'Jet_release_data:' 1e+30
'./CM42EW_ls1_gr2_q02_ws12_wd315/Pipefailure' 'Jet_release_data:' 1e+30
'./CM42EW_ls1_gr2_q08_ws02_wd120/Pipefailure' 'Jet_release_data:' 1e+30
'./CM42EW_ls1_gr2_q08_ws08_wd120/Pipefailure' 'Jet_release_data:' 1e+30
'./CM42EW_ls1_gr2_q08_ws12_wd120/Pipefailure' 'Jet_release_data:' 1e+30
'./CM42EW_ls1_gr2_q08_ws02_wd315/Pipefailure' 'Jet_release_data:' 1e+30
'./CM42EW_ls1_gr2_q08_ws08_wd315/Pipefailure' 'Jet_release_data:' 1e+30
'./CM42EW_ls1_gr2_q08_ws12_wd315/Pipefailure' 'Jet_release_data:' 1e+30
'./CM42EW_ls1_gr2_q32_ws02_wd120/Pipefailure' 'Jet_release_data:' 1e+30
'./CM42EW_ls1_gr2_q32_ws08_wd120/Pipefailure' 'Jet_release_data:' 1e+30
'./CM42EW_ls1_gr2_q32_ws12_wd120/Pipefailure' 'Jet_release_data:' 1e+30
'./CM42EW_ls1_gr2_q32_ws02_wd315/Pipefailure' 'Jet_release_data:' 1e+30
'./CM42EW_ls1_gr2_q32_ws08_wd315/Pipefailure' 'Jet_release_data:' 1e+30
'./CM42EW_ls1_gr2_q32_ws12_wd315/Pipefailure' 'Jet_release_data:' 1e+30
'./CM42EW_ls1_gr2_q128_ws02_wd120/Pipefailure' 'Jet_release_data:' 1e+30
'./CM42EW_ls1_gr2_q128_ws08_wd120/Pipefailure' 'Jet_release_data:' 1e+30
'./CM42EW_ls1_gr2_q128_ws12_wd120/Pipefailure' 'Jet_release_data:' 1e+30
'./CM42EW_ls1_gr2_q128_ws02_wd315/Pipefailure' 'Jet_release_data:' 1e+30
'./CM42EW_ls1_gr2_q128_ws08_wd315/Pipefailure' 'Jet_release_data:' 1e+30
'./CM42EW_ls1_gr2_q128_ws16_wd315/Pipefailure' 'Jet_release_data:' 1e+30
'./CM42EW_ls1_gr2_q512_ws02_wd120/Pipefailure' 'Jet_release_data:' 1e+30
'./CM42EW_ls1_gr2_q512_ws08_wd120/Pipefailure' 'Jet_release_data:' 1e+30
'./CM42EW_ls1_gr2_q512_ws12_wd120/Pipefailure' 'Jet_release_data:' 1e+30
'./CM42EW_ls1_gr2_q512_ws02_wd315/Pipefailure' 'Jet_release_data:' 1e+30
'./CM42EW_ls1_gr2_q512_ws08_wd315/Pipefailure' 'Jet_release_data:' 1e+30
'./CM42EW_ls1_gr2_q512_ws12_wd315/Pipefailure' 'Jet_release_data:' 1e+30
'./CM42EW_ls1_gr2_q0.5_ws18_wd120/Pipefailure' 'Jet_release_data:' 1e+30
'./CM42EW_ls1_gr2_q0.5_ws18_wd315/Pipefailure' 'Jet_release_data:' 1e+30
'./CM42EW_ls1_gr2_q512_ws18_wd120/Pipefailure' 'Jet_release_data:' 1e+30
'./CM42EW_ls1_gr2_q512_ws18_wd315/Pipefailure' 'Jet_release_data:' 1e+30
```

Figure 4.2: Naming system of a completed (.scn) file of the base case scenario.

In the naming system shown in Figure 4.2, CM42EW is the name of the module used in this study. The other short forms are ls = leak scenario, gr = grid resolution (gr2 = grid resolution 200000), q = initial leak rate, ws = wind speed, wd = wind direction. The ".scn" file for the base case is named as *Pipefailure.scn*. A detailed *"Pipefailure.scn"* file for the base case scenario is attached to the Appendix E, Table 10.11.

The scenario input files are generated by using the command *"powerscan"* in the terminal window launched by clicking the cmd button in the KFX license client. In this

case, the command would be *" powerscan Pipefailure.scn"*. Powerscan generates a sub-directory for each case that is specified on the *Pipefailure.scn* file, as shown in Figure 4.3. The auto-generated scenario files can be loaded into and run from the KFX GUI. Note that each sub-directory will also be supplied with shell scripts for running the scenario in batch, and for stopping the simulation.

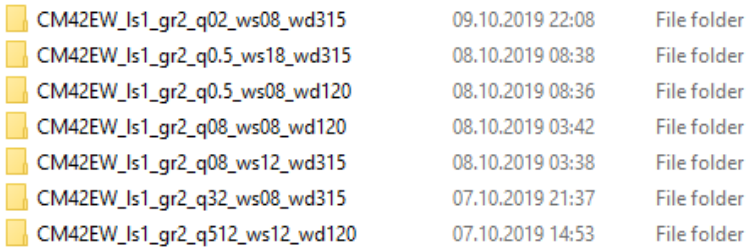

Figure 4.3: Directories created upon running powerscan.

Upon a successful powerscan, the simulations could be started from the GUI as mentioned above. The user could start the simulations either case by case which would be time consuming. Instead, the users could also send all the cases for simulation at once. This is done by writing a short script which would enable KFX to accept and queue multiple cases for simulation as shown in Figure 4.4. This reduces time and efforts significantly while running huge number of cases simultaneously.

```
universe = vanilla
executable = /usr/local/bin/runkfx_rbm

transfer_executable = False

requirements = HAS_KFXRBM == True

error = kfx.error
log = kfx.log
output = kfx.out

environment = "KAM3ROOT=/opt/computit/kfx_pakke_test"

Concurrency_Limits = FURCIFER

Initialdir = /data/proj/P10475_RA/STUDENTS/2019/sgo/Thesis/RBM/PrvntRls/
CM42EW/BaseCase/LS_1_Pipe/Saikrishna/CM42EW_ls1_gr2_q02_ws12_wd120
arguments = Pipefailure
Queue

Initialdir = /data/proj/P10475_RA/STUDENTS/2019/sgo/Thesis/RBM/PrvntRls/
CM42EW/BaseCase/LS_1_Pipe/Saikrishna/CM42EW_ls1_gr2_q32_ws12_wd315
arguments = Pipefailure
Queue
```

Figure 4.4: Script to submit multiple cases to the cluster for simulation.

Once submitted to the cluster, the queue could be monitored as to which of the simulations are running and those that are idle and waiting to be run. The python scripts used to run number of simulations simultaneously are attached to the Appendix D, Figure 10.3.

The base case simulations were completed in 15 days. Once all the cases in the scenario file have been simulated, the ignition probability window, which is a unique feature in KFX-RBM version shall be opened from the cmd window by typing the command *"gfl ignprob"*. This opens the following window shown in Figure 4.5.

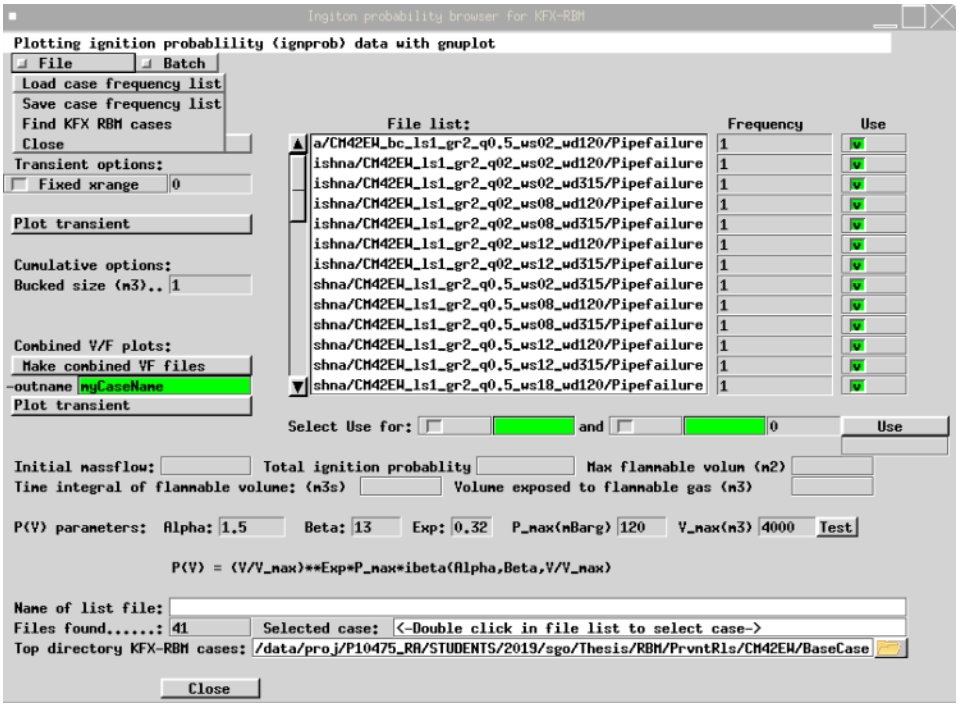

Figure 4.5: Ignition probability browser for KFX-RBM.

In the above wizard, the option " Find KFX RBM cases" from the file menu loads all the cases that have been simulated, along with a value in the respective frequency columns. This has to be extracted by choosing "Save case frequency list" from file menu for post processing.

The PLOFAM leak frequency model forms the basis for the loss of containment model, [9] [8]. The approximations allow for effective estimation of the distribution of a given total leak frequency for the chosen module. The complementary cumulative leak frequency fraction distribution, denoted *A (Q)*, is approximated by the following function:

$$A(Q) = C * Q^{-k} \tag{4.2.1}$$

where Q is the leak rate, C and K are PLOFAM constants. The parameter values for *C* and

K can be found from Table 4.6. Values of C are given by K requiring that the distribution is continuous and starts at 1.0 for Q = 0.1 Kg/s [9].

$$C_{0.1-1} = \frac{1}{0.1^{-0.5}} \tag{4.2.2}$$

which also applies for Q $>$ 1 kg/s as the distribution must be continuous

$$C_{>1} = \frac{C_{0.1-1} * 1^{-0.5}}{1^{-0.7}} \tag{4.2.3}$$

	PLOFAM
K	For Q <= 1 kg/s : -0.50 For Q >1 kg/s : -0.70
C	For Q 1 kg/s: 0.3162 For Q >1 kg/s: 0.3162

Table 4.6: Parameters for approximate leak frequency model [9].

In order to identify the frequencies associated with each case shown in the Figure 4.5, it is necessary to identify the total leak frequency of the module CM42EW. This is given by the product of the volume of the module (30 * 15.9 * 8.25 m^3) and the value for total ignition probability specified in the MISOF report, 4.7*E-6 [9].

The value of A(Q) is derived as explained above and frequency values for each leak rate specified is arrived by multiplying A(Q) with the total leak frequency of the module. These values are then categorically sorted to find the frequency value for each chosen leak rate presented in Table 4.1. This gives us six different frequency figures corresponding to each leak rate. These values are then divided by the number of cases with that particular leak rate in order to arrive at the final frequency value for each and every case that could be substituted in the previously saved "Case frequency list" which could in turn be imported into the frequency column of the RBM cases as shown in Figure 4.6.

The loaded case frequency list is then used to generate plot files which enables to view various result plots including all cases. The option named "Make combined VF files" is activated to generate plot files combining all 40 scenarios in the base case. This bit of post processing to generate result plots has to be carried out for each scenario but this is explained only for the "Base case scenario". A spreadsheet depicting post processing calculations is attached to Appendix F, Figure 10.9.

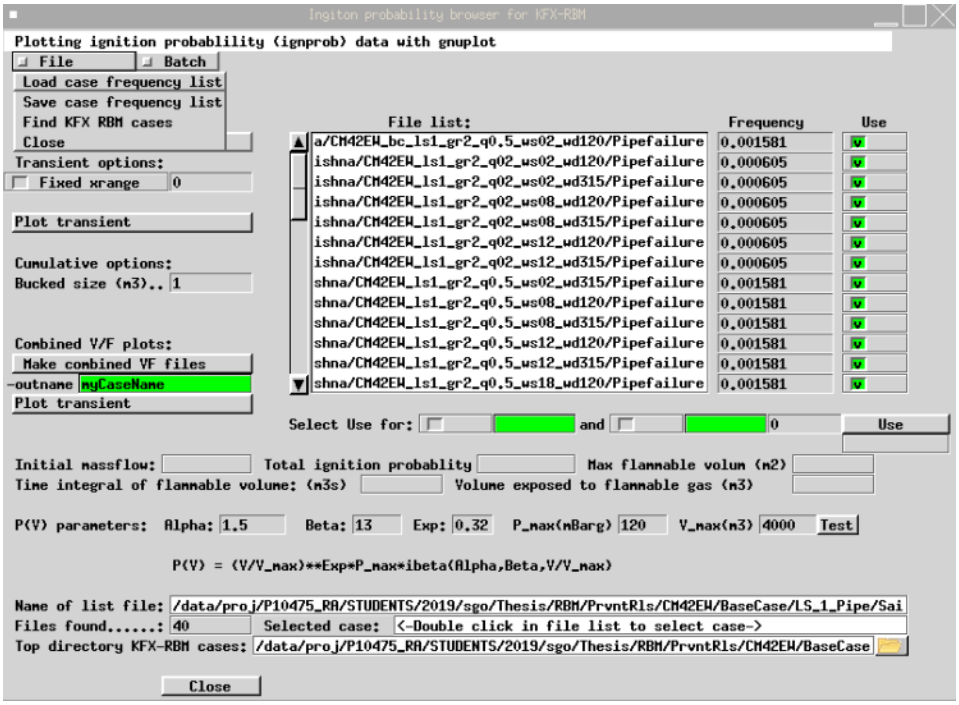

Figure 4.6: Ignition probability wizard with updated case frequency list.

4.2.2 Results

The KFX-RBM feature calculates the ignition probability per control volume in the domain per ignition mechanism and per equipment type. For the generic ignition sources, results can be divided according to any volumetric representations put into the module [9] [8].

It is important to note that the probability distributions generated here are based on a limited number of scenarios (i.e., leak scenarios). Few hundred scenarios are a few too less to give an accurate prediction of probability distributions for the chosen module. This study has been conducted with a representative set of scenarios with few most practically reasonable leak rates, wind speeds and wind directions. In other words, if the simulations were to be re-run with the same module but with higher number of scenarios including even wider combinations of leak rates, wind speeds and wind directions, the chances are that the results could depict either higher or lower ignition probabilities [9].

Contribution from continuous vs discrete sources

This result depicts the frequency distributions per module per ignition mechanism in the MISOF model. The results shows that the contribution from continuous sources were higher initially till the gas cloud volume reached 500 cubic meters. Beyond that the contribution from discrete sources has been dominant as shown in Figure 4.7. This could be

due to the poor ventilation in the module and hence has caused a prolonged exposure to potential sources of ignition compared to contribution from continuous sources.

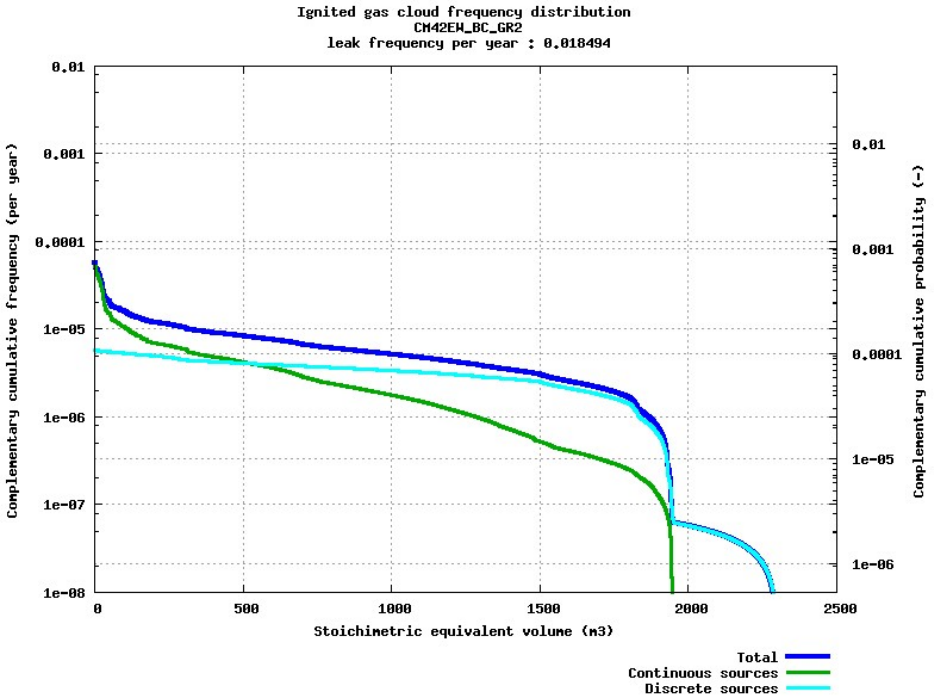

Figure 4.7: Complementary cumulative frequency distribution for stoichiometric cloud.

Ignition time

Figure 4.8 presents the frequency distributions with respect to the ignition time. The results depict that the ignition tend to occur before 1 minute after the start of the leak when the contribution from the continuous sources are highest. After approximately a minute, the discrete sources seem dominant.

The reason for this, as explained in the MISOF report is that the continuous ignition mechanisms are the dominant idealisation of ignition mechanisms in the MISOF model. The continuous ignition mechanism is materialized upon first time exposure, and the effect of the safety functions is relatively small within the initial half a minute or so. It is hard to find basis for the ignition time. The statistical basis for the MISOF model indicates that ignitions take place rather early [9].

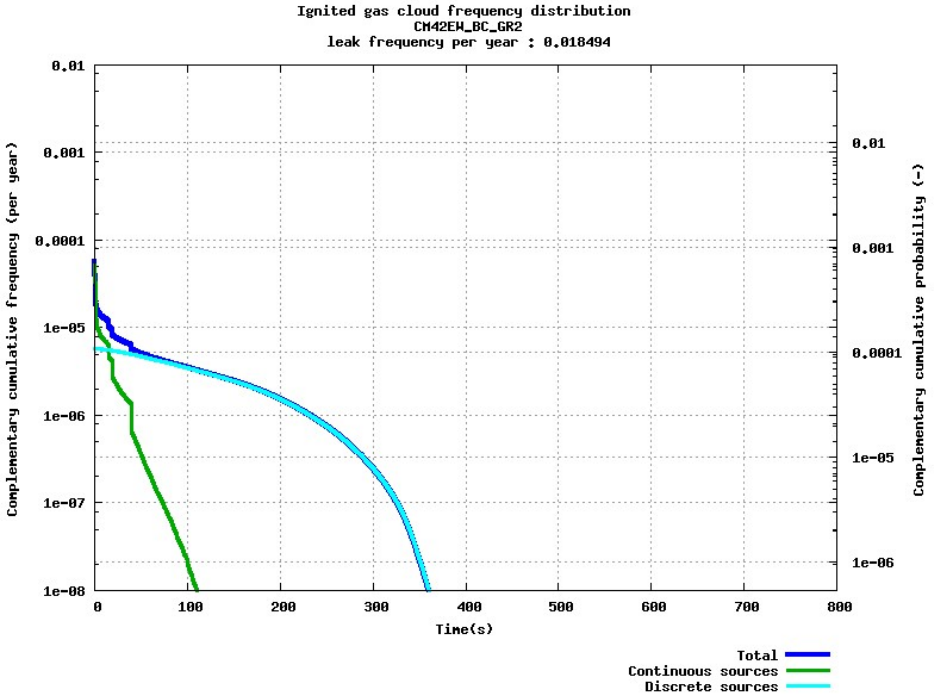

Figure 4.8: Complementary cumulative frequency distribution for time of ignition of stoichiometric equivalent gas cloud.

Pressure frequency distribution

In the MISOF model, the complementary cumulative distribution for the dimensioning explosion pressure (mbarg) is obtained by combining the relevant complementary cumulative distribution for the ignited stoichiometric equivalent gas cloud with the Equation 4.2.4. The dimensioning pressure in this context is considered to be the global pressure acting on walls and decks in the module [9].

$$P_{ExDim}(V) \;=\; P_{max} \;*\; \left(\frac{v}{v_{max}}\right)^{m} \;*\; B(V,\alpha,\beta) \tag{4.2.4}$$

where B(V, α, β) is the regularized incomplete beta function, which is a cumulative probability distribution [9]. Figure 4.9 shows that the complementary cumulative frequency is approximately of the order between 10^{-4} and 10^{-5} during the start of the leak and decreasing henceforth. Therefore, explosions are not a dimensioning event for the module in this study. This aligns well with the MISOF study. Figure 4.10 presents frequency vs flammable cloud plot. Contribution from continuous sources seem dominant till 800 cu.m. volume, thereafter discrete sources dominate

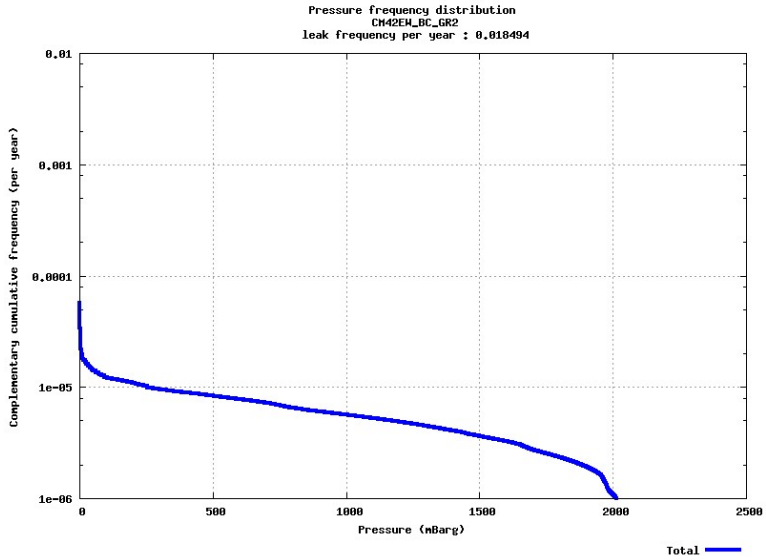

Figure 4.9: Complementary cumulative frequency distribution for dimensioning explosion load.

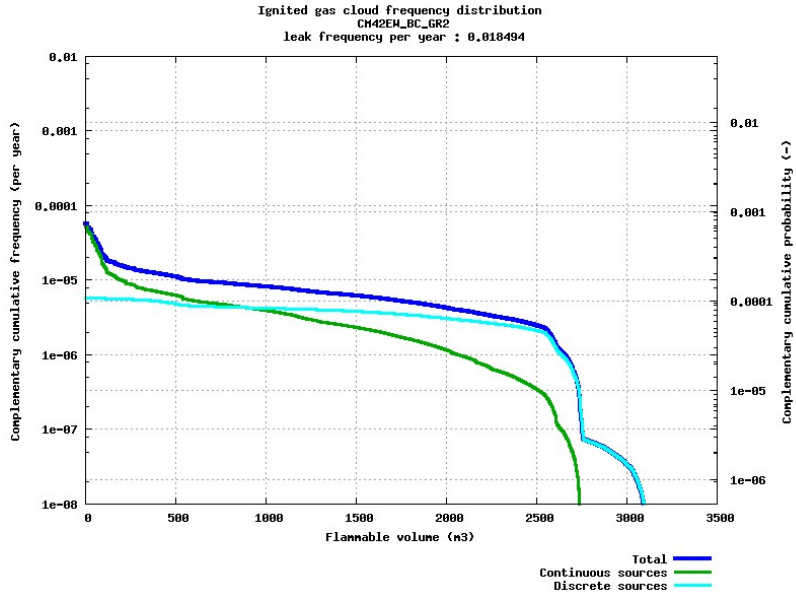

Figure 4.10: Complementary cumulative frequency distribution for flammable gas cloud.

The following chapter presents the results of re-simulated base case with different grid resolutions carried out to save simulation time without affecting the result quality.

Chapter 5

Grid optimisation

This objective of this chapter is to present and analyse the results of a sub-study which was performed to identify the optimal number of grids cells sufficient enough to produce reasonably good quality results in a shortest time possible.

KFX simulations operate based on the principles of finite volumes, as explained in Section 4.2. In general, higher the number of grids, the higher the quality of the results since the grids are distributed finely. However, this requires enormous simulation time considering the fact that each case contains at least 34 scenarios in this study. Therefore the challenge is to find the optimal number of grids for the chosen module such that the simulations does not take longer time and at the same time the quality of the results are not compromised. Since the base case simulations presented in the previous chapter took 12 days to run 40 scenarios, there arose a strong desire to reduce the simulation time in order to finish this study within the specified deadline.

This can be achieved in two ways. The first way is to decrease the number of grid points. These are essentially the boundary points of the finite number of control volumes, which was 200000 for the base case. The second way is by increasing the Courant number to a maximum.

5.1 Jet grid smoothing algorithm

There are various options available for modeling of the grid around the release point. The "Grow" option was selected in as basis for the simulations executed. The "Grow" option models the release using a single release cell. This makes the simulation more efficient, but results in a relatively poor resolution of the gas cloud concentration gradients as the transient leak rate decreases. This is because the grid is optimized for the initial leak rate, and in the late phase of the leak it could results in significant deviations due to numerical diffusion.

An alternative option has been developed which is denoted as "Ring9". This resolves the release by 9 grid cells. This alternative option helps to mitigate deviations due to

numerical diffusion, but would be more costly in terms of Central Processing Unit (CPU) hours.

Therefore, due to time constraints in terms of available CPU hours in the project, "Grow" was selected as the basis. It is judged that the potential deviations due to the smoothing algorithm only has limited effect on the conclusions in the study. All simulations are based on the same set up and the relative effects of the changes in barrier properties are not expected to be affected much. However, the effect of the smoothing algorithm should be investigated more systematically to understand how to select algorithm's weighting precision with respect to the use of CPU hours.

5.2 The Time steps

KFX has a feature called the time step generators and the purpose of that wizard is to calculate time steps that gives stability and accuracy in the time developments in the fire and gas dispersion simulations. The most important aspect of time accuracy is conservation of mass, energy, species and elements [2] [10].

Typically in explicit codes, the Courant number criterion is used to estimate stable time steps. This criteria ensures that no fluid particle entering the control volume travels longer than the length of the control volume multiplied by the specified Courant number, during one time step.

Courant number

The Courant number is a non-dimensional parameter widely used in CFD and its applications. Simply put, the Courant number describes how fast the information is allowed to propagate in the system. It is defined as:

$$C = \left| \frac{\vec{u} \triangle t}{\triangle x} \right| \tag{5.2.1}$$

It has been documented that too large time steps leads to loss of transient conservation. In explicit codes the Courant number shall not be greater than unity. But for an implicit code such as KFX, the Courant number can be larger than unity. According to KFX manual [2], the initial Courant number can be increased if a quicker starts are desired with a safe value being between 5 and 10.

The *'Maximum Courant number'* is another way of specifying the level of accuracy desired. This would then be followed by a *'Courant number increase factor'*, which governs the maximum permitted change in the Courant number from one time step to the next. If increasing the time step quickly is desired, this number can be increased to a value of 1.5 or perhaps even 2. If high time accuracy is desired, the Courant number increase factor should be set at 1.05. KFX allows to set and change these parameters from the wizard shown in Figure 5.1.

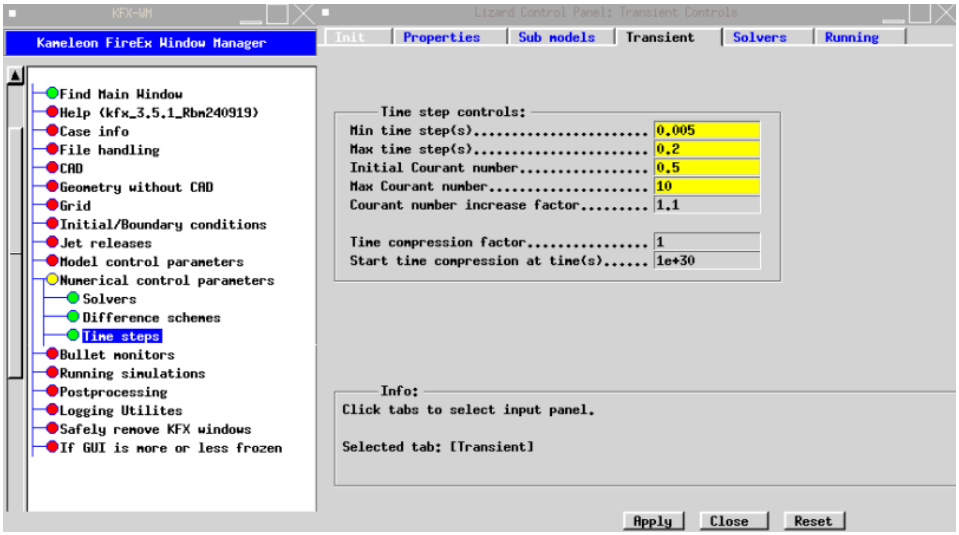

Figure 5.1: The KFX Transient panel.

5.3 Re-simulating base case

In order to reduce simulation time, experiments were carried out by reducing the grid resolutions to 125000 and 75000 and by increasing the Courant number. With the remaining parameters staying constant, the exact set of simulations were subjected to a re-run to compare the accuracy of the results and to explore the possibly to save some simulation running time.

Table 5.1 presents the modified parameters used to identify the optimal grid resolution for this study. The Courant number "Max" is an option in KFX which lets the simulations to be run at a Courant number of 15, but the code will adjust this parameter automatically if a smaller Courant number is required for accurate results.

Case name	Grid resolution	Courant number	Number of scenarios
Base case	200000	10	40
Base case - Re-run 1	125000	15 (Max)	34
Base case - Re-run 2	75000	15 (Max)	34

Table 5.1: Case set-up parameters to identify optimal grid resolution.

5.4 Grid resolution - 125000 and Courant number - Max

This section presents the results of re-simulation of base case with a grid resolution of 125000 and a maximum courant number of 15. There was a significant reduction in the simulation time from 12 days for grid 200000 to 3 days in this case.

Contribution from continuous vs discrete sources

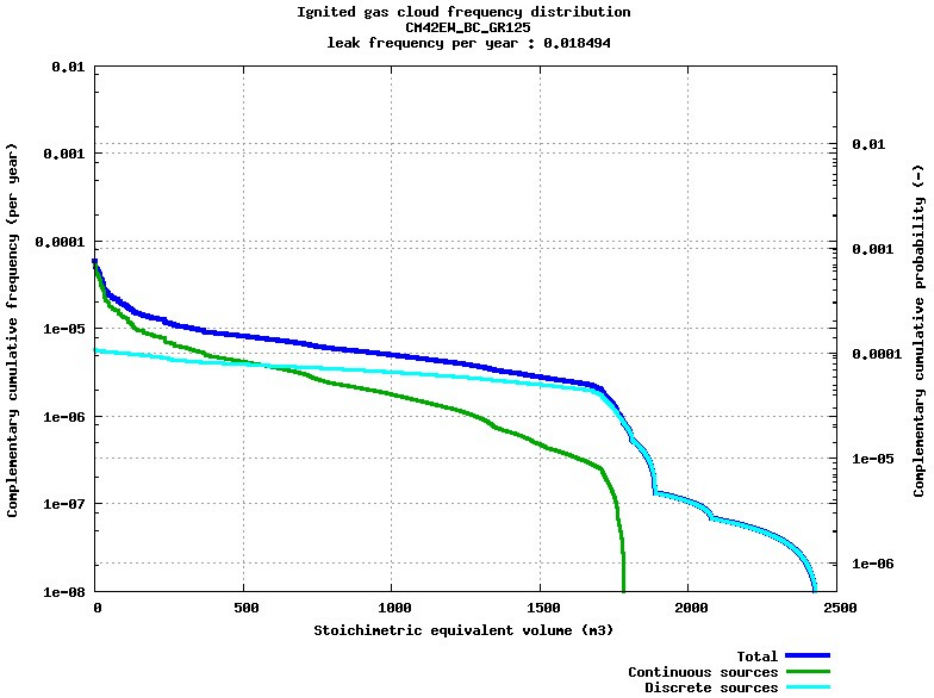

Figure 5.2: Complementary cumulative frequency distribution for stoichiometric equivalent gas cloud for grid resolution 125000.

Figure 5.2 depicts that the contribution from continuous sources were higher initially till the gas cloud volume decreases to approximately 550 cubic meters where the contribution from discrete sources begin to take over. Contribution from continuous sources decreases gradually and reaches a negligible frequency when the cloud volume is approximately 1750 cubic meters.

On the other hand, the contribution from discrete sources shows a prolonged exposure to ignition sources which could be attributed to poor ventilation in the module. There seems to be no significant changes in comparison to the plot with grid resolution 200000 presented in Figure 4.7.

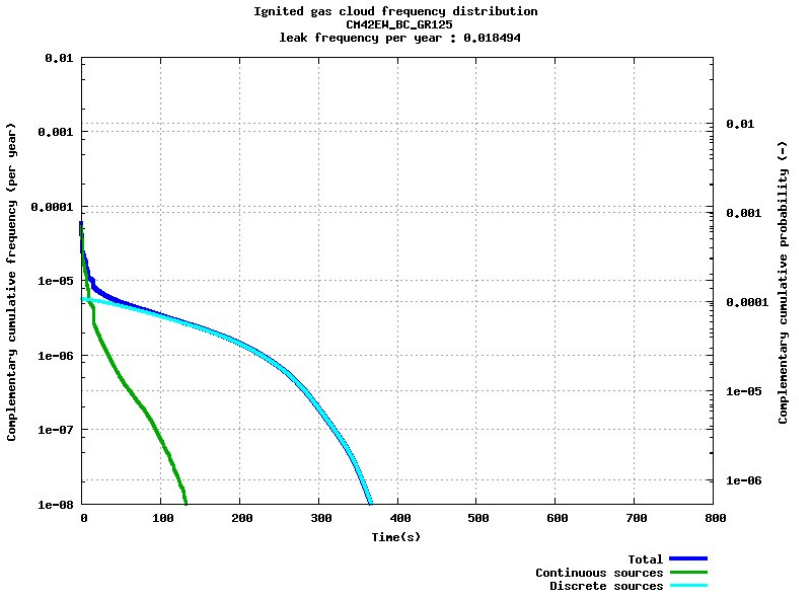

Figure 5.3: Cumulative frequency distribution for time of ignition of stoichiometric equivalent cloud for grid resolution 125000.

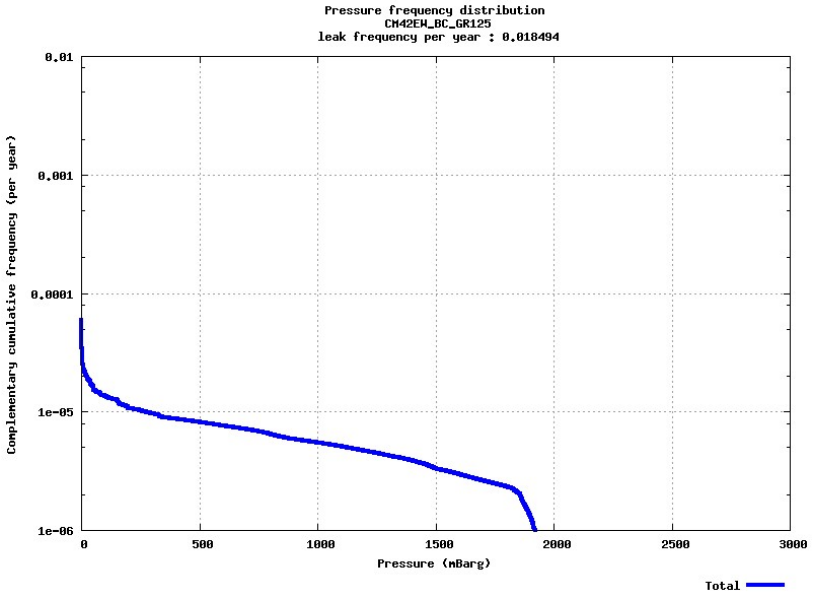

Figure 5.4: Complementary cumulative frequency distribution for dimensioning explosion load for grid resolution 125000.

The plot shown in Figure 5.3 is almost identical to that in Figure 4.8. Ignition could occur within half a minute from the start of release but the probability of it occurring is very low. Here again, the discrete sources contribute to a prolonged exposure but the probabilities are very low. Figure 5.4 depicts that the initial frequency is of the order between 10^{-4} and 10^{-5} and therefore eliminating the possibilities of any explosions.

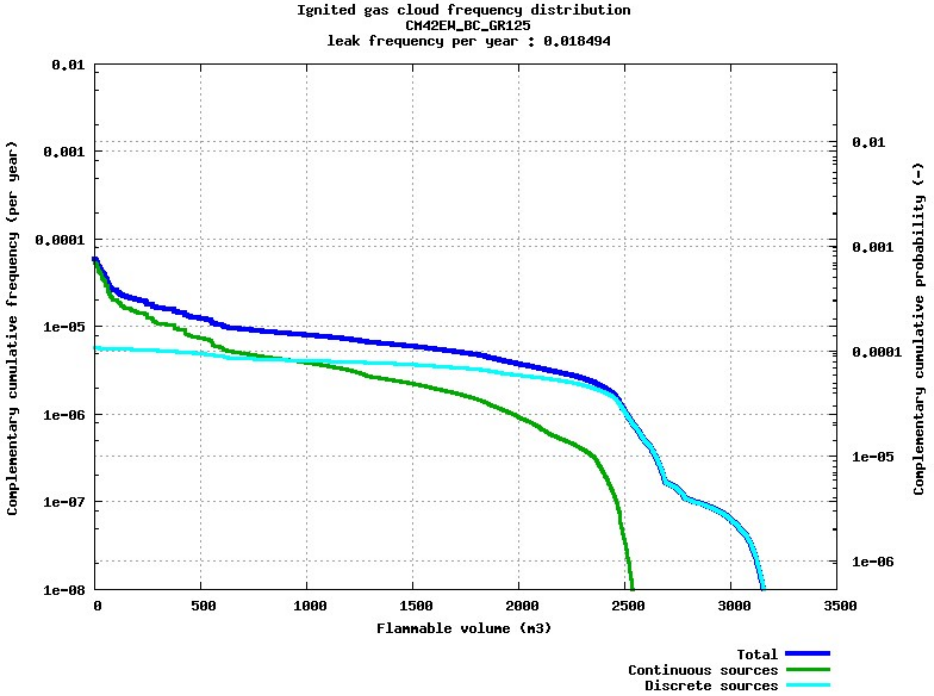

Figure 5.5: Complementary cumulative frequency distribution for flammable gas cloud for grid resolution 125000.

The flammable cloud plot shown in Figure 5.5 is almost identical to that shown in Figure 4.10. Although the discrete sources contribute to a prolonged exposure, the probabilities are insignificant.

5.5 Grid resolution - 75000 and Courant number - Max

This section presents the results of re-simulation of base case with a grid resolution of 75000 and a maximum courant number, 15. The simulation time was further reduces to 1.5 days in this case, in comparison to 3 days with a grid resolution of 125000. Although the reduction in simulation time seem convincing, the accuracy of result plots is questionable.

In general, the results of this simulation had significant deviations in comparison to results with grid resolutions 125000 and 200000. The Figure 5.6 shows an increase in the cumulative frequency immediately after the release started. This seems similar with continuous as well as discrete sources. Unlike the former cases where the contribution from continuous sources seemed dominant till the cloud reached approximately 500 to 550 m^3, this case depicts a prolonged contribution from continuous sources till the cloud reaches a volume of 1000 m^3 and falls rapidly thereafter. Then, the contribution from discrete sources seems to have a prolonged contribution despite with negligible frequencies.

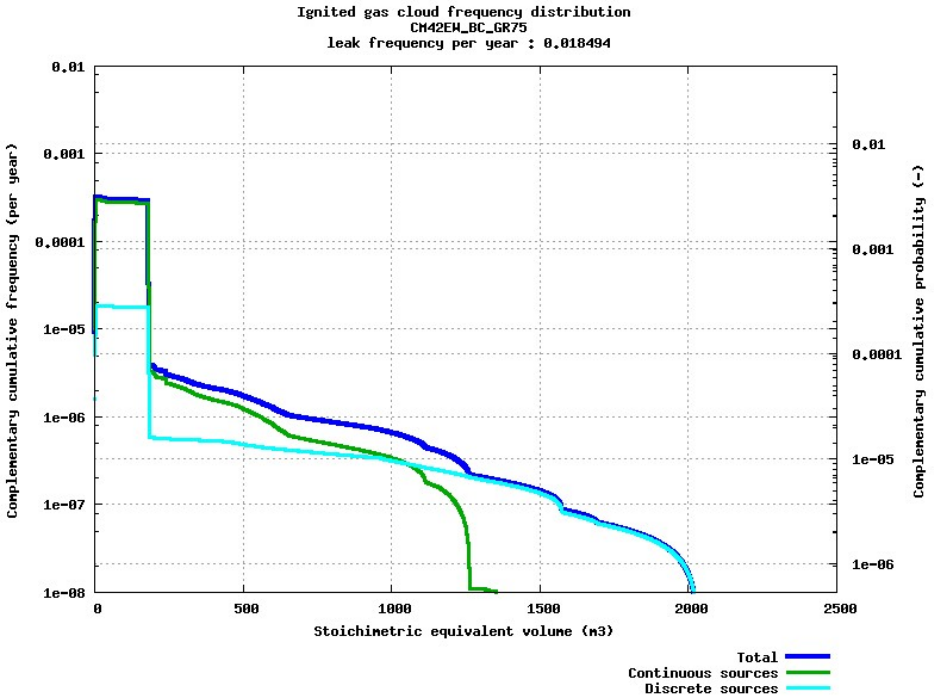

Figure 5.6: Complementary cumulative frequency distribution for stoichiometric equivalent gas cloud for grid resolution 75000.

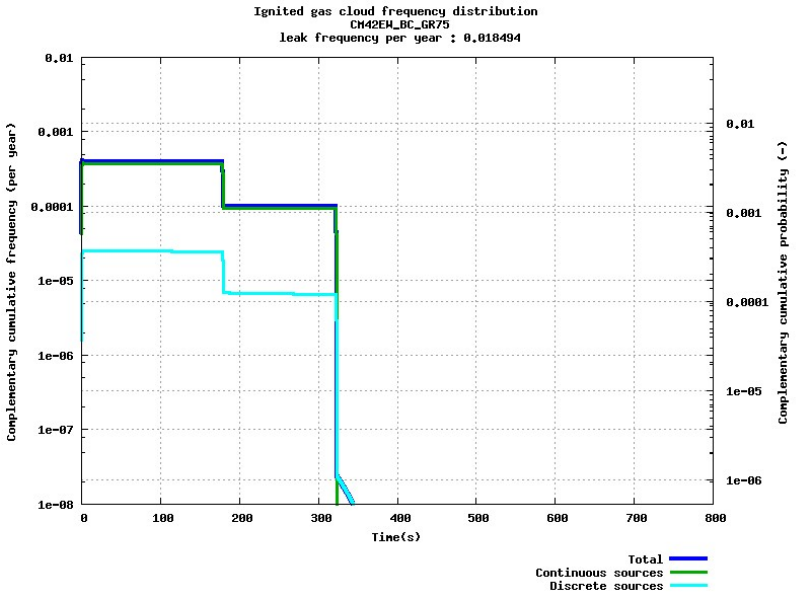

Figure 5.7: Cumulative frequency distribution for ignition time of stoichiometric equivalent cloud.

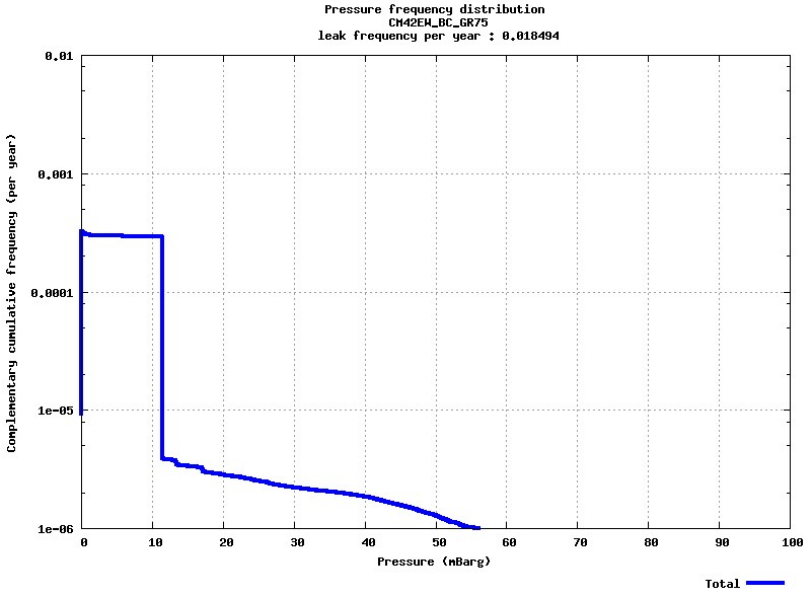

Figure 5.8: Complementary cumulative frequency distribution for dimensioning explosion load.

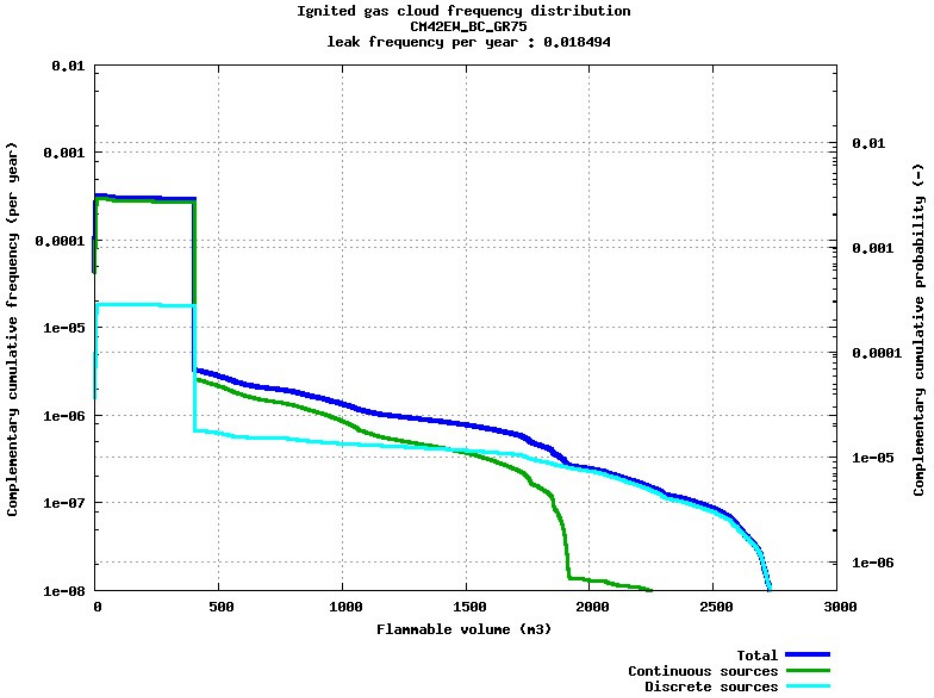

Figure 5.9: Complementary cumulative frequency distribution for flammable gas cloud for grid resolution 75000.

5.6 Inferences

From the base case simulation carried out with 75000 grid cells, the trend of high deviations are evident in the transient, pressure and flammable cloud plots shown in Figures 5.7, 5.8 and 5.9.

This suggests that choosing a very coarse grid resolution for a case that contains multiple scenarios with leak rates ranging from as low as 0.5 kg/s to as high as 512 kg/s produces results that could be questionable for accuracy and quality. On the other hand, there are other inferences that could be obtained from such results, which are analysed in detail in Section 7.1.

Case name	Grid resolution	Courant number	Number of scenarios	Simulation time (days)
Base case	200000	10	40	12
Base case - Re-run 1	125000	15 (Max)	34	3
Base case - Re-run 2	75000	15 (Max)	34	1.5

Table 5.2: Results of optimal grid resolution study depicting simulation time.

Hence, considering the quality of results obtained and the significant reduction in the simulation time, the sensitivity cases are simulated with a grid resolution of 125000 and a maximum courant number 15. Hence, the aforementioned case with grid resolution of 125000 will be referred to as the base case in the rest of the study for further comparisons and analyses.

Chapter 6

Parametric variations

The objective of this chapter is to present and discuss the results of various simulations that were carried out by incorporating different parametric changes. The cases chosen to study the sensitivities are in line with practical scenarios on-board the installations in the NCS. The resulting plots are compared with the base case and the inferences are presented in the respective sections.

6.1 Sensitivity 1 - Delays in shutdown time due to manual activation of ESD system

The underlying rational behind this sensitivity case is to understand the changes in the consequences if the emergency shut down had to be activated manually. To account for that, the parameter responsible for "ESD activation time" in the scenario file, which was set to "2 s" for the base case simulation, has been increased to "300 s" in this case. In addition, the response time of the gas detectors, which was previously set to "1 s" for the base case simulation, has been increased to "180 s" in this case. The result plots of this simulation are presented in the figures below.

The Figure 6.1 shows that the contribution from the continuous begin to dominate when the stoichiometric cloud volume reaches approximately 250 m^3, which in the base case occurred when the cloud reached a volume of 500 m^3, while the rest of the plot seems much similar to that of the base case shown in Figure 5.2.

The transient plot shown in Figure 6.2 depicts that the possibility of an ignition is after 60 s unlike less than 30 s in the base case as in Figure 5.3. As a result of delayed activation of shut down, the exposure from continuous sources seems to be almost twice as much, in comparison to that of the base case shown in Figure 5.3. The plot depicts that an ignition could occur just after a minute upon the release, which is still considered as immediate ignition upon release. It is to be noted that since the chosen module is assumed to have less ignition sources, the frequencies are of negligible order. The probabilities of ignition could have been high had the module been complex and contains more ignition sources.

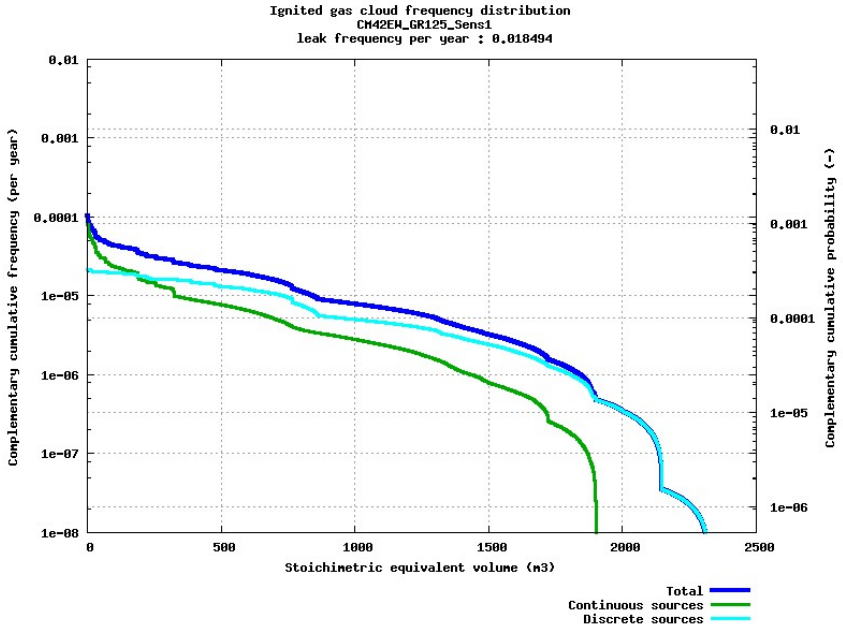

Figure 6.1: Cumulative frequency distribution for stoichiometric equivalent gas cloud.

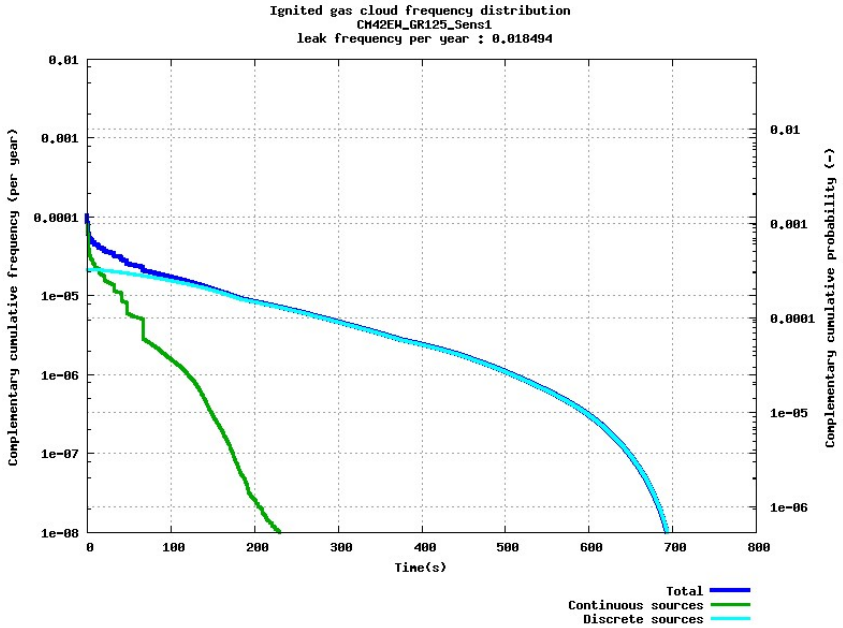

Figure 6.2: Cumulative frequency distribution for ignition time of stoichiometric gas cloud.

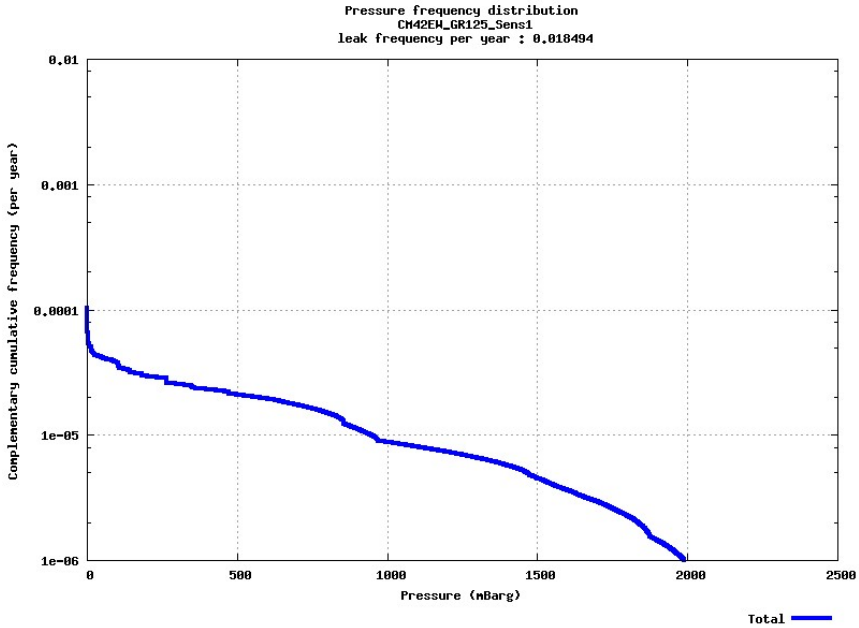

Figure 6.3: Complementary cumulative frequency distribution for dimensioning explosion load.

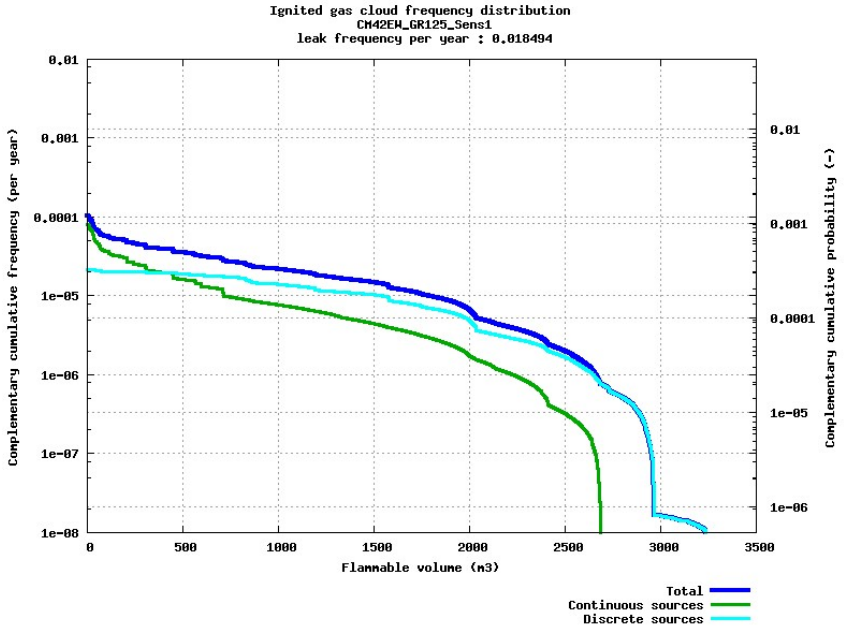

Figure 6.4: Complementary cumulative frequency distribution for flammable gas cloud.

In case of pressure plot, unlike the plot of the base case shown in Figure 5.4, where the cumulative frequency rapidly decreased and reached a value of 10^{-5} at the pressure of 250 mBarg, this plot of this case depicts a prolonged exposure due to slightly higher pressures and reaches a frequency of 10^{-5} when the pressure is approximately 950 mBarg as shown in Figure 6.3. Although the probability of explosions are low in this case, such effects could prove to be extremely dangerous for a different module with very poor ventilation, with more ignition sources and high pressure releases.

The flammable cloud plot presented in Figure 6.4 shows a similar trend as the stoichiometric cloud plot with respect to contribution from continuous sources. In this case, the continuous sources begin to dominate at a much earlier could size of approximately 400 m^3 in comparison to the base case wherein the similar trend occurs when the cloud volume reaches approximately 900 m^3, as shown in Figure 5.5.

6.2 Sensitivity 2 - Partial isolation of gas detectors

This section presents results of a sensitivity case wherein the base case with grid resolution of 125000 was re-simulated with seven gas detectors isolated. The detectors have been isolated for one complete zone and not random isolation. The rationale behind this scenario is that there have been a number of cases in NCS where gas leaks have occurred in isolated sections of modules during preventive or corrective maintenance activities. Therefore, it is vital to document the influence of partially isolating gas detection system on the ignition probabilities.

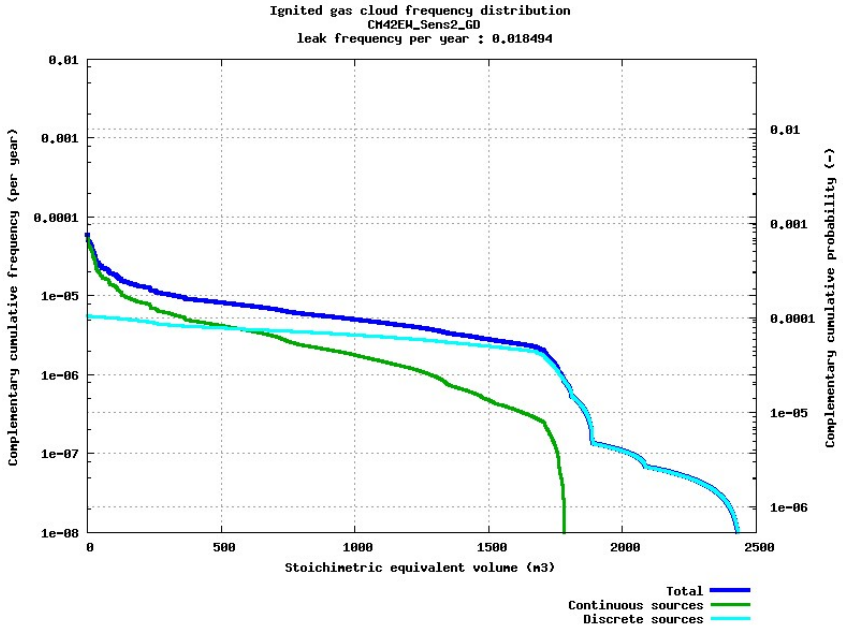

Figure 6.5: Cumulative frequency distribution for stoichiometric equivalent gas cloud.

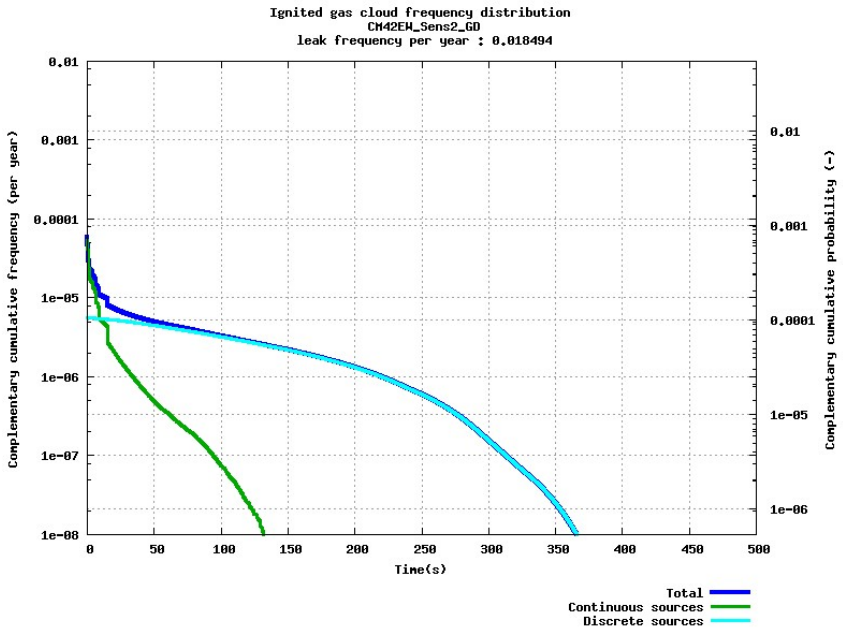

Figure 6.6: Cumulative frequency distribution for ignition time of stoichiometric cloud.

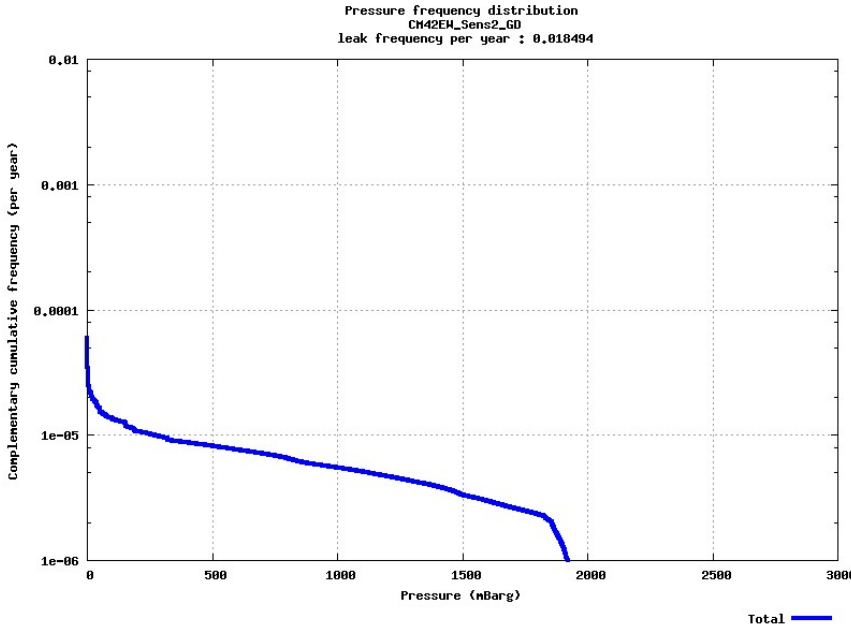

Figure 6.7: Complementary cumulative frequency distribution for dimensioning explosion load.

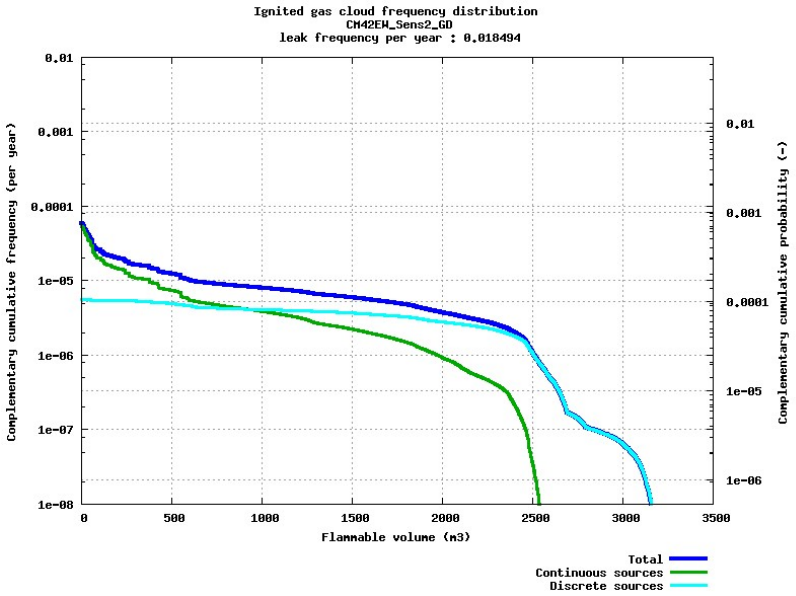

Figure 6.8: Complementary cumulative frequency distribution for flammable gas cloud.

The results shown in Figures 6.5, 6.6, 6.7 and 6.8 depicted no evidence of increase in the ignition probability in comparison to that of the base case with 125000 grid cells, as presented in Section 5.4. One of the major reasons for this could be related to the size of the module. Since the chosen module is relatively small, isolating a small section in this module does not create any significant delays in gas detection since the density of gas detectors is sufficient enough for detection of any leaks. However, it would be worthwhile to perform similar experiments with relatively bigger modules. In addition, plots comparing the base case results with the sensitivities are presented in Section 7.3.

6.3 Sensitivity 3 - Increased ignition sources

In this sensitivity case, the objective was to see the changes in the cumulative frequencies in the consequence plots upon inducing an additional source of ignition into the chosen module. In this case, the ".xml" file which is used to run powerscan was incorporated with a pump which acts as a source of ignition. The modified ".xml" file used in this case is attached to Appendix H, Figure 10.12 and Figure 10.13. In general, the result plots presented below depicts that the cumulative frequencies are of the order between 10^{-3} and 10^{-4}, which is higher in comparison to the base case and the other sensitivity cases.

Figure 6.9, in comparison to that of the base case shown in Figure 5.2, shows no changes in the contribution from discrete sources whereas the contribution from continuous sources is rather high as expected. Continuous sources also dominate for a prolonged period till the cloud reaches a volume of 1350 m^3. Similar trend is observed in the flammable cloud plot shown in Figure 6.12.

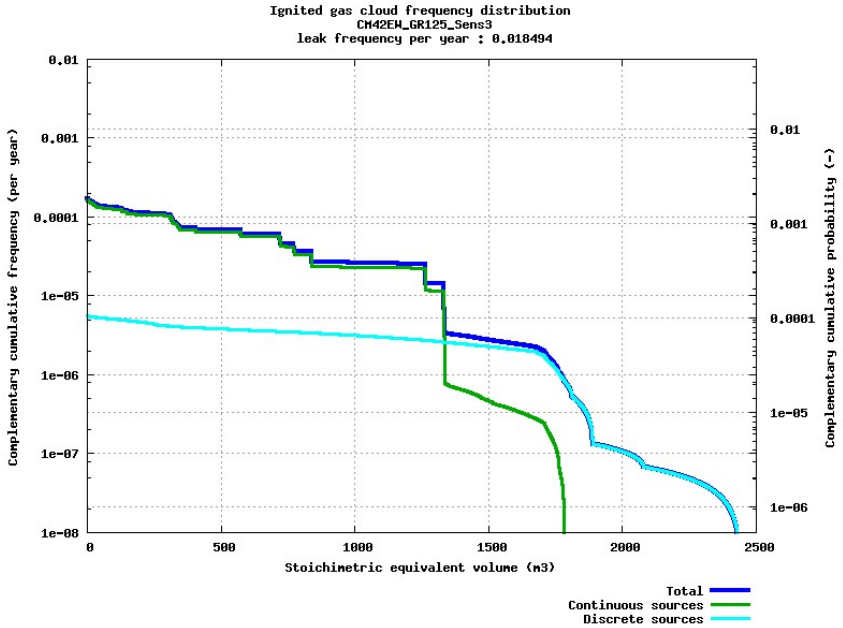

Figure 6.9: Cumulative frequency distribution for stoichiometric equivalent gas cloud.

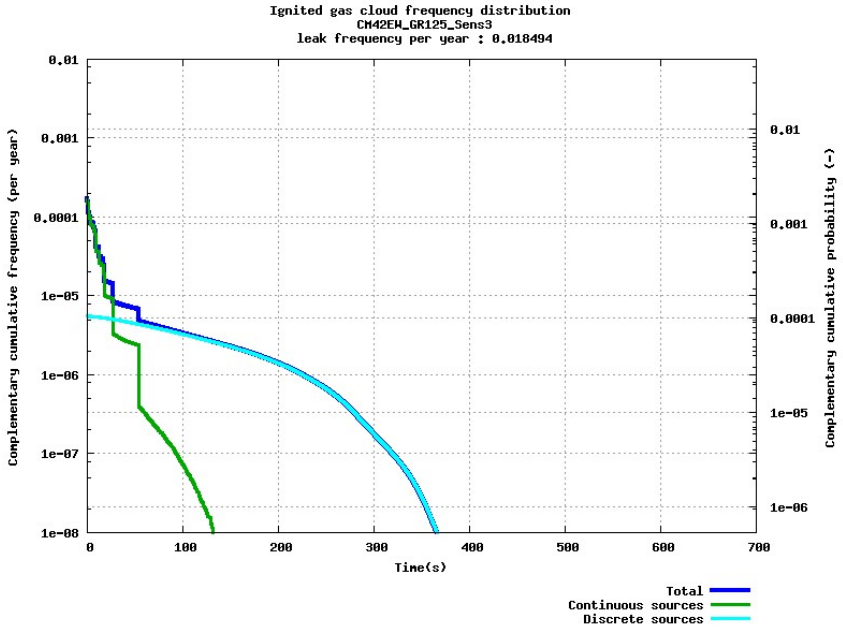

Figure 6.10: Cumulative frequency distribution for ignition time of stoichiometric cloud.

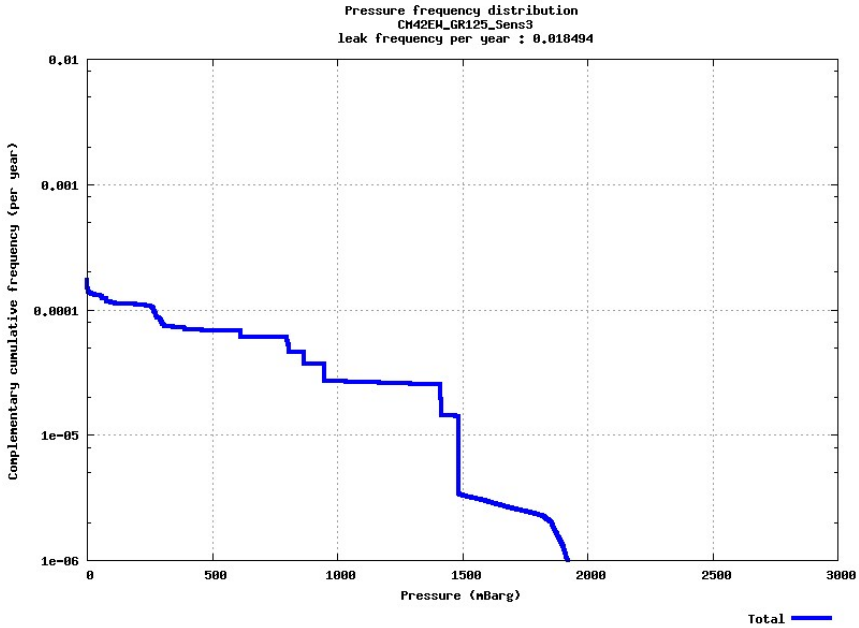

Figure 6.11: Complementary cumulative frequency distribution for dimensioning explosion load.

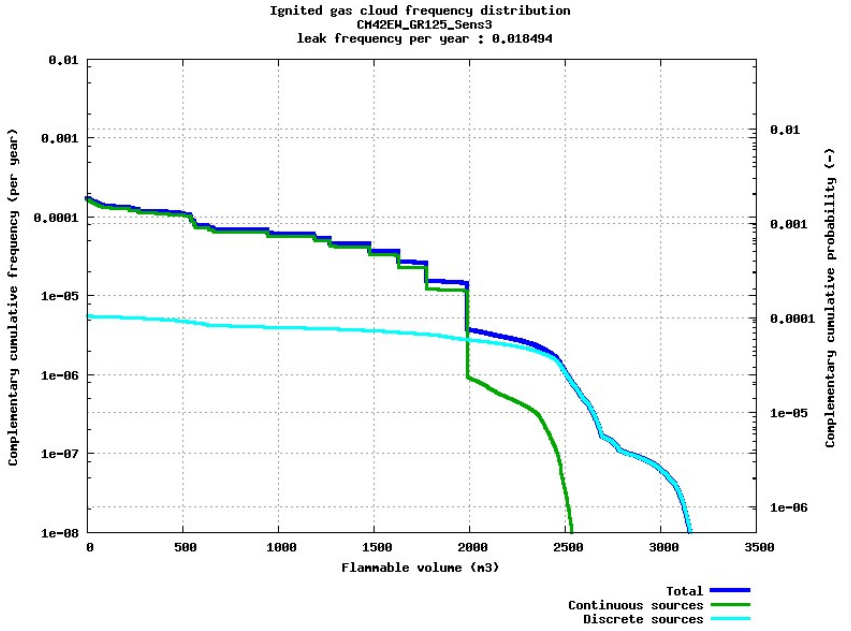

Figure 6.12: Complementary cumulative frequency distribution for flammable cloud.

The transient plot shown in Figure 6.10 depicts that an ignition could occur typically within less than 60 s from the start of the release. The probability of such ignition occurring immediately is slightly higher in comparison to that of the base case shown in Figure 5.3. The immediate pressure frequency shown in Figure 6.11 also predicts an higher possibilities of explosion compared to base case shown in Figure 5.4. The flammable could plot shown in Figure 6.12 depicts prolonged exposure due to increased ignition sources.

This result depicts that the presence of ignition sources such as running pumps or hot works such as welding, grinding, cutting etc. in a section of the module does have a significant influence in increasing the cumulative frequencies. Such additional sources of ignitions when combined with even poorly ventilated modules and high pressure releases could bring nothing less than adverse consequences. Plots comparing the base case results with the sensitivities are presented in Section 7.3.

6.4 Sensitivity 4 - Temporary weather cladding to prevent cold winds during winters

In view of analysing the influence of temporary weather cladding (a porous curtain to prevent cold winds, typically during winters) on the probability of ignition in the module in question, the module was incorporated with a porous cladding on one of the open ends and the simulation was re-run. The grid resolution, number of detectors and other parameters remain unchanged. The results are presented in the following figures:

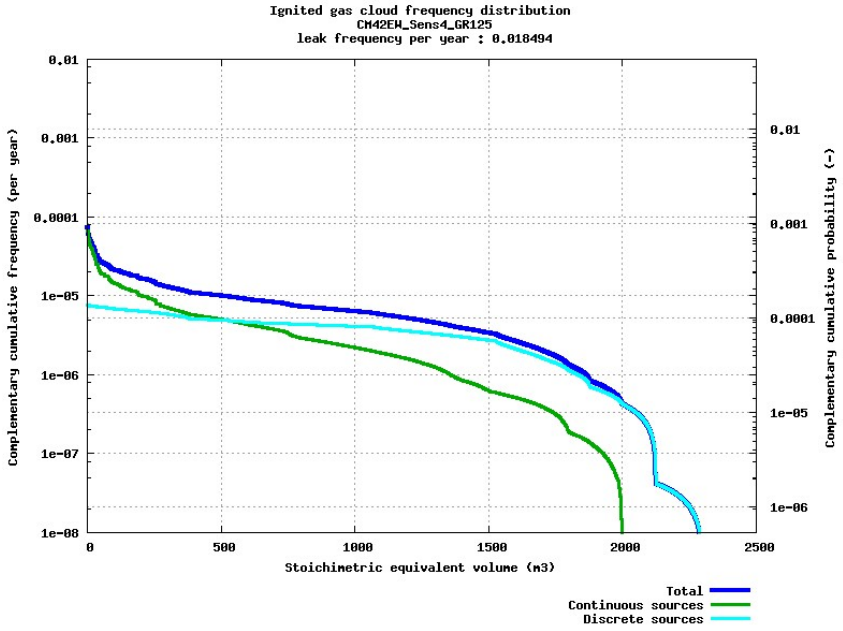

Figure 6.13: Cumulative frequency distribution for stoichiometric equivalent cloud.

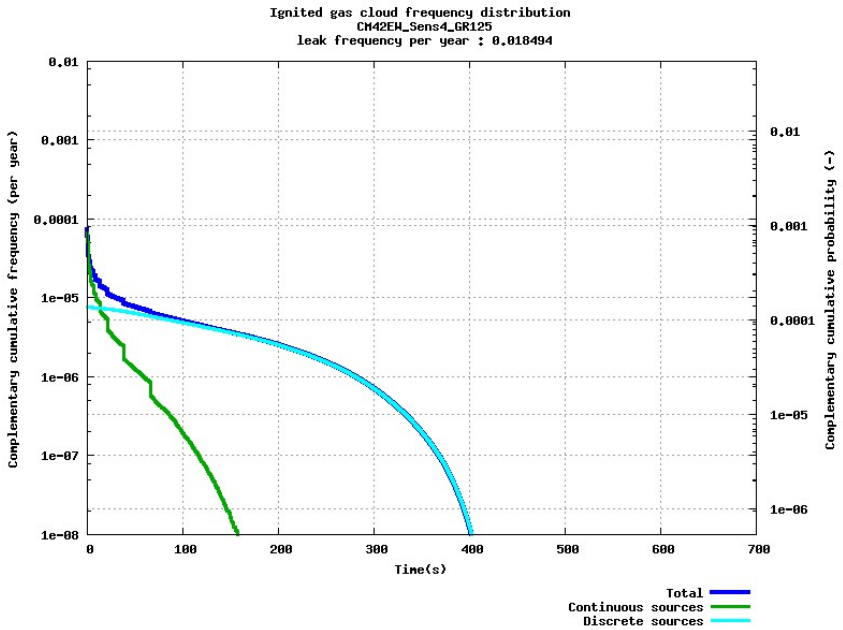

Figure 6.14: Cumulative frequency distribution for ignition time of stoichiometric cloud.

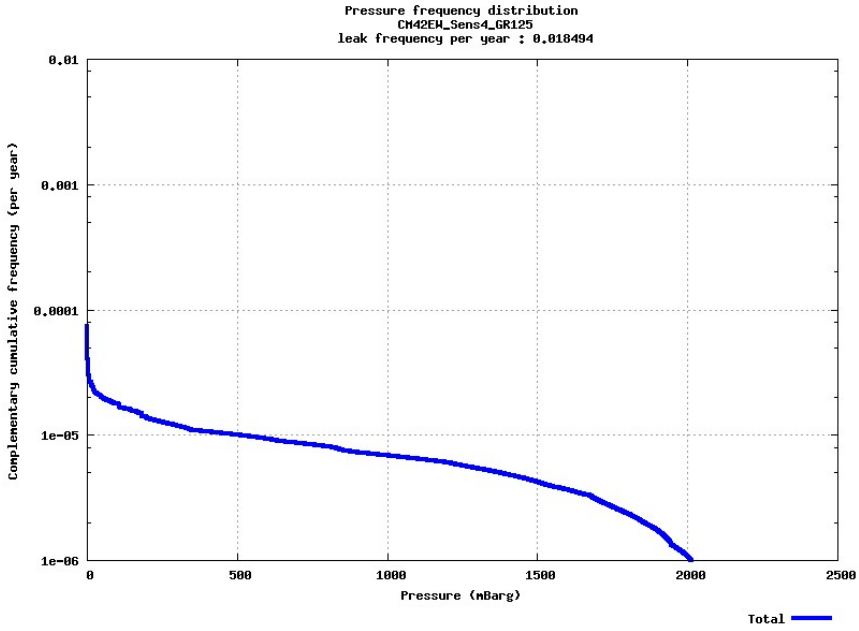

Figure 6.15: Complementary cumulative frequency distribution for dimensioning explosion load.

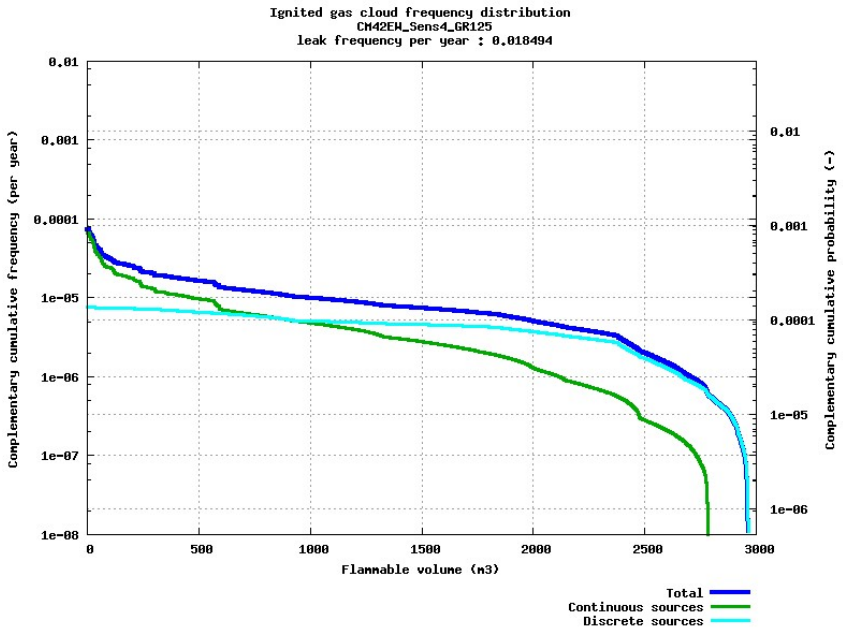

Figure 6.16: Complementary cumulative frequency distribution for flammable cloud.

The Figure 6.13 shows a prolonged contribution from the discrete sources in comparison to that of base case presented in the Figure 5.2. In the latter, a rapid decrease in the frequency curve is evident when the stoichiometric equivalent volume is between 1700 and 1800 m^3 approximately and at a volume of 2000 m^3, the cumulative frequency is of a negligible order of 10^{-7}. In comparison, there is a gradual decrease in the continuous source contribution curve between the stoichiometric volumes of 1500 and 2000 m^3 and at 2000 m^3, the cumulative frequency is still of the order 10^{-6} and plummeting down rapidly after the gas cloud volume of 2000 m^3.

The complementary cumulative frequencies are of a negligible order in the result plots. However, the trend of prolonged gas exposure is evident in plots presented in the Figure 6.14, Figure 6.15 and Figure 6.16.

This prolonged exposure is the effect of reduced ventilation due to temporary weather protection on one of the open ends of the module. It is to be noted that such reduction in ventilation is a function of the porosity of the temporary cladding erected. If the porosity is lesser, the higher the ventilation loss and longer the exposure to gas as a result. The results could be even worse if there were multiple temporary weather protections erected in the same module. Plots comparing the base case results with the sensitivities are presented in Section 7.3.

6.5 Base case - Valve failure

In order to study the influence of a release point and release direction on the cumulative probabilities, the base case was re-simulated with a different release point and release direction with a grid resolution of 125000. The resulting plots are presented in the figures below.

The stoichiometric equivalent plot shown in Figure 6.17 depicts a prolonged contribution from continuous sources till the gas cloud reaches a volume of approximately 1025 m^3 and then decreases rapidly thereafter. In comparison to the base case plot shown in Figure 5.2, the cumulative probabilities in this case are much lower. The contribution from continuous sources are of the order 10^-6 immediately upon release. Similar trend is observed in the flammable cloud plot presented in Figure 6.20. The transient plot shown in Figure 6.18 depicts that there could be possibilities of ignition within 60 s from the initiation of the leak as was the case with base case scenario shown in Figure 5.3.

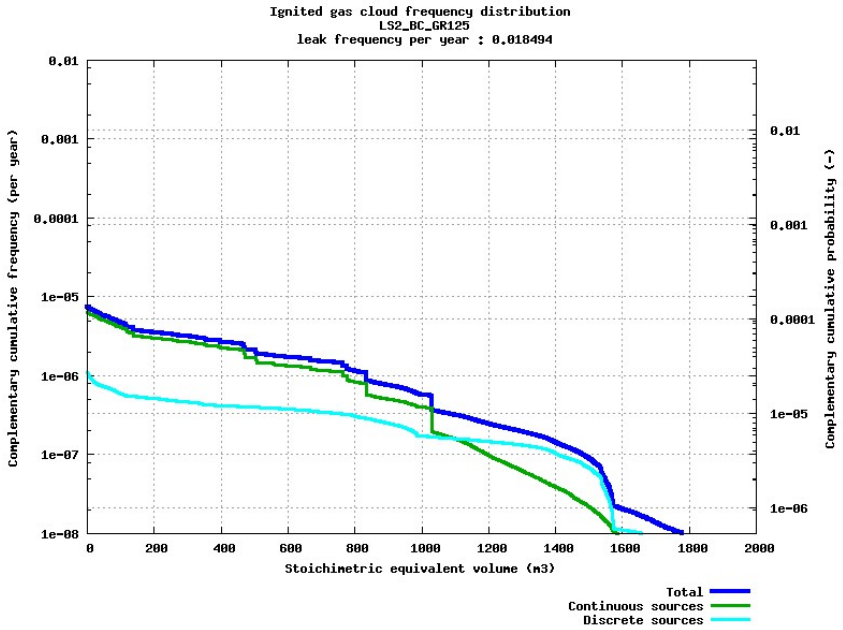

Figure 6.17: Cumulative frequency distribution for stoichiometric equivalent cloud.

The pressure plot shown in Figure 6.19 depicts significantly low pressure in comparison to that of the base case plot, Figure 5.4. The reason is that the release point in this case is much closer to one of the open ends, which means that the ventilation is much better and the released gas is diluted immediately upon release. This in turn means that the explosion risk is highly insignificant.

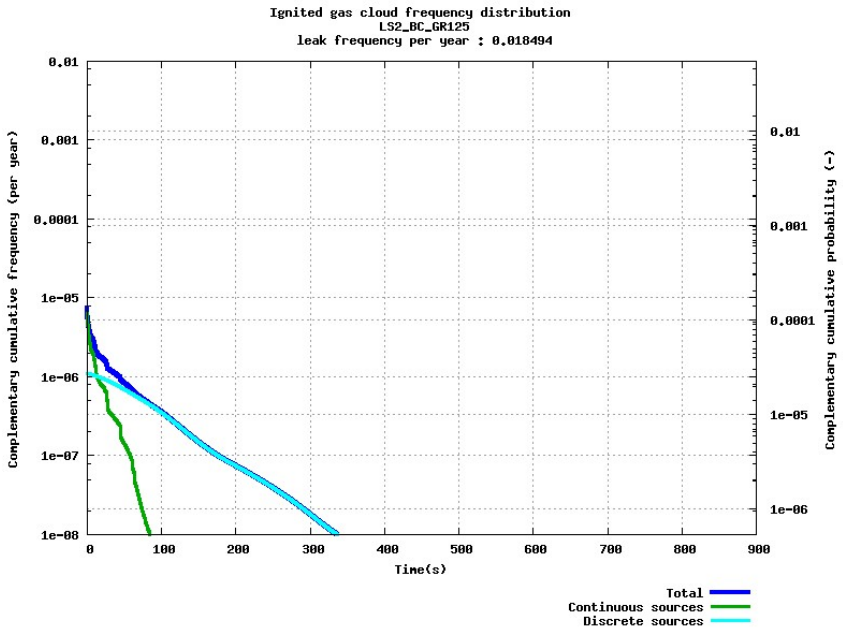

Figure 6.18: Cumulative frequency distribution for ignition time of stoichiometric cloud.

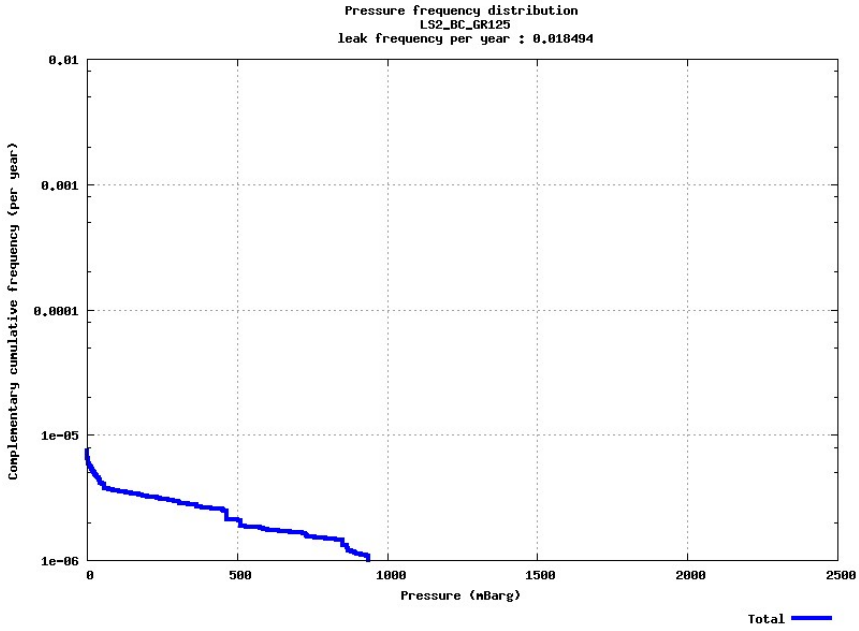

Figure 6.19: Complementary cumulative frequency distribution for dimensioning explosion load.

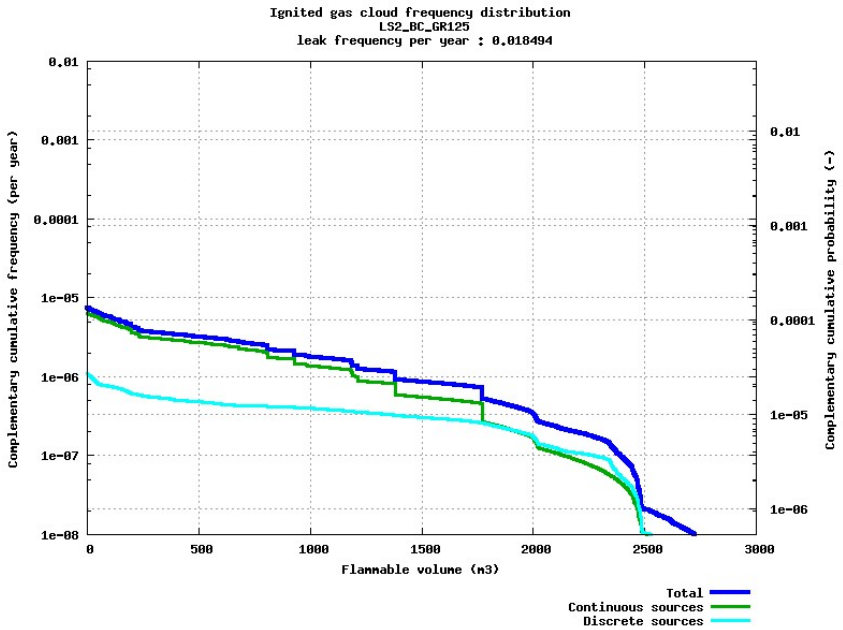

Figure 6.20: Complementary cumulative frequency distribution for flammable cloud.

The result plots shows significant influence upon changing the release point and release direction. Such changes in influence yields valuable inputs in terms of identifying the most critical zones with the modules. Such critical zones could be targeted and strengthened with additional barriers if deemed necessary. Further insights and detailed comparisons are delineated in Section 7.2 and plots comparing the results of simulations with different barriers are presented in Section 7.3.

Chapter 7

Findings and Comparisons

This chapter presents comparisons of results between different sets of simulations and discusses the inferences gained in detail.

7.1 Optimal grid resolution

This section presents and discusses various combined result plots of the base case simulations performed with different grid resolutions such as 200000, 125000 and 75000.

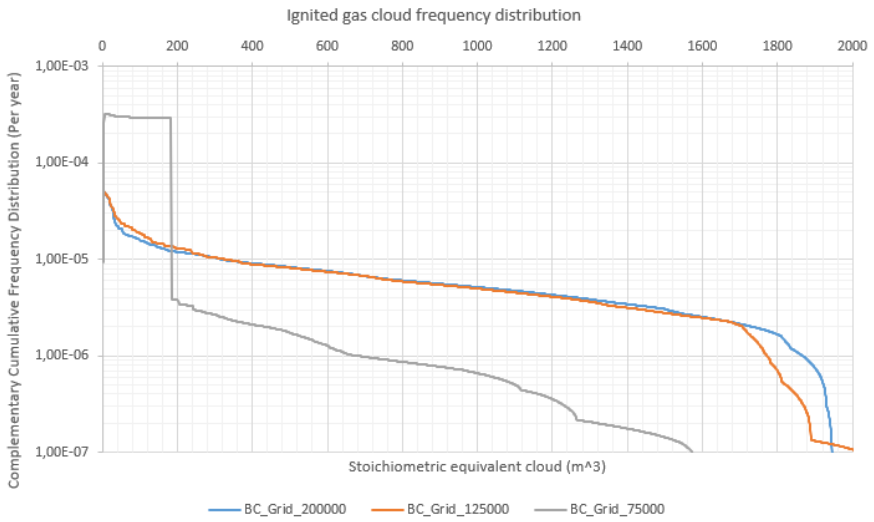

Figure 7.1: Comparison of stoichiometric cloud volume for different grid resolutions.

The Figure 7.1 depicts a plot of complementary cumulative frequency vs stoichiomet-

ric gas cloud volume for the aforementioned grid resolutions. The plots of grid resolutions 200000 and 125000 are almost identical from leak initiation till the cloud reaches a volume of 1700 m^3 and the deviations after that are acceptable since the frequencies have reached insignificant levels. Whereas the plot with a resolution of 75000 depicts significant deviations. This shows that the for cases which contain numerous scenarios with different release rates ranging from 0.5 kg/s to 512 kg/s, a coarse grid resolution is not suitable.

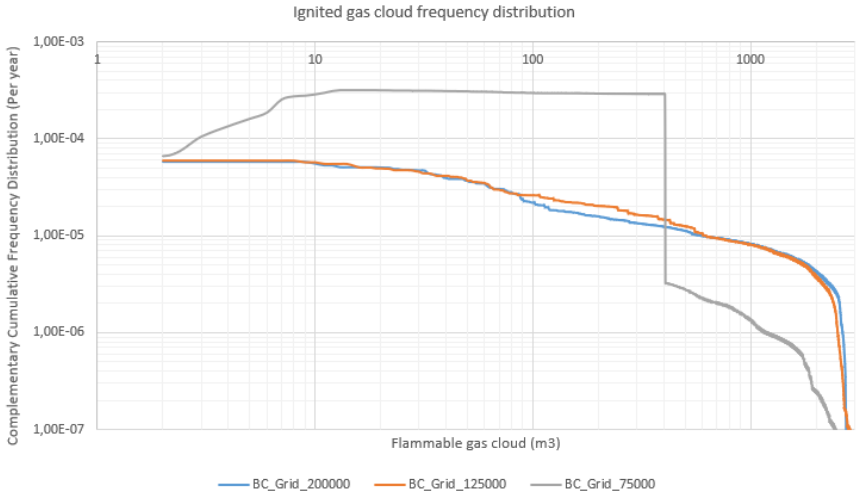

Figure 7.2: Comparison of flammable gas cloud volume for different grid resolutions.

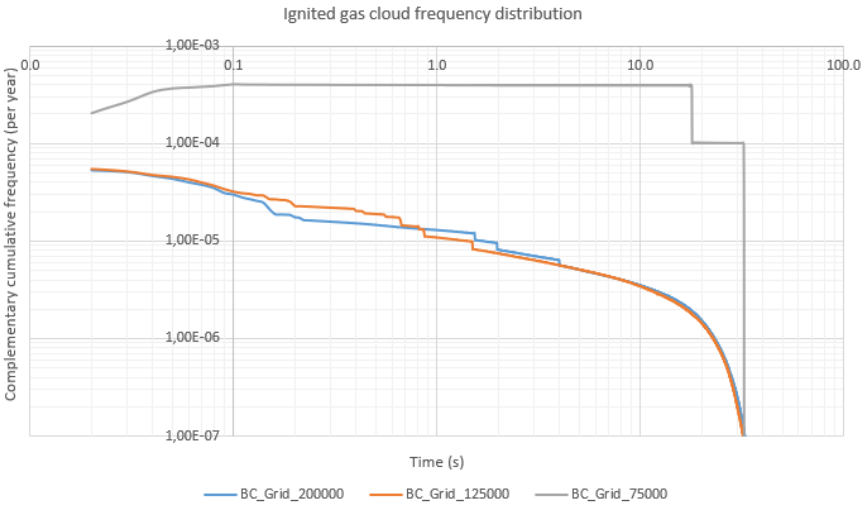

Figure 7.3: Transient cumulative frequency comparison for different grid resolutions.

The inaccuracies in the plots as a result of choosing a coarser grid resolution of 75000 is also evident in cumulative frequency vs flammable gas cloud plots and time dependent transient plots shown in Figure 7.2 and Figure 7.3 respectively. Therefore, further analysis is necessary to identify the reasoning behind such inaccuracies in the results.

In an effort to identify the influence of the grid resolutions on one particular release rate, similar plots are presented for small releases of 2 kg/s and a big releases of 512 kg/s for all three grid resolutions. Thereafter, Section 7.1.3 presents result plots of the analysis carried out to identify the threshold for release rate beyond which the plots are reasonably accurate for a coarse resolution.

7.1.1 Small release - 2 kg/s

For a 2 kg/s release, there seems to be minor deviations in the results plots for the grid resolution 200000 and 125000 whereas the deviations are quiet significant with a resolution of 75000 as shown in Figures 7.4, 7.5 and 7.6. This is in line with the results of the plots which included several leak rates, presented in Section 7.1.

The reason for such significant deviations in the plots for small releases with coarse grid resolution is that, immediately after the release, the volume of fuel entering a relatively big control volume is low. Such low volumes combined with low pressure presents inconsistencies in the flow of fuel into adjacent control volumes and subsequently, there arise inaccuracies in the calculations. The combination of these factors results in large deviations in results for small releases with coarse resolution.

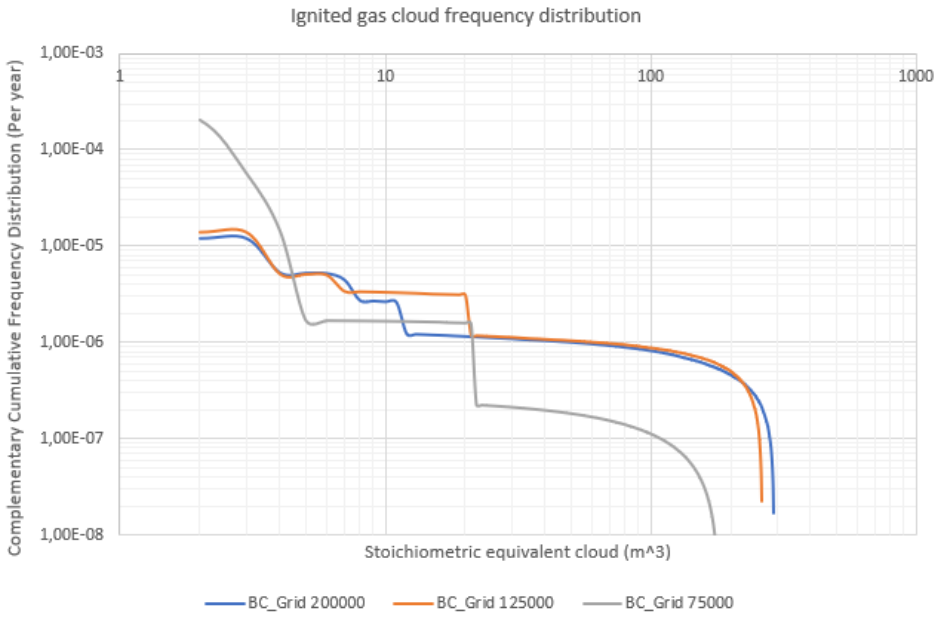

Figure 7.4: Comparison of stoichiometric cloud volume for different grid resolutions.

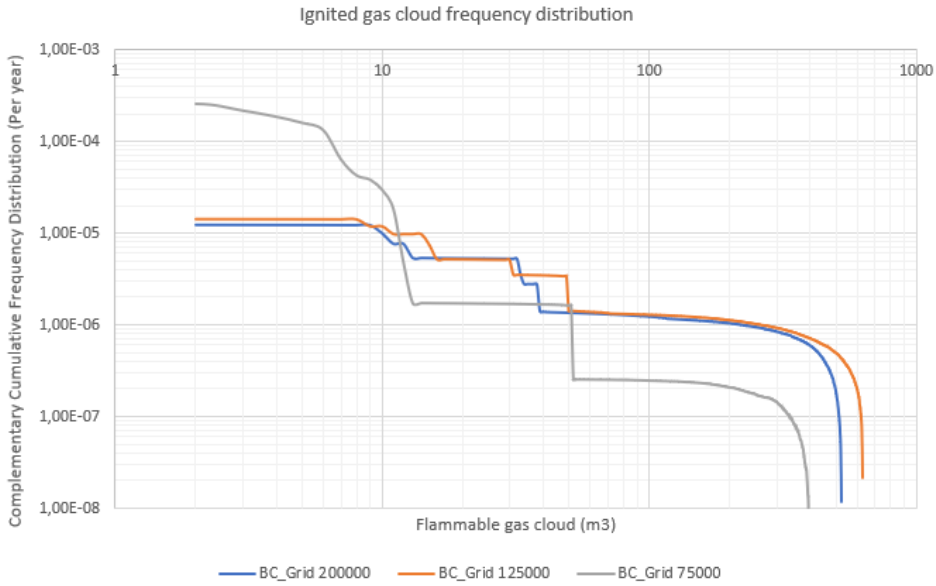

Figure 7.5: Comparison of flammable cloud volume for different grid resolutions.

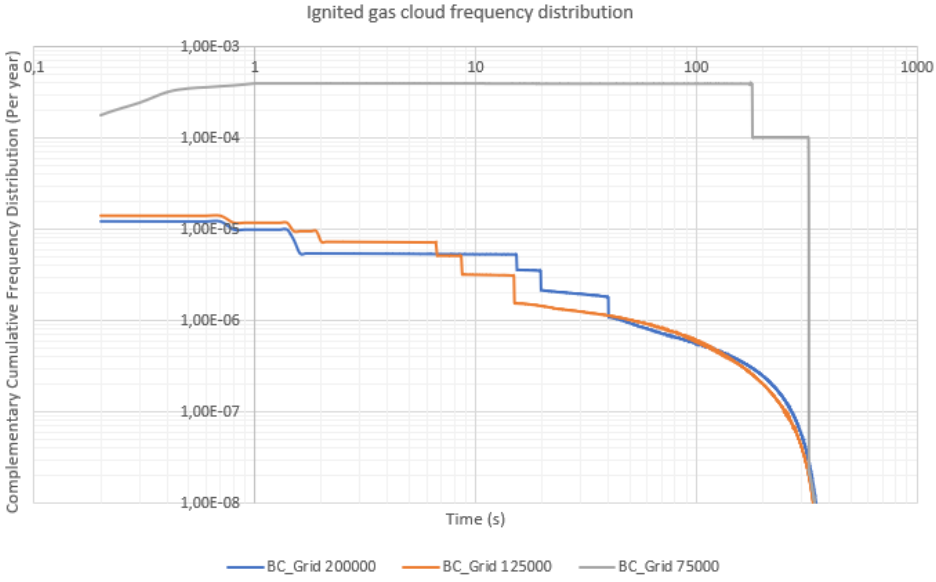

Figure 7.6: Transient cumulative frequency comparison for different grid resolutions.

Therefore, it is fair to conclude that for relatively small releases such as 2 kg/s, choosing a coarse grid resolution is not recommended as the results are significantly inaccurate.

7.1.2 Big release - 512 kg/s

For releases as big as 512 kg/s, the is observed that the deviation of the plot corresponding to 75000 grid resolution is negligible in comparison to grid resolutions of 200000 and 125000, as presented in the Figures 7.7, 7.8 and 7.9.

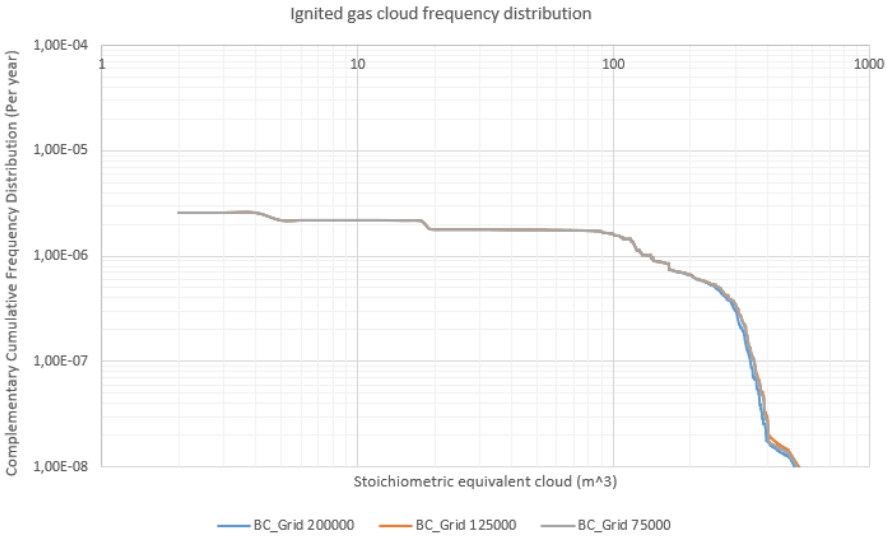

Figure 7.7: Comparison of stoichiometric cloud volume for different grid resolutions.

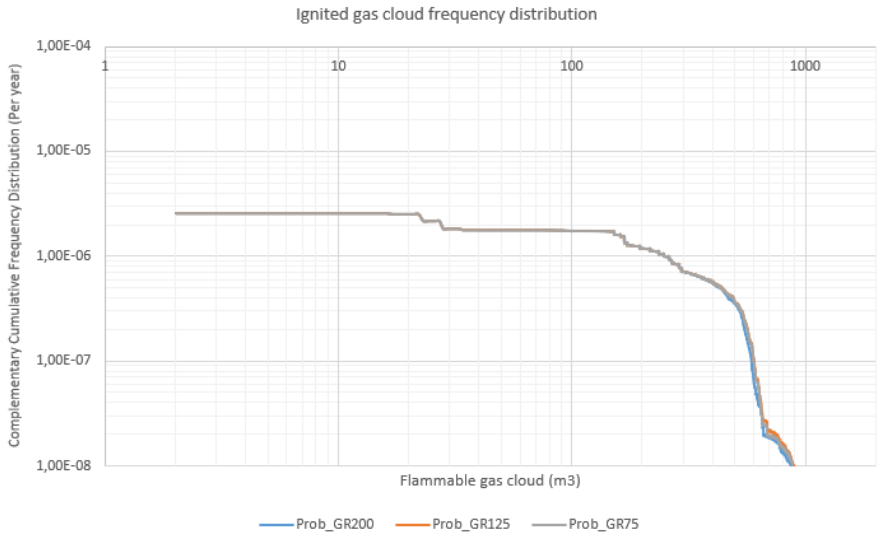

Figure 7.8: Comparison of flammable cloud volume for different grid resolutions.

The reason for this is that the volume of fuel entering a relatively big control volume is large. This large volume combined with the high pressure from the release posts no troubles for the flow of fuel into subsequent control volumes. Hence the calculations are stable and deviations are insignificant.

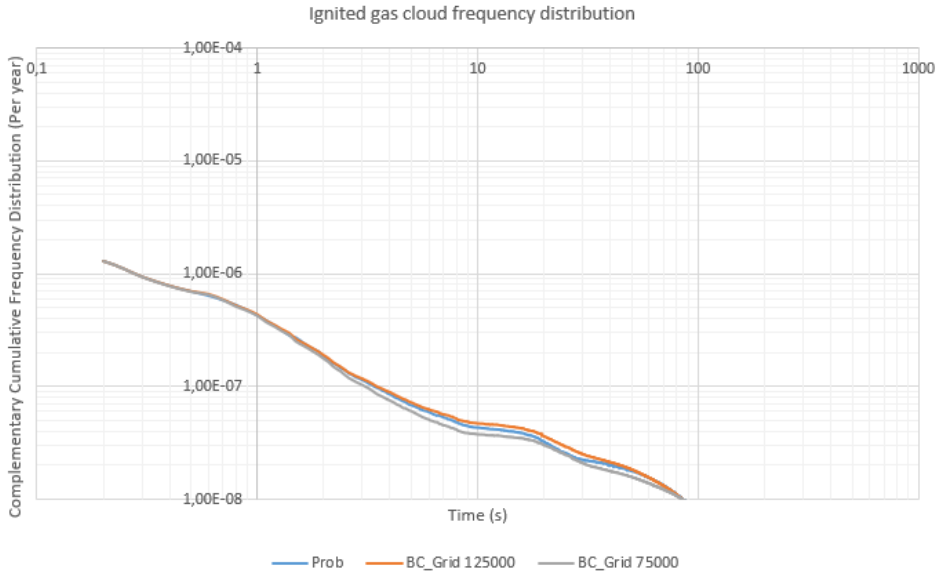

Figure 7.9: Transient cumulative frequency comparison for different grid resolutions.

Based on this, it is fair to conclude that the grid resolution is a function of leak rate. The higher the leak rate, the lower can be the grid resolution. With this, the simulation time is reduced significantly without affecting the stability of calculations and quality of results. But this section could leave the readers with a question "What would then be the threshold for release rate below which the results deviate significantly?" which is analysed in the following section.

7.1.3 Release threshold for coarse grid resolution - 32 kg/s

To identify the release rate threshold, beyond which, even a coarse grid resolution yield results that are fairly accurate as fine grid resolutions, a leak rate of 8 kg/s was first analysed. The result plots of the release rate 8 kg/s still depicted significant deviations for a coarse grid resolution of 75000 grids. The result plots of the leak rates 8 kg/s are attached to Appendix I, Figure 10.14, Figure 10.15 and Figure 10.16.

The analysis then moved to the subsequent higher release rate studies in this thesis, which was 32 kg/s based on Table 4.1.

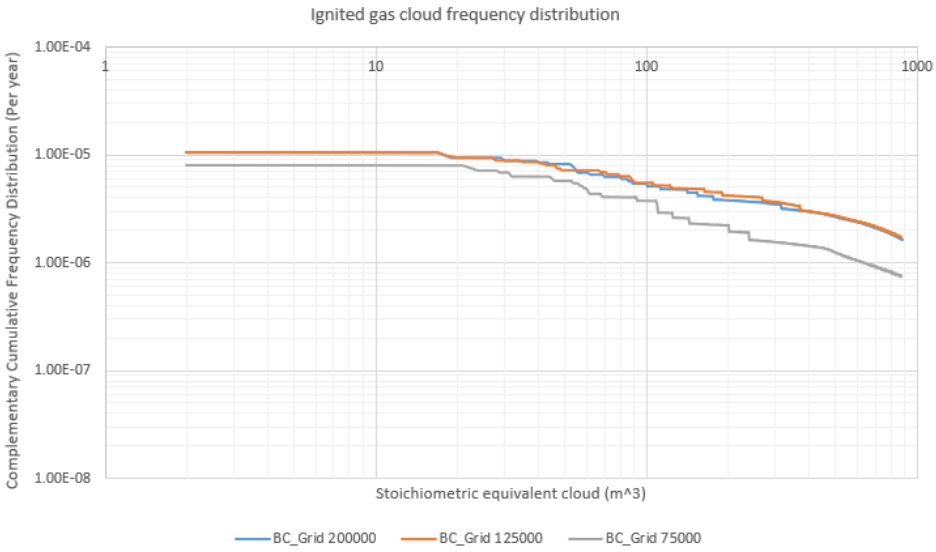

Figure 7.10: Comparison of stoichiometric cloud volume for different grid resolutions.

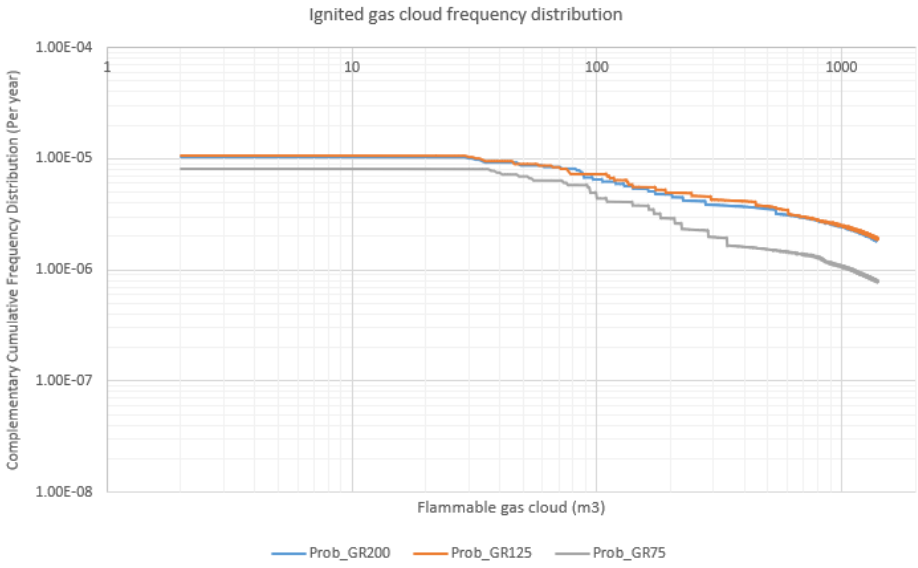

Figure 7.11: Comparison of flammable cloud volume for different grid resolutions.

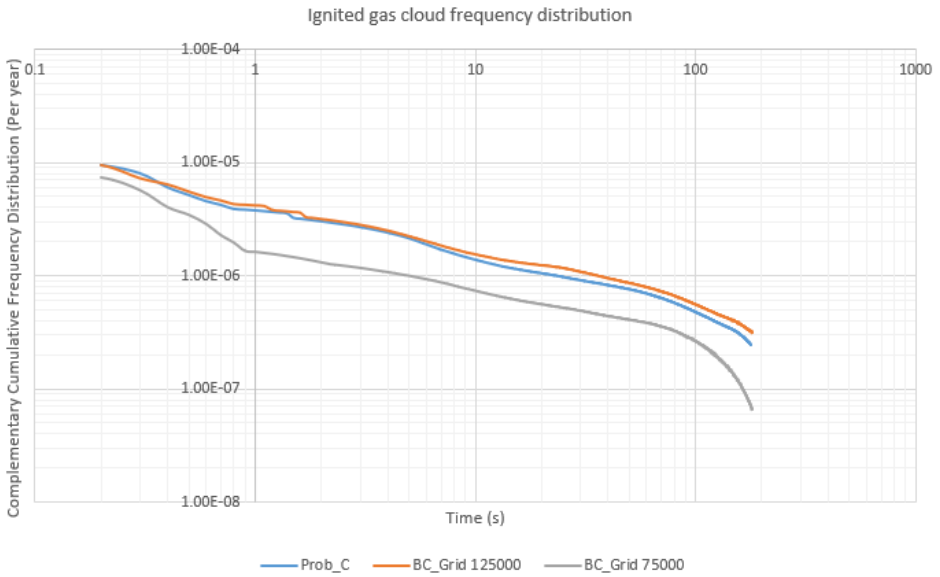

Figure 7.12: Transient cumulative frequency comparison for different grid resolutions.

The plots shown in Figure 7.10, Figure 7.11 and Figure 7.12 depict that for a release rate of 32 kg/s, the plots for grid resolution 75000 has only a minor deviation with an order of magnitude 10^{-5}. Since the cumulative frequencies for grid resolutions 200000 and 125000 are also fairly low and of the same order 10^{-5}, the result plots could be regarded as reasonably accurate.

Therefore, it could be concluded that the threshold for release rate beyond which a coarser grid resolution could be chosen to obtain reasonably accurate result plots is 32 kg/s. It is to be noted that this assessment may not hold sufficiently enough for significantly bigger and complex modules with high details. A re-assessment would be desirable in such cases.

7.2 Influence of release point location and direction

This section presents a comparison of results from the base case simulations performed with a same module but changing the release point and the direction of release. In both cases, the grid resolution was set to 125000. The results are presented in the following Figures 7.13, 7.14 and 7.15.

The comparison plot for pipe and valve failure scenarios depict that the cumulative probability for valve failure scenario is clearly lower than that in the pipe failure scenario. The stoichiometric as well as flammable cloud volumes are also clearly low in case of valve failure. This is because the release point in the case of valve failure was closer to one of the open ends and pointed towards positive x direction. This rendered that the ventilation was much better in this case and the gas cloud was diluted with air as soon as the release started.

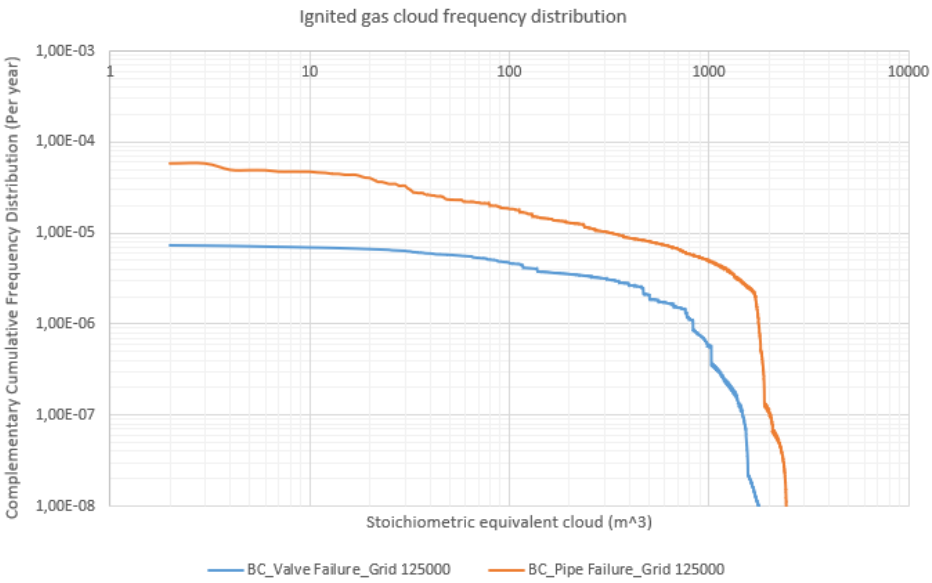

Figure 7.13: Comparison of stoichiometric cloud volume for different leak scenarios.

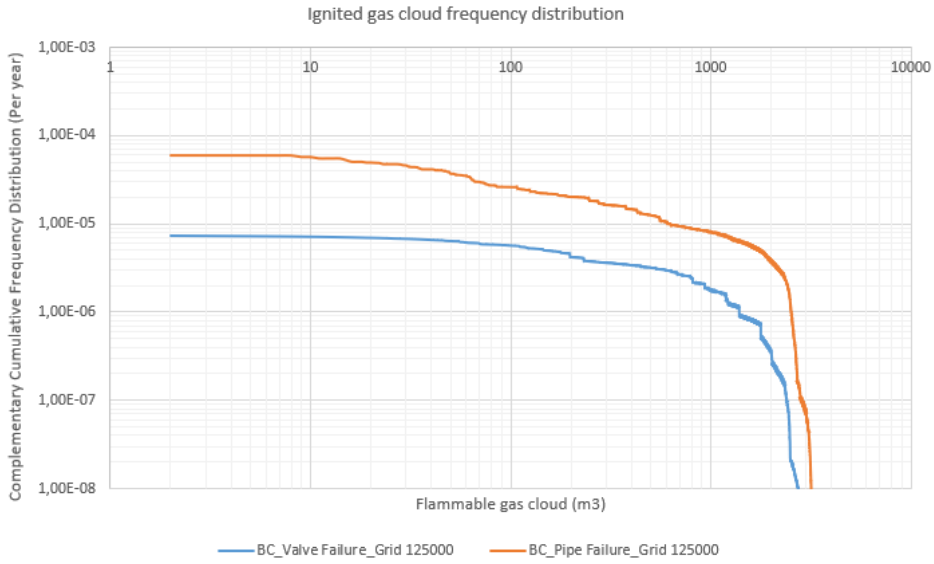

Figure 7.14: Comparison of flammable cloud volume for different leak scenarios.

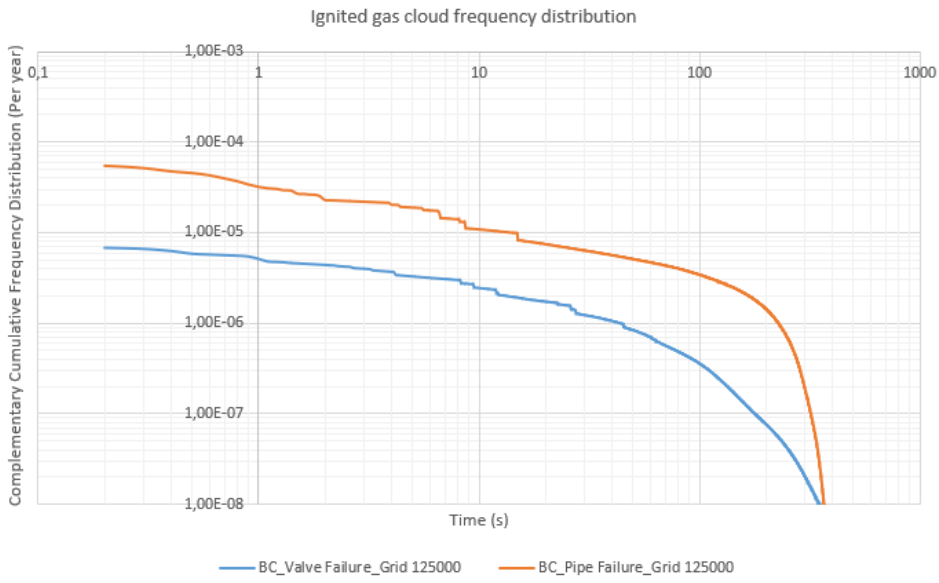

Figure 7.15: Transient cumulative frequency comparison for different leak scenarios.

On the contrary, the release point in the pipe failure scenario was approximately in the middle of the module, the farthest distance from either of the open ends and pointed in negative z direction. Hence, the ventilation was poor in comparison to that of the former case which clearly reflects in the higher probabilities and cloud volume in this case. From this, it is fair to say that the release point and release direction could have significant influence to the overall risk picture either by enhancing or decreasing the probabilities of ignition depending on poor or good ventilation respectively.

7.3 Comparison of base case and sensitivities

In order to obtain key insights concerning which of the barriers presented in Table 2.4 is the most influential in increasing the risk of ignition if failed to work as intended, a comparison of the result plots of the base case to that of the sensitivity scenarios is presented in this section. It is to be noted that some of the curves in the combined graphs have to be re-plotted in order to account for plot accuracy and to account for a practical error probability factor. Hence the plots are presented in multiple sub-sections below.

7.3.1 Actual plots as generated

This section presents the plots of the base case and sensitivities exactly as generated by the software. The curve depicting the cumulative frequencies due to “hot works” is based on the assumption that the hot works are taking place in a section of the module throughout the year. Hence that particular curve does not yield reasonably practical frequencies in all the plots in this section.

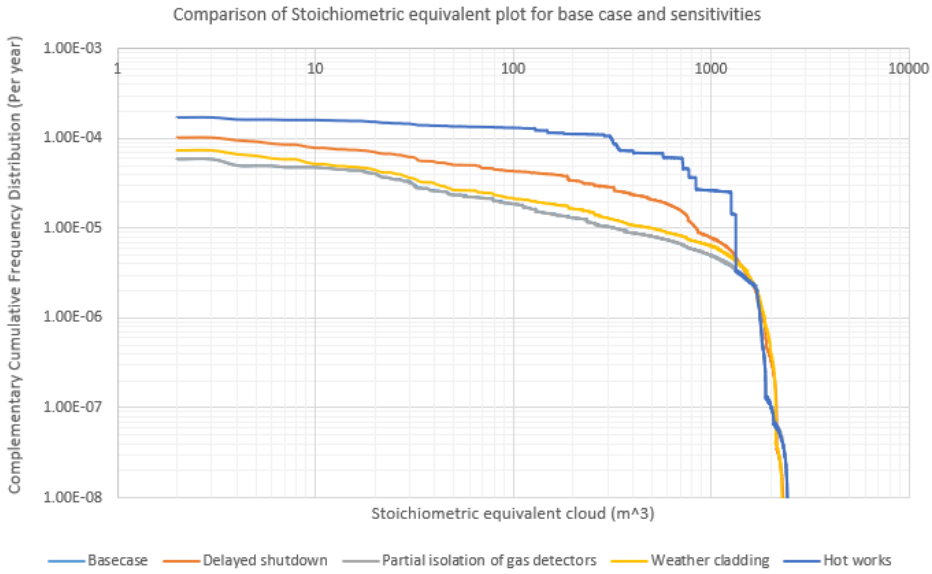

Figure 7.16: Comparison of stoichiometric equivalent volume for different leak scenarios.

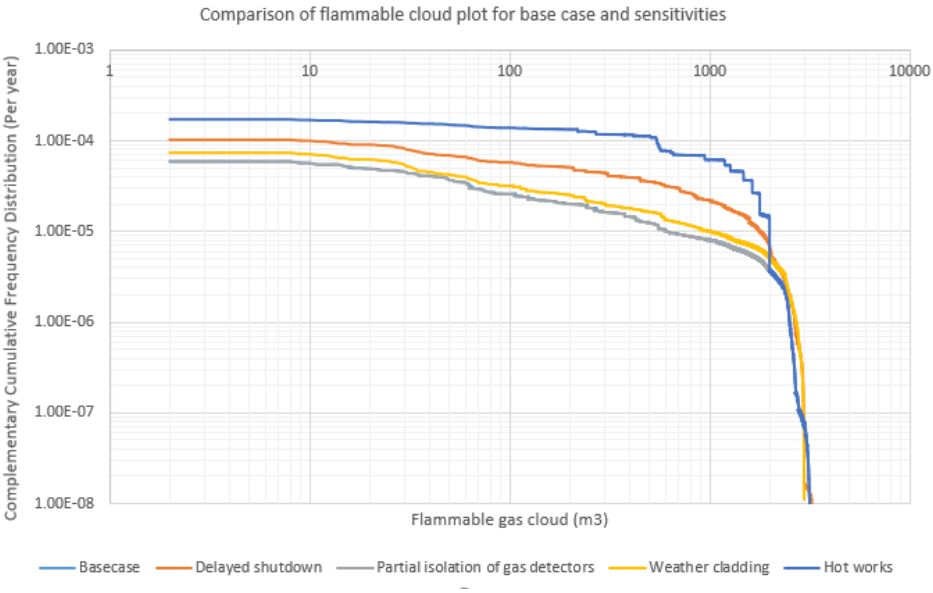

Figure 7.17: Comparison of flammable cloud volume for different leak scenarios.

The plots pertaining to weather cladding and delayed shutdown are fairly close to that of then base case. The plot corresponding to isolation of gas detectors show zero deviation compared to respective base case plots.

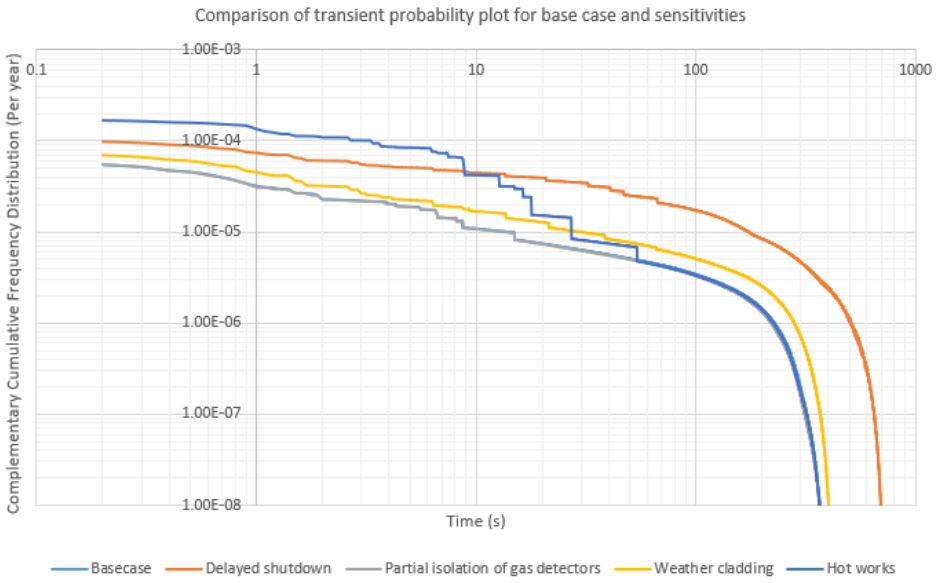

Figure 7.18: Transient cumulative frequency comparison for different leak scenarios.

The comparison plots shown in Figure 7.16, 7.17 and 7.18 depict that the plot corresponding to "Hot works" depicts high frequencies due to aforementioned reason. Hence, comparing this plot to others might not yield the best of the insights regarding that particular barrier and other barriers. Therefore, a manual correction of data is desired to account for the accuracy of the plots, which is detailed in Section 7.3.2.

7.3.2 Comparison-plots incorporated with manual corrections

To account for the accuracy of the "hot works" plot, a practical assumption is made pertaining the number of hours per year that the chosen section in the module would be subjected to any hot works. To be reasonably practicable, it is assumed that the section would be subjected to hot works for 1% of the hours per year. This corresponds to 87.6 hours or 3.65 days per year. In order to account for the remaining 99%, the 1% results of the above mentioned sensitivity case is merged with 99% of the base case results. In this way, we could visualize a practical plot wherein the influence of hot works for 1% of the time of the year is accounted for.

It is to be noted that, the frequencies depicted by the "hot work" plot is based on the assumption that hot works are carried out only in one section of the module. In reality, there could also be hot works carried out in multiple locations in the same module which is not a part of this study. The plot of hot works corresponding to 1% of hot works per year are presented in Figures 7.19, 7.20 and 7.21.

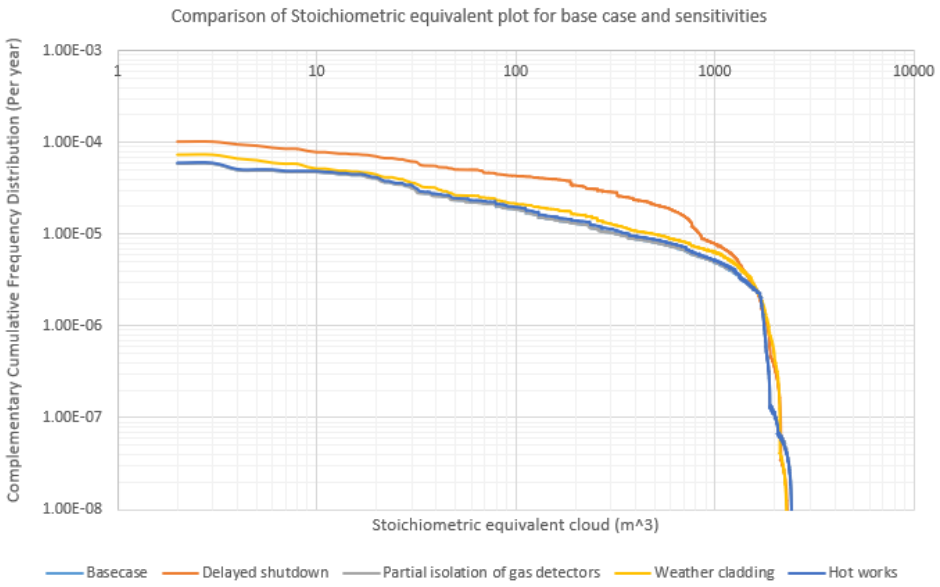

Figure 7.19: Comparison of stoichiometric equivalent volume for different leak scenarios.

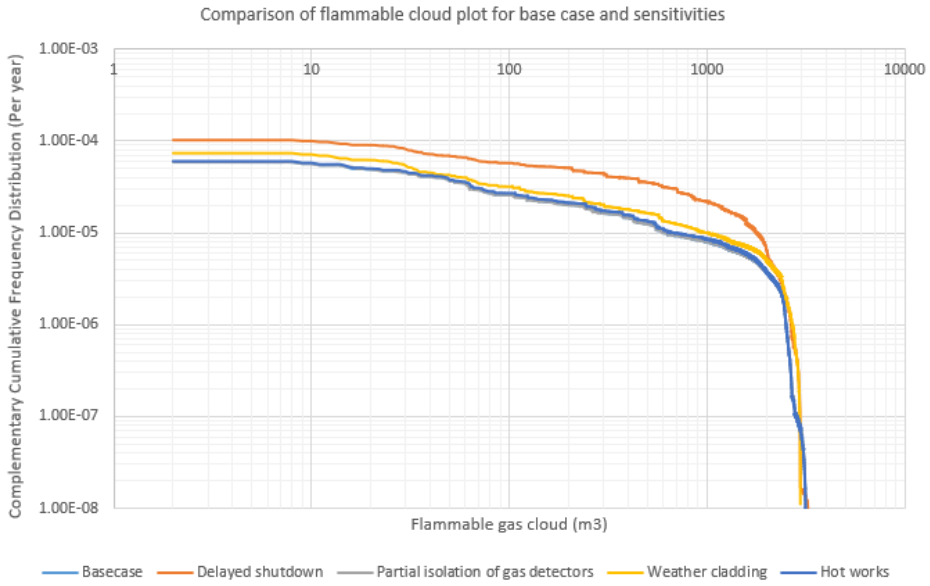

Figure 7.20: Comparison of flammable cloud volume for different leak scenarios.

Although the plots corresponding to different barriers depict minor changes in ignition probabilities, all the plots are between an order of magnitude of 10^{-4} and 10^{-5}.

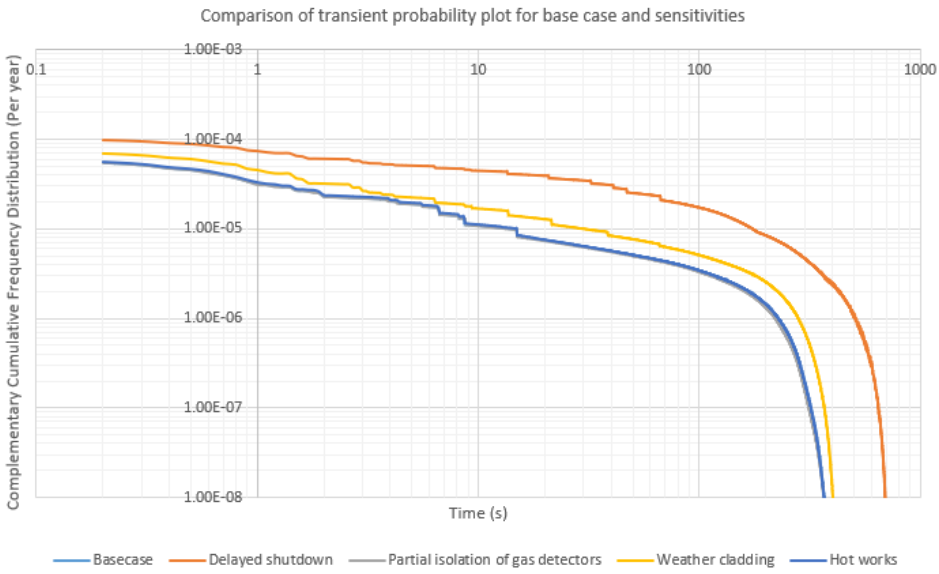

Figure 7.21: Transient cumulative frequency comparison for different leak scenarios.

All the above plots depict that "delays in shutdown time" has the maximum influence on the probabilities of ignition. The second highest influence is from the "temporary porous weather cladding" erected during winters to reduce the effects of cold winds while the crew are performing tasks in some exposed locations on-board the installations. "Hot works in one section of the module" has the third highest contribution to the complementary cumulative frequencies, which is marginally higher than the influence from "partial isolation of gas detectors". As explained in Section 6.2, for this module, there was no influence observed between the "base case" and "partial isolation of gas detectors" owing to the ratio between the size of the module and the number of detectors installed.

7.3.3 Comparison of various risk plots for the "hot-works in one section of the module" case

On the other hand, rather than neglecting the plots of the case "hot works in one section of the module", presented in Figure 7.16, Figure 7.17 and Figure 7.18, it would be reasonably practical to regard these plots as depicting instantaneous cumulative frequencies at any particular instant while the hot works are being performed.

While discussing about instantaneous risks, there could be many factors influencing the cumulative frequencies. Therefore, it is fair to add a small factors to account for such influences in the frequencies. Since the study presented by the Figure 2.5, shows a contribution of 56% from technical and human factors to the causation of leaks, the same factor of 0.56 is added as an influence to the complementary cumulative frequencies corresponding to the case "hot works in one section of the module". The resulting plots presented in the figures below compares the actual, corrected and instantaneous risk probabilities.

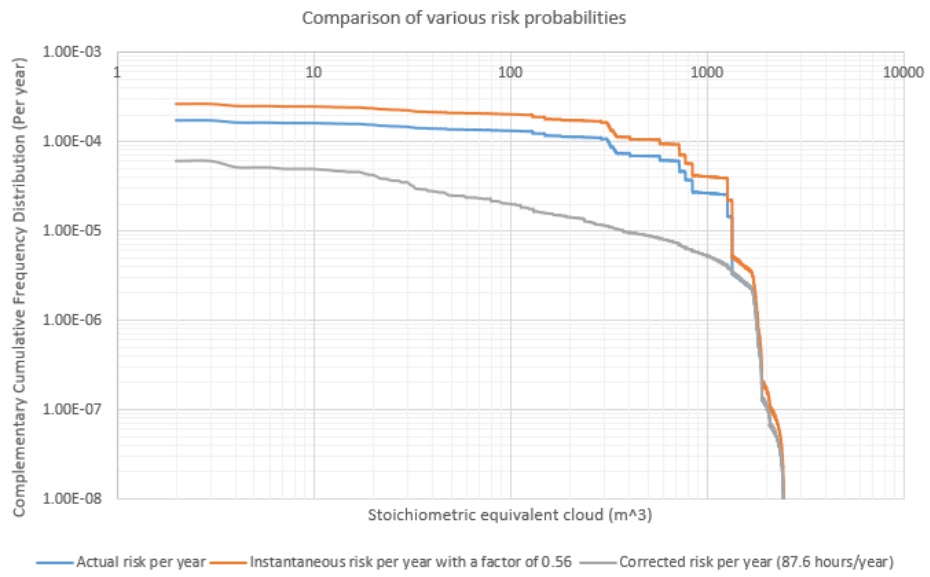

Figure 7.22: Comparison of stoichiometric equivalent volume for different leak scenarios.

The plots depict that the instantaneous risk probability, while any hot-work is in progress is the chosen section of the module is high with an order of magnitude 10^{-3}, beyond which the risk could be unacceptable.

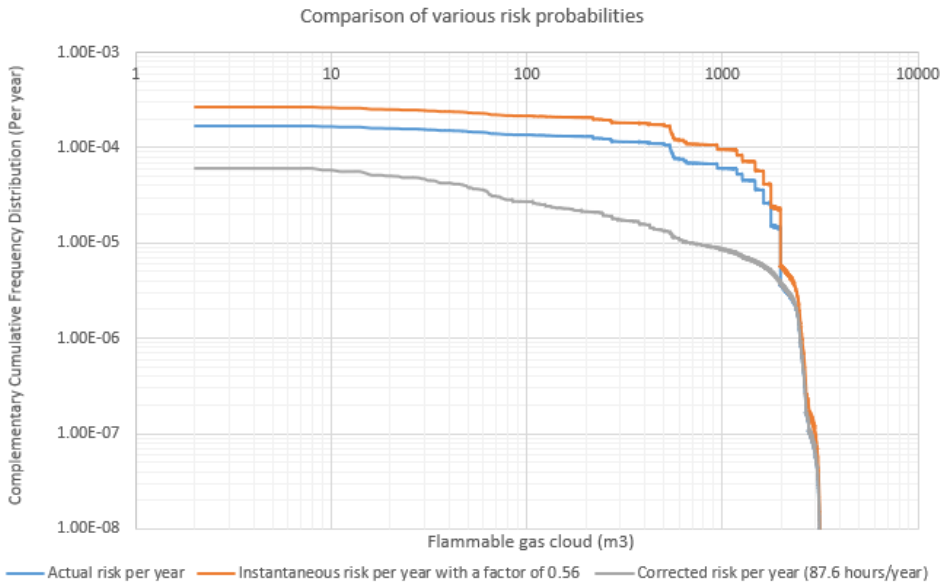

Figure 7.23: Comparison of flammable cloud volume for different leak scenarios.

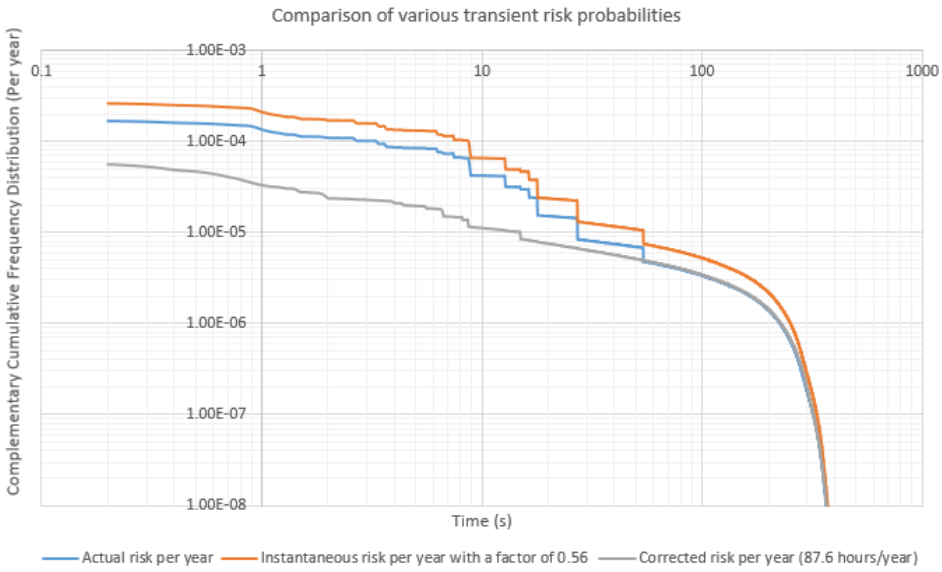

Figure 7.24: Transient cumulative frequency comparison for different leak scenarios.

The plots shown in Figure 7.22, Figure 7.23 and Figure 7.24 depict that the annual frequencies are of the order 10^{-4}. However, the instantaneous risk combined with a factor to account for technical and human errors is reasonably high.

7.4 Comparison of contribution from various sources

Since the results presented in Section 7.3.2 depicts the case of "delayed shutdown" as the highest contributor to cumulative frequencies, this section captures the which of the equipment contributes highest to the frequencies. This is done so as a comparison to the results of the base case scenario. Similar plots for rest of the scenarios depicting contribution from various sources are attached to Appendix 10.

7.4.1 Complementary cumulative frequency vs stoichiometric equivalent cloud (m^3)

The Figure 7.25 shows that the contribution from pump 2 and pump 3 has been highest, at least immediately after the release following which the contributions from pump 4, electrical equipment and generic sources seem high. However, in the case with delayed shutdown shown in Figure 7.26, initially the contribution from pump 2, pump 3 and generic sources have been high. In addition, the high contribution from generic sources seem to prolong until the cloud volume reached 1000 m^3 before plummeting down to negligible levels. The electrical equipment had also contributed for some prolonged period similar to the contributions from the generic sources.

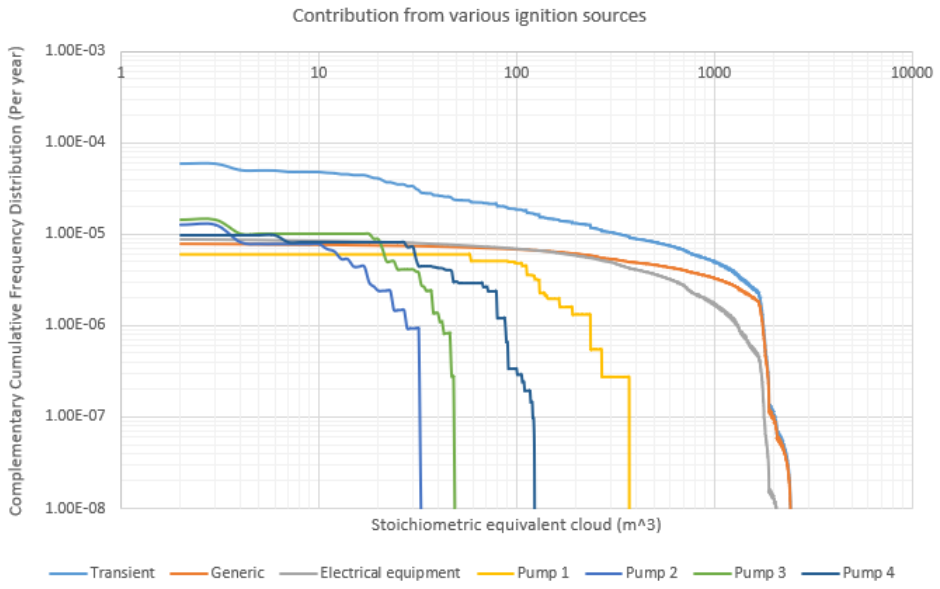

Figure 7.25: Base case - Cumulative frequency vs stoichiometric cloud contribution.

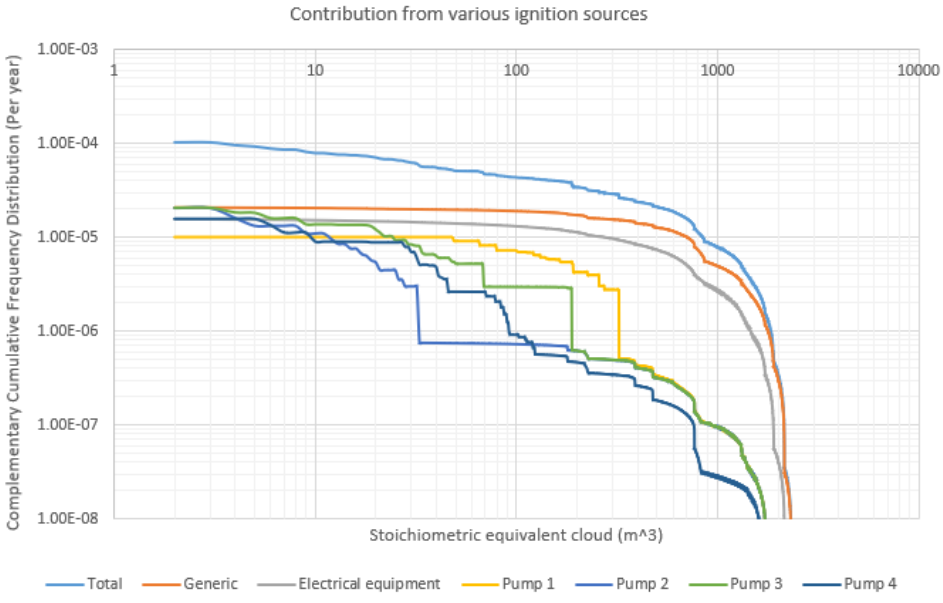

Figure 7.26: Delayed SD - Cumulative frequency vs stoichiometric cloud contribution.

7.4.2 Complementary cumulative frequency vs Flammable cloud (m^3)

This section presents the cumulative frequencies contribution by various sources with respect to flammable gas cloud volume.

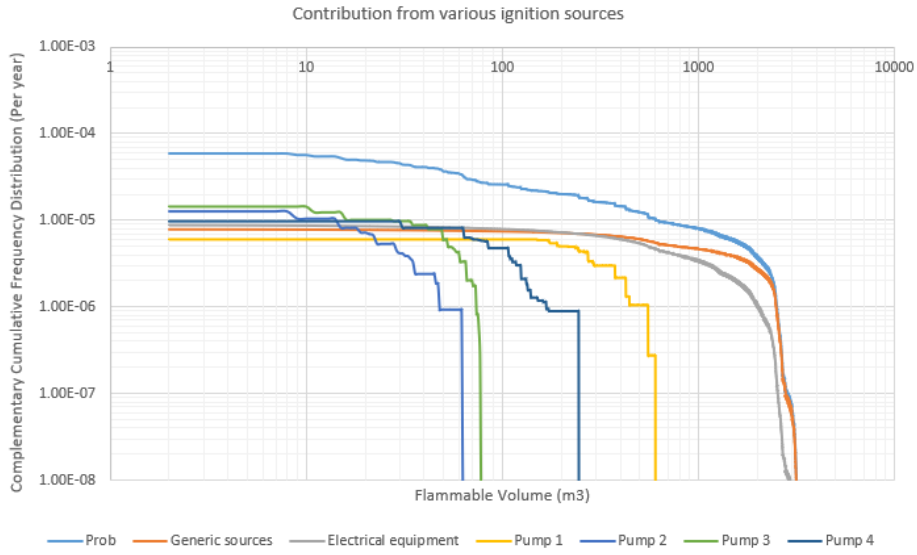

Figure 7.27: Base case - Cumulative frequency vs flammable cloud contribution.

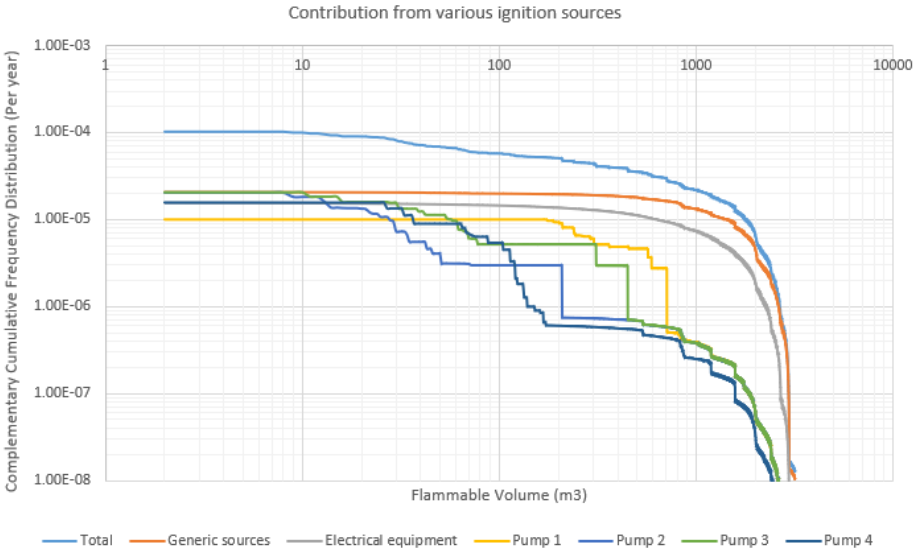

Figure 7.28: Delayed SD - Cumulative frequency vs flammable cloud contribution.

In the base case scenario shown in Figure 7.27, pumps 2 and 3 have contributed the highest initially followed by pump 4 and electrical equipment. Whereas in the case of delayed shutdown presented in Figure 7.28, pump 2, pump 3 and generic sources had contributed the highest with generic sources depicting prolonged contribution. The trend of prolonged contribution is also observed with the the electrical source contribution.

7.4.3 Transient distribution of complementary cumulative frequency

The contribution trend observed in the Section 7.4.1 and Section 7.4.2 is prominent also in the case of transient distribution in the base case scenario presented in Figure 7.29. The case with delays in shutdown time presented in Figure 7.30, the contribution from the generic sources clearly dominate the remaining sources and does so for a prolonged period of time. The rest of the plot follows a similar trend to that presented in Figure 7.28 and 7.26.

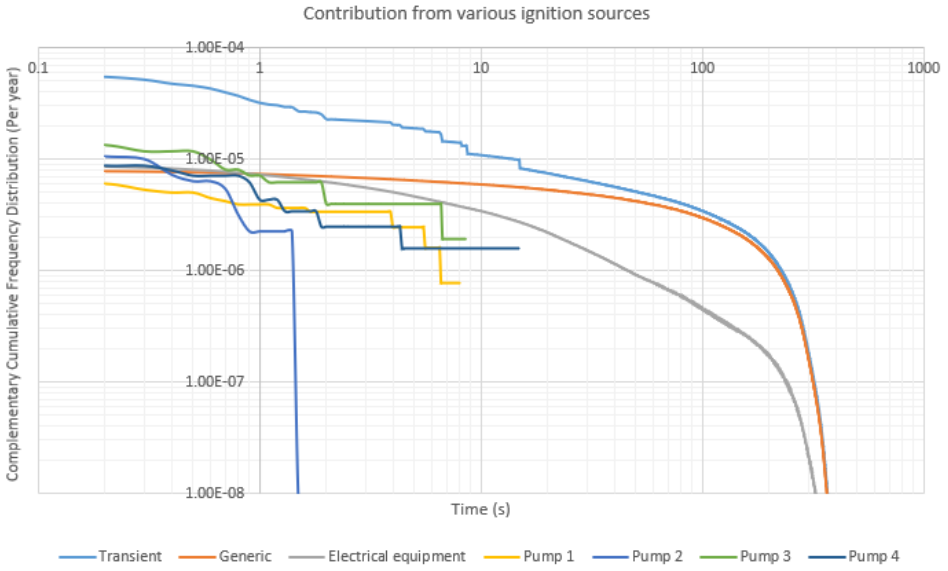

Figure 7.29: Base case - transient cumulative frequency contribution.

Figure 7.29 shows that there are possibilities of ignitions caused by various pumps in the module. Most of the ignitions tend to occur within 8 seconds from the start of the leak in the base case. This inference is in line with that put forward in the MISOF study.

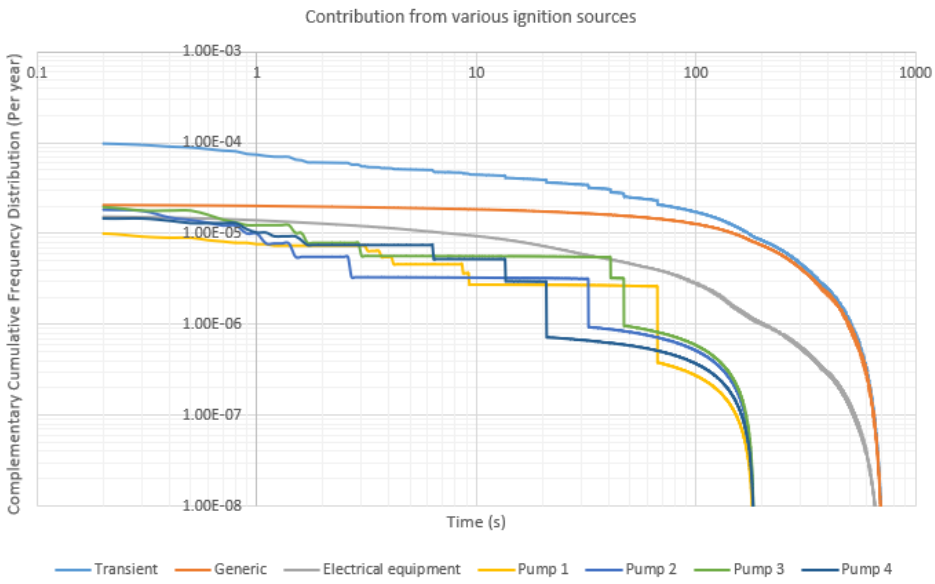

Figure 7.30: Delayed SD - transient cumulative frequency contribution..

The contribution plot for the case of delayed activation of shutdown presented in Figure 7.30, depicts possibilities of ignitions within 10 seconds from the start of the leak. In addition, the curves of contribution from the pumps shows possibilities of delayed ignitions that could occur between 10 and 70 seconds from the start of the leak. However, the cumulative frequencies of such event is quiet low of the order of magnitude between 10^{-5} and 10^{-6}.

By comparing the results of two simulations or group of simulations, this chapter has presented several inferences and insights gained from combined plots. Some key inferences gained through the study to identify the optimal grid resolution, influence of release location and direction, as well as the most influential barriers etc., could be regarded as valuable outputs of this thesis work. The rationale behind why some of these insights could prove to be meaningful to the owners of KFX, its users and to the CFD based dynamic risk analysis industry as a whole are delineated in the next chapter.

Chapter 8

Discussions

Since the results of the simulations have been presented, compared and thoroughly discussed in the chapters 6 and 7, this chapter discusses the validity of the results obtained in terms of its quality and some of the constraints to this thesis work.

The first and foremost limitation of this study is the size of the module subjected to various simulations. Being a relatively small module with a volume of 4000 m^3, the generated results may not hold accurately good to some of the biggest modules located in NCS. Secondly, the simulations were executed with a very finite combination of six leak rates, four wind speeds and two wind directions based on past trends and practical assumptions. The fact that in reality these parameters could combine in an infinite number of ways is unaccounted for in this thesis work. Finally, KFX being a software which is being constantly developed could possess some inherent levels of inaccuracies in its calculations and result generations. These aforementioned factors could present a certain degree of uncertainty to the thesis work as a whole. However, considering that the standard version of KFX has been commercial for some years now, and the results generated from it have been generally accepted and used as a decision support tool by some leading oil and gas operators in Norway, the value of the results generated in this thesis work cannot be deemed insignificant.

The experiment carried out to identify the optimal grid resolution that could be sufficient enough to yield good quality results within the shortest possible time has produced results of high significance. The generated results adds value not only to this thesis, but also to the KFX users within the industry and the owners of the software. One could argue that choosing optimal number of grids depends on the size and complexity of the module as well as the domain of interest within the chosen module. However, the conclusion of this experiment that the grid resolution is a function of leak rate could serve as a rule of thumb to KFX users, thereby enabling them to narrow down on the number of grids to be chosen. This would also partially eliminate the need to run multiple simulations just to optimize the resolution. Since the courant number factor in KFX could be manipulated to

increase the number of time steps, this result also helps to understand how and when to push the limits of KFX codes. Hence, this result, if perceived well, not only saves simulation time, but also contributes to the reputation of the software tool among the oil and gas operators globally by serving as a quick decision support tool.

As a result of subjecting the chosen module to numerous simulations incorporated with various critical barriers, a number of valuable insights were gained. The positive influence on the cumulative frequencies due to the erection of porous weather shielding sets aside a clear need to develop alternative methods to tackle the effects of cold winds during winters. This would answer the question as to whether or not to increase the ventilation if erection of weather cladding was inevitable. The results of the case "Hot works in a section of the module" has depicted an increase in the instantaneous risk figure when coupled with a small fraction in order to account for technical and human errors. This risk picture would certainly increase if there would be other activities in the same module in the near vicinity of hot works. Hence, the need to ensure that there shall be no other activities carried out simultaneously with hot works in the same module is clearly evident.

The combined plots showing the effects of various barriers in influencing the complementary cumulative frequencies is a very useful result to understand the hierarchy of barriers in terms of influencing ability. These plots could serve as guidelines in perceiving which of the barriers, if failed, would contribute the most to the probability of ignition. This information is necessary to strengthen the safety measures with the module by utilizing barriers in combinations.

One of the sub-study carried out was to identify the influence of release point and release direction on the ignition probabilities in the module. The results depicted a significant influence of the two aforementioned aspects on ignition probability. This results will certainly be valuable to enhance the understanding on the number of barriers required in a particular location in the module depending on the levels of natural ventilation available at that location.

Finally, this thesis work proved to be beneficial to the owners of the software in more than one way. Since certain features of KFX-RBM is still under development, there were some bugs encountered with the software tool during the span of this study. The developers of the software quoted that some of the bugs were unique and known to have never occurred before. The uniqueness of some of the bugs rendered fixing the bugs challenging as well as time consuming, yet, it proved to be beneficial for the owners as it contributed to the robustness of the software tool. Some of the bugs encountered are mentioned below:

- **Quick run wizard** - Upon selecting the composition of the fuel and pushing the calculate button, the code could not generate the formula of composite fuel. This rendered that the case files could not be generated and subsequently, the simulation could not be initiated.

- **KFX View** - As it is essential to choose the exact point of release from the module using KFX View window, the geometry file seemed to vanish when the model was

zoomed-in to inspect/select the release point. This rendered that the leak point could not be accurately chosen unless the co-ordinates were known.

- **Powerscan** - "Powerscan" is a tool used to generate flow script files which are essential for running simulations. This feature was not functioning as intended from the KFX RBM license installed at Safetec. This rendered that the scenario ".scn" and the geometry files had to be sent to DNV GL, just to run "powerscan" and re-send the files back to Safetec to initiate the simulations.
- **Gnuplot** - Gnuplot is a feature in KFX that enables plotting of various graphical result files. While trying to plot transient files using gnuplot feature, the Y-axis of the combined transient plot seemed erroneous. For example: The Y-axis was depicting leak rates of the order 10^{12}, which was clearly erroneous.

In addition to the aforementioned issues which were purely software-related, there were other issues that induced delays in running the simulations. Some of them are issues establishing a separate terminal for KFX-RBM, terminal not working as intended, cluster being overloaded which rendered that any new cases for submission had to wait for days before they actually began to run, crashing of server when the simulations were more than half completed etc. Some of these issues were very practical and resolved itself with time or with little assistance.

This study, comprising of eight different scenarios which consists of 278 separate cases were run just using 8 nodes in the server, which was a major factor affecting the simulation time. Despite being plagued with some inevitable constraints during the execution of simulations, the quality of insights gained through this study could not be deemed insignificant.

Chapter 9

Conclusions and Future work

This chapter summarises some of the important finding that emerged through this strenuous thesis plagued with numerous practical and software-related challenges along the way. In addition, this chapter also presents some recommendations for potential future work that could be carried out.

9.1 Conclusions

As a result of performing numerous simulations in order to quantify the effect of some of the critical barriers that are governing ignition control, the study has stumbled into some interesting findings as listed below:

- Among the barriers analysed, it was identified that case with "delayed activation of ESD" assuming that the shut down had to be activated manually, had the highest influence on the ignition probabilities. This validates the importance of gas detection and automatic triggering of ESD system at the earliest possible time.
- Experimenting with various grid resolutions inferred that the grid resolution is a function of leak rate. Beyond a leak rate of 32 kg/s, the results presented insignificant deviations between the grid resolution of 200000 and 75000. The key take away here is that the simulation time was reduced significantly with the quality of results remaining reasonably accurate.
- The results of the simulations carried out by changing the leak point and leak direction within the same module, depicted a significant influence on the probabilities of ignition of an order between 5 and 6. This points out the need further investigate the ways to optimize the placement of barriers based on the criticality of locations within the modules.
- A significant difference was observed between the comparison of risk-per-year with 1% of hot-work days per year and the instantaneous risk at any given instant during

the hot-work. Since the instantaneous risk is of an order of magnitude that is close to be regarded unacceptable, it necessitates a recommendation that there shall be no other activity performed in the same module where hot-works are underway.

- The simulation carried out by partially isolating the number of gas detectors did not depict any significant changes in the risk picture. This result may not hold good for much bigger and complex modules, wherein re-simulations are recommended.

- It was observed that the erection of porous weather cladding does have some influence in driving up the ignition probabilities. Although not significant, it is recommended to consider increasing the ventilation measures if erecting such protections are inevitable.

Finally, by stumbling into some unique bugs in the software tool, KFX-RBM, and by notifying the developers to analyse and fix them, the study contributed towards making the software tool robust.

9.2 Future work

The biggest constraint, the"time", has pushed a number of analysis and simulations to be summarised in this section, which could have otherwise been a part of this thesis work. Listed below are some simulation cases, which I felt would be practical to study and analyse its effects.

- Firstly, since this study utilized a reasonably small module and smaller boundary conditions for the performed simulations, it would be interesting to perform similar study with a relatively bigger module with increased boundary conditions. The effect of isolating partially isolating the gas detectors in bigger modules could be studied.

- Secondly, if provided with a possibility of running simulations with more number of nodes, the same set of simulations could be re-run with more scenarios. In this way, the accuracy of the study could be increased by considering more wind speeds, wind directions and release rates. This could result in a sub-study to identify the optimal number of cases required to produce results that could account for all the reasonably practicable wind speeds and wind directions.

- Subsequently, it would be interesting to simulate and study the effect of gas detectors and their air intake could have on the ignition and explosion probabilities. If performed accurately, this study has the potential to question the distance of hazardous zone for air intakes followed in most of the installations in the NCS as of today.

- Finally, simulations could be set-up to study the effect of hot-works in multiple locations in the same module. In addition, the effect of heat loads on the adjacent modules as a result of leaving the fire proof doors open could also be studied.

Bibliography

[1] International Energy Agency. World enerygy outlook 2019, 2019. URL https://www.iea.org/statistics/.

[2] B.Grimsmo N.I. Lilleheie K.E. Rian R. Olsen B. Lakså V. Nilsen J.E. Vembe T Evanger B.E. Vembe, R.N. Kleiveland. Kfx - user manual, 2017.

[3] B.Grimsmo N.I. Lilleheie K.E. Rian T. Myhrvold B.E. Vembe, J.K.Holen. Kfx - theory manual, 2001.

[4] B.Lakså B.Grimsmo N.I. Lilleheie R.N. Kleiveland T. Evanger B.E. Vembe, K.E.Rian. Kfx - validation handbook, 2016.

[5] United Nations Population division. World population prospects 2019, 2019. URL https://population.un.org/wpp/Graphs/Probabilistic/POP.

[6] United States EIA. World fuel production and consumption forecast, 2019. URL https://www.eia.gov/outlooks/steo/report/global_oil.php.

[7] EquinorAS. Accident investigation of heimdal hydrocarbon leaks 2012, 2012. URL https://www.equinor.com/no/news/archive/2012/Granskning.

[8] A.O. Sæbø I Fossan. Process leak for offshore installations frequency assessment model - plofam, 2018.

[9] Are Opstad Sæbø Ingar Fossan. Modelling of ignition sources on offshore oil and gas facilities - misof(2), 2018.

[10] Randall J LeVeque et al. *Finite volume methods for hyperbolic problems*, volume 31. Cambridge university press, 2002.

[11] B.F. Magnussen and Bjørn Hjertager. On mathematically modeling with special emphasis on soot formation and combustion. 16:719–728, 08 1977.

[12] Aud Nistov. Process safety performance indicators for major accident prevention, 2012.

[13] K. Gloppestad O.M. Nyheim S. Haugen J.E. Vinnem T. Zhu N.J. Edwin, O. Brautset. Modelling instantaneous risk for major accident prevention, 2017.

[14] Petroleum Safety Authority of Norway. Trends in risk level in petroleum activity. URL https://www.ptil.no/contentassets.

[15] Petroleum Safety Authority of Norway. Heimdal accident investigation report, 2012. URL https://www.norskoljeoggass.no/globalassets/dokumenter/2012_966_granskingsrapport-heimdal.pdf.

[16] Petroleum Safety Authority of Norway. Trends of risk level in norwegian petroleum activities, 2019.

[17] International Association of Oil and Gas Producers (IOGP). Safety performance indicators-process safety events – 2018 data. URL https://www.iogp.org/bookstore.

[18] International Association of Oil and Gas Producers (IOGP). Process safety, 2008. URL https://www.iogp.org/oil-and-gas-safety/process-safety/.

[19] Oil and UK Gas. The health and safety report 2018, 2018. URL https://oilandgasuk.cld.bz/Health-Safety-Report-2018/2/.

[20] The Norwegian Oil and Gas. Statement from the norwegian oil and gas association, 2012. URL http://www.csb.gov/userfiles/file/statement.pdf.

[21] Hamid Omidvarborna, Ashok Kumar, and Dong-Shik Kim. Recent studies on soot modeling for diesel combustion. *Renewable and Sustainable Energy Reviews*, 48: 635–647, 2015.

[22] Norwegian Petroleum. Norwegian historical production forecast., 2019. URL https://www.norskpetroleum.no/en/facts/historical-production/.

[23] Stephen B Pope. Turbulent flows, 2001.

[24] Marvin Rausand. *Risk assessment: theory, methods, and applications*, volume 115. John Wiley & Sons, 2013.

[25] G Saikrishna and J.E Vinnem. Influence of human-organisational factors in major hydrocarbon leaks in norwegian continental shelf. 2019.

[26] Statista. Number of offshore rigs worldwide - 2018., 2018. URL https://www.statista.com/statistics/279100/number-of-offshore-rigs-worldwide-by-region/.

[27] PA Tesner. Formation of soot particles. In *Faraday Symposia of the Chemical Society*. Royal Society of Chemistry, 1973.

[28] Henk Kaarle Versteeg and Weeratunge Malalasekera. *An introduction to computational fluid dynamics: the finite volume method*. Pearson education, 2007.

[29] Jan-Erik Vinnem. *Offshore risk assessment: principles, modelling and applications of QRA studies*. Springer Science & Business Media, 2013.

[30] Jan Erik Vinnem and Willy Røed. Root causes of hydrocarbon leaks on offshore petroleum installations. *Journal of Loss Prevention in the Process Industries*, 2015.

[31] Jan Erik Vinnem, Jorunn Seljelid, Stein Haugen, Snorre Sklet, and Terje Aven. Generalised methodology for operational risk analysis. In *Proceedings of ESREL*, 2007.

Chapter 10

Appendix

Appendix A - Man Technology Organization diagram

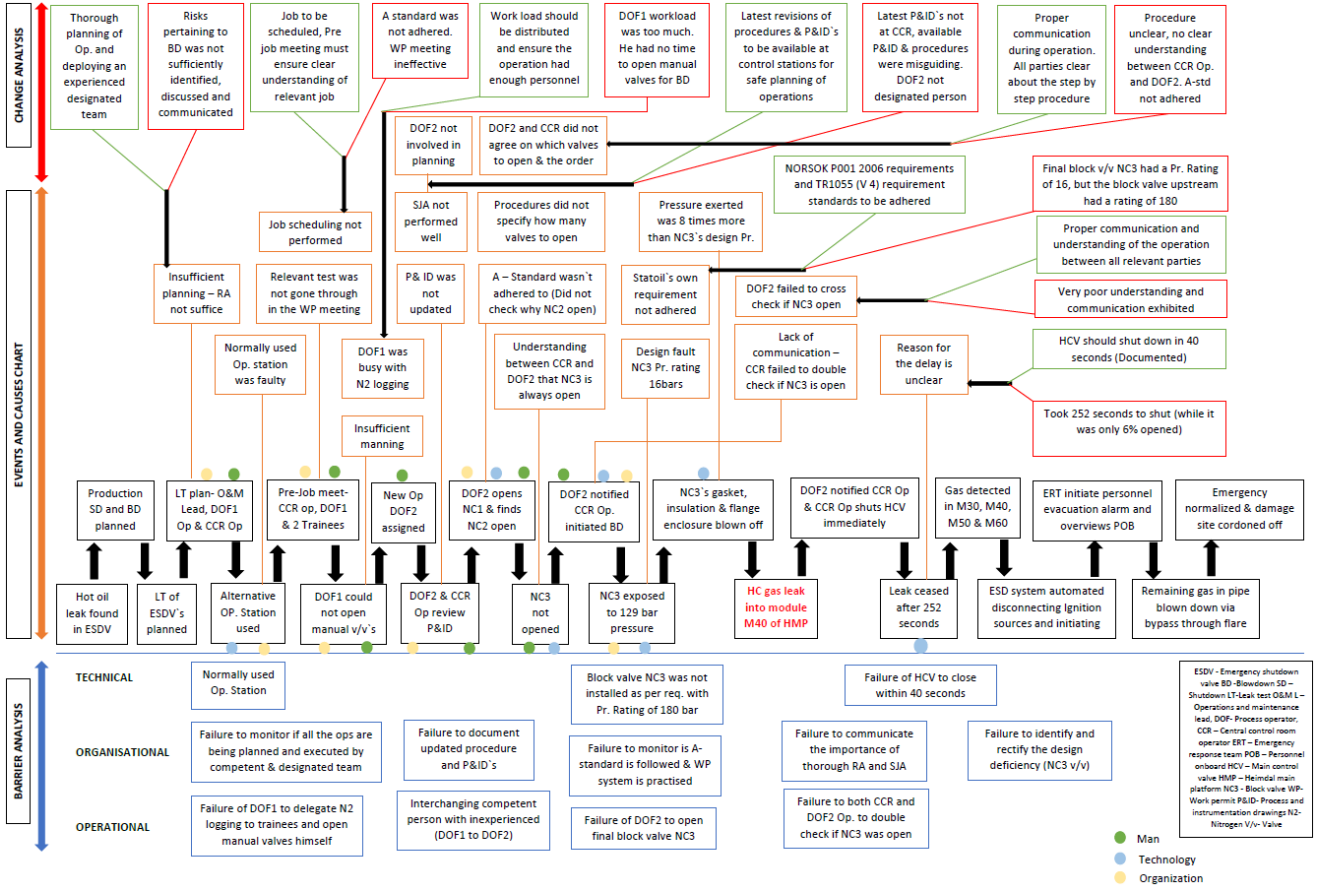

Figure 10.1: Heimdal - MTO analysis

Appendix B - Number of offshore installations operating worldwide

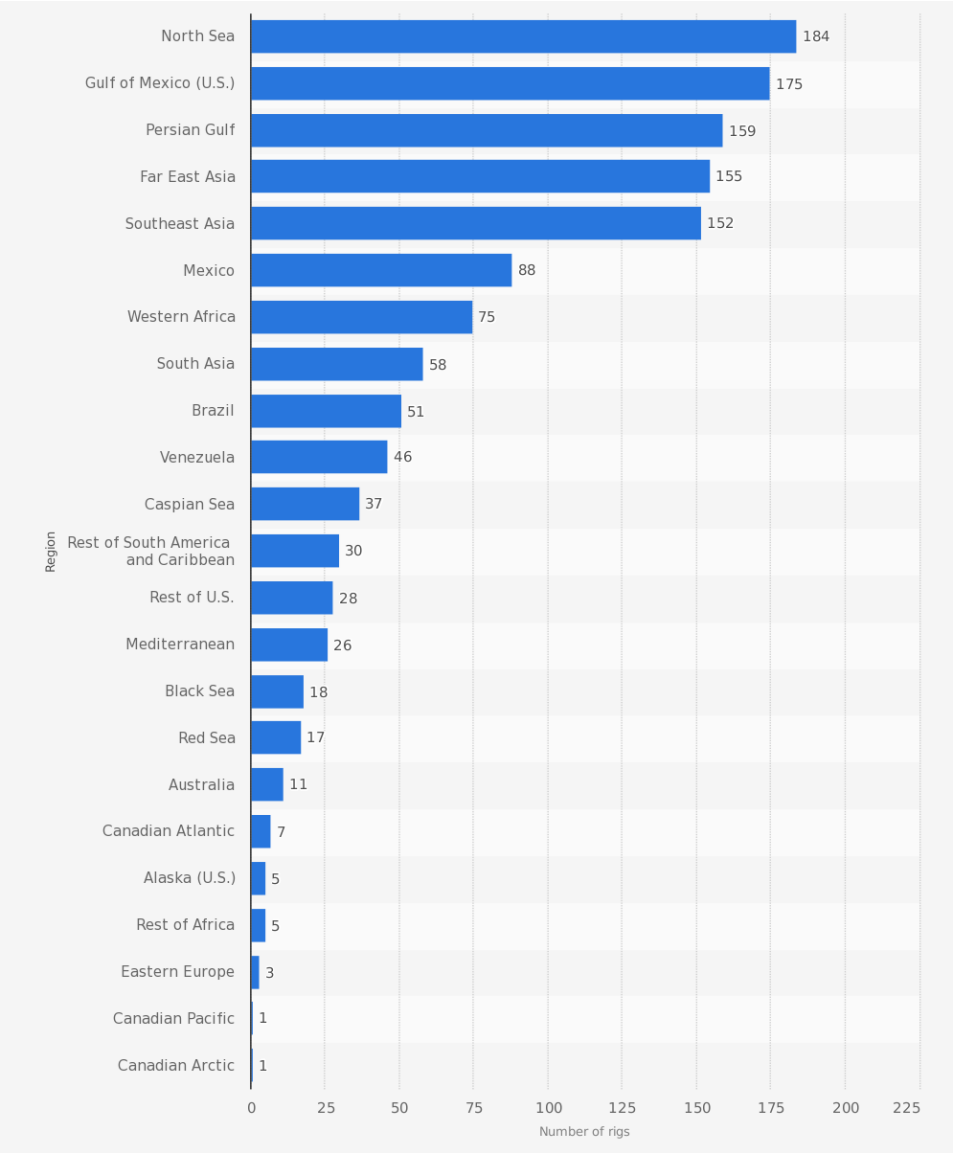

Figure 10.2: Number of offshore rigs operating worldwide as of January 2018 by region, Source: Statista, [26].

Appendix C - List of scenarios simulated

Module	
Name	CM42EW
Length	30 meters
Breadth	16 meters
Height	8 meters
Volume	4000 cubic meters
Open walls	East & West

Table 10.1: Dimensions and size of module CM42EW.

Leak Point A	X=15.502, Y=7.9996, Z=4.6937
Leak Point B	X=5.40, Y=9.58, Z=0.74

Table 10.2: Coordinates for leak points in the module CM42EW.

ID	Module	Leak Point	Leak direction	Wind direction	Wind speed (m/s)	Fluid	Leak rate (Kg/s)
1	CM42EW	A	(0,0,-1)	120	2	Gas	0.5
2	CM42EW	A	(0,0,-1)	120	8	Gas	0.5
3	CM42EW	A	(0,0,-1)	120	12	Gas	0.5
4	CM42EW	A	(0,0,-1)	315	2	Gas	0.5
5	CM42EW	A	(0,0,-1)	315	8	Gas	0.5
6	CM42EW	A	(0,0,-1)	315	12	Gas	0.5
7	CM42EW	A	(0,0,-1)	120	2	Gas	2
8	CM42EW	A	(0,0,-1)	120	8	Gas	2
9	CM42EW	A	(0,0,-1)	120	12	Gas	2
10	CM42EW	A	(0,0,-1)	315	2	Gas	2
11	CM42EW	A	(0,0,-1)	315	8	Gas	2
12	CM42EW	A	(0,0,-1)	315	12	Gas	2
13	CM42EW	A	(0,0,-1)	120	2	Gas	8
14	CM42EW	A	(0,0,-1)	120	8	Gas	8
15	CM42EW	A	(0,0,-1)	120	12	Gas	8
16	CM42EW	A	(0,0,-1)	315	2	Gas	8
17	CM42EW	A	(0,0,-1)	315	8	Gas	8
18	CM42EW	A	(0,0,-1)	315	12	Gas	8
19	CM42EW	A	(0,0,-1)	120	2	Gas	32
20	CM42EW	A	(0,0,-1)	120	8	Gas	32
21	CM42EW	A	(0,0,-1)	120	12	Gas	32
22	CM42EW	A	(0,0,-1)	315	2	Gas	32
23	CM42EW	A	(0,0,-1)	315	8	Gas	32
24	CM42EW	A	(0,0,-1)	315	12	Gas	32
25	CM42EW	A	(0,0,-1)	120	2	Gas	128
26	CM42EW	A	(0,0,-1)	120	8	Gas	128
27	CM42EW	A	(0,0,-1)	120	12	Gas	128
28	CM42EW	A	(0,0,-1)	315	2	Gas	128
29	CM42EW	A	(0,0,-1)	315	8	Gas	128
30	CM42EW	A	(0,0,-1)	315	12	Gas	128
31	CM42EW	A	(0,0,-1)	120	2	Gas	512
32	CM42EW	A	(0,0,-1)	120	8	Gas	512
33	CM42EW	A	(0,0,-1)	120	12	Gas	512
34	CM42EW	A	(0,0,-1)	315	2	Gas	512
35	CM42EW	A	(0,0,-1)	315	8	Gas	512
36	CM42EW	A	(0,0,-1)	315	12	Gas	512
37	CM42EW	A	(0,0,-1)	120	18	Gas	0.5
38	CM42EW	A	(0,0,-1)	315	18	Gas	0.5
39	CM42EW	A	(0,0,-1)	120	18	Gas	512
40	CM42EW	A	(0,0,-1)	315	18	Gas	512

Table 10.3: Base case scenarios with grid resolution 200000 and Courant number 10

ID	Module	Leak Point	Leak direction	Wind direction	Wind speed (m/s)	Fluid	Leak rate (Kg/s)
41	CM42EW	A	zn	120	2	Gas	2
42	CM42EW	A	zn	120	8	Gas	2
43	CM42EW	A	zn	120	12	Gas	2
44	CM42EW	A	zn	315	2	Gas	2
45	CM42EW	A	zn	315	8	Gas	2
46	CM42EW	A	zn	315	12	Gas	2
47	CM42EW	A	zn	120	2	Gas	8
48	CM42EW	A	zn	120	8	Gas	8
49	CM42EW	A	zn	120	12	Gas	8
50	CM42EW	A	zn	315	2	Gas	8
51	CM42EW	A	zn	315	8	Gas	8
52	CM42EW	A	zn	315	12	Gas	8
53	CM42EW	A	zn	120	2	Gas	32
54	CM42EW	A	zn	120	8	Gas	32
55	CM42EW	A	zn	120	12	Gas	32
56	CM42EW	A	zn	315	2	Gas	32
57	CM42EW	A	zn	315	8	Gas	32
58	CM42EW	A	zn	315	12	Gas	32
59	CM42EW	A	zn	120	2	Gas	128
60	CM42EW	A	zn	120	8	Gas	128
61	CM42EW	A	zn	120	12	Gas	128
62	CM42EW	A	zn	315	2	Gas	128
63	CM42EW	A	zn	315	8	Gas	128
64	CM42EW	A	zn	315	12	Gas	128
65	CM42EW	A	zn	120	2	Gas	512
66	CM42EW	A	zn	120	8	Gas	512
67	CM42EW	A	zn	120	12	Gas	512
68	CM42EW	A	zn	315	2	Gas	512
69	CM42EW	A	zn	315	8	Gas	512
70	CM42EW	A	zn	315	12	Gas	512
71	CM42EW	A	zn	120	2	Gas	0.5
72	CM42EW	A	zn	315	8	Gas	0.5
73	CM42EW	A	zn	120	12	Gas	512
74	CM42EW	A	zn	315	2	Gas	512

Table 10.4: Base case re-run with grid resolution 125000 and Courant number Max

ID	Module	Leak Point	Leak direction	Wind direction	Wind speed (m/s)	Fluid	Leak rate (Kg/s)
75	CM42EW	A	zn	120	2	Gas	2
76	CM42EW	A	zn	120	8	Gas	2
77	CM42EW	A	zn	120	12	Gas	2
78	CM42EW	A	zn	315	2	Gas	2
79	CM42EW	A	zn	315	8	Gas	2
80	CM42EW	A	zn	315	12	Gas	2
81	CM42EW	A	zn	120	2	Gas	8
82	CM42EW	A	zn	120	8	Gas	8
83	CM42EW	A	zn	120	12	Gas	8
84	CM42EW	A	zn	315	2	Gas	8
85	CM42EW	A	zn	315	8	Gas	8
86	CM42EW	A	zn	315	12	Gas	8
87	CM42EW	A	zn	120	2	Gas	32
88	CM42EW	A	zn	120	8	Gas	32
89	CM42EW	A	zn	120	12	Gas	32
90	CM42EW	A	zn	315	2	Gas	32
91	CM42EW	A	zn	315	8	Gas	32
92	CM42EW	A	zn	315	12	Gas	32
93	CM42EW	A	zn	120	2	Gas	128
94	CM42EW	A	zn	120	8	Gas	128
95	CM42EW	A	zn	120	12	Gas	128
96	CM42EW	A	zn	315	2	Gas	128
97	CM42EW	A	zn	315	8	Gas	128
98	CM42EW	A	zn	315	12	Gas	128
99	CM42EW	A	zn	120	2	Gas	512
100	CM42EW	A	zn	120	8	Gas	512
101	CM42EW	A	zn	120	12	Gas	512
102	CM42EW	A	zn	315	2	Gas	512
103	CM42EW	A	zn	315	8	Gas	512
104	CM42EW	A	zn	315	12	Gas	512
105	CM42EW	A	zn	120	2	Gas	0.5
106	CM42EW	A	zn	315	8	Gas	0.5
107	CM42EW	A	zn	120	12	Gas	512
108	CM42EW	A	zn	315	2	Gas	512

Table 10.5: Base case re-run with grid resolution 75000 and Courant number Max

ID	Module	Leak Point	Leak direction	Wind direction	Wind speed (m/s)	Fluid	Leak rate (Kg/s)
109	CM42EW	A	zn	120	2	Gas	2
110	CM42EW	A	zn	120	8	Gas	2
111	CM42EW	A	zn	120	12	Gas	2
112	CM42EW	A	zn	315	2	Gas	2
113	CM42EW	A	zn	315	8	Gas	2
114	CM42EW	A	zn	315	12	Gas	2
115	CM42EW	A	zn	120	2	Gas	8
116	CM42EW	A	zn	120	8	Gas	8
117	CM42EW	A	zn	120	12	Gas	8
118	CM42EW	A	zn	315	2	Gas	8
119	CM42EW	A	zn	315	8	Gas	8
120	CM42EW	A	zn	315	12	Gas	8
121	CM42EW	A	zn	120	2	Gas	32
122	CM42EW	A	zn	120	8	Gas	32
123	CM42EW	A	zn	120	12	Gas	32
124	CM42EW	A	zn	315	2	Gas	32
125	CM42EW	A	zn	315	8	Gas	32
126	CM42EW	A	zn	315	12	Gas	32
127	CM42EW	A	zn	120	2	Gas	128
128	CM42EW	A	zn	120	8	Gas	128
129	CM42EW	A	zn	120	12	Gas	128
130	CM42EW	A	zn	315	2	Gas	128
131	CM42EW	A	zn	315	8	Gas	128
132	CM42EW	A	zn	315	12	Gas	128
133	CM42EW	A	zn	120	2	Gas	512
134	CM42EW	A	zn	120	8	Gas	512
135	CM42EW	A	zn	120	12	Gas	512
136	CM42EW	A	zn	315	2	Gas	512
137	CM42EW	A	zn	315	8	Gas	512
138	CM42EW	A	zn	315	12	Gas	512
139	CM42EW	A	zn	120	2	Gas	0.5
140	CM42EW	A	zn	315	8	Gas	0.5
141	CM42EW	A	zn	120	12	Gas	512
142	CM42EW	A	zn	315	2	Gas	512

Table 10.6: Module with a temporary weather cladding with grid resolution 125000 and Courant number Max

ID	Module	Leak Point	Leak direction	Wind direction	Wind speed (m/s)	Fluid	Leak rate (Kg/s)
143	CM42EW	A	zn	120	2	Gas	2
144	CM42EW	A	zn	120	8	Gas	2
145	CM42EW	A	zn	120	12	Gas	2
146	CM42EW	A	zn	315	2	Gas	2
147	CM42EW	A	zn	315	8	Gas	2
148	CM42EW	A	zn	315	12	Gas	2
149	CM42EW	A	zn	120	2	Gas	8
150	CM42EW	A	zn	120	8	Gas	8
151	CM42EW	A	zn	120	12	Gas	8
152	CM42EW	A	zn	315	2	Gas	8
153	CM42EW	A	zn	315	8	Gas	8
154	CM42EW	A	zn	315	12	Gas	8
155	CM42EW	A	zn	120	2	Gas	32
156	CM42EW	A	zn	120	8	Gas	32
157	CM42EW	A	zn	120	12	Gas	32
158	CM42EW	A	zn	315	2	Gas	32
159	CM42EW	A	zn	315	8	Gas	32
160	CM42EW	A	zn	315	12	Gas	32
161	CM42EW	A	zn	120	2	Gas	128
162	CM42EW	A	zn	120	8	Gas	128
163	CM42EW	A	zn	120	12	Gas	128
164	CM42EW	A	zn	315	2	Gas	128
165	CM42EW	A	zn	315	8	Gas	128
166	CM42EW	A	zn	315	12	Gas	128
167	CM42EW	A	zn	120	2	Gas	512
168	CM42EW	A	zn	120	8	Gas	512
169	CM42EW	A	zn	120	12	Gas	512
170	CM42EW	A	zn	315	2	Gas	512
171	CM42EW	A	zn	315	8	Gas	512
172	CM42EW	A	zn	315	12	Gas	512
173	CM42EW	A	zn	120	2	Gas	0.5
174	CM42EW	A	zn	315	8	Gas	0.5
175	CM42EW	A	zn	120	12	Gas	512
176	CM42EW	A	zn	315	2	Gas	512

Table 10.7: Module with partially isolated gas detectors with grid resolution 125000 and Courant number Max

ID	Module	Leak Point	Leak direction	Wind direction	Wind speed (m/s)	Fluid	Leak rate (Kg/s)
177	CM42EW	B	xp	120	2	Gas	2
178	CM42EW	B	xp	120	8	Gas	2
179	CM42EW	B	xp	120	12	Gas	2
180	CM42EW	B	xp	315	2	Gas	2
181	CM42EW	B	xp	315	8	Gas	2
182	CM42EW	B	xp	315	12	Gas	2
183	CM42EW	B	xp	120	2	Gas	8
184	CM42EW	B	xp	120	8	Gas	8
185	CM42EW	B	xp	120	12	Gas	8
186	CM42EW	B	xp	315	2	Gas	8
187	CM42EW	B	xp	315	8	Gas	8
188	CM42EW	B	xp	315	12	Gas	8
189	CM42EW	B	xp	120	2	Gas	32
190	CM42EW	B	xp	120	8	Gas	32
191	CM42EW	B	xp	120	12	Gas	32
192	CM42EW	B	xp	315	2	Gas	32
193	CM42EW	B	xp	315	8	Gas	32
194	CM42EW	B	xp	315	12	Gas	32
195	CM42EW	B	xp	120	2	Gas	128
196	CM42EW	B	xp	120	8	Gas	128
197	CM42EW	B	xp	120	12	Gas	128
198	CM42EW	B	xp	315	2	Gas	128
199	CM42EW	B	xp	315	8	Gas	128
200	CM42EW	B	xp	315	12	Gas	128
201	CM42EW	B	xp	120	2	Gas	512
202	CM42EW	B	xp	120	8	Gas	512
203	CM42EW	B	xp	120	12	Gas	512
204	CM42EW	B	xp	315	2	Gas	512
205	CM42EW	B	xp	315	8	Gas	512
206	CM42EW	B	xp	315	12	Gas	512
207	CM42EW	B	xp	120	2	Gas	0.5
208	CM42EW	B	xp	315	8	Gas	0.5
209	CM42EW	B	xp	120	12	Gas	512
210	CM42EW	B	xp	315	2	Gas	512

Table 10.8: Base case with different leak point and leak direction with grid resolution 125000 and Courant number Max

ID	Module	Leak Point	Leak direction	Wind direction	Wind speed (m/s)	Fluid	Leak rate (Kg/s)
211	CM42EW	A	zn	120	2	Gas	2
212	CM42EW	A	zn	120	8	Gas	2
213	CM42EW	A	zn	120	12	Gas	2
214	CM42EW	A	zn	315	2	Gas	2
215	CM42EW	A	zn	315	8	Gas	2
216	CM42EW	A	zn	315	12	Gas	2
217	CM42EW	A	zn	120	2	Gas	8
218	CM42EW	A	zn	120	8	Gas	8
219	CM42EW	A	zn	120	12	Gas	8
220	CM42EW	A	zn	315	2	Gas	8
221	CM42EW	A	zn	315	8	Gas	8
222	CM42EW	A	zn	315	12	Gas	8
223	CM42EW	A	zn	120	2	Gas	32
224	CM42EW	A	zn	120	8	Gas	32
225	CM42EW	A	zn	120	12	Gas	32
226	CM42EW	A	zn	315	2	Gas	32
227	CM42EW	A	zn	315	8	Gas	32
228	CM42EW	A	zn	315	12	Gas	32
229	CM42EW	A	zn	120	2	Gas	128
230	CM42EW	A	zn	120	8	Gas	128
231	CM42EW	A	zn	120	12	Gas	128
232	CM42EW	A	zn	315	2	Gas	128
233	CM42EW	A	zn	315	8	Gas	128
234	CM42EW	A	zn	315	12	Gas	128
235	CM42EW	A	zn	120	2	Gas	512
236	CM42EW	A	zn	120	8	Gas	512
237	CM42EW	A	zn	120	12	Gas	512
238	CM42EW	A	zn	315	2	Gas	512
239	CM42EW	A	zn	315	8	Gas	512
240	CM42EW	A	zn	315	12	Gas	512
241	CM42EW	A	zn	120	2	Gas	0.5
242	CM42EW	A	zn	315	8	Gas	0.5
243	CM42EW	A	zn	120	12	Gas	512
244	CM42EW	A	zn	315	2	Gas	512

Table 10.9: Module with higher immediate ignition probability due to increased ignition sources and with grid resolution 125000 and Courant number Max

ID	Module	Leak Point	Leak direction	Wind direction	Wind speed (m/s)	Fluid	Leak rate (Kg/s)
245	CM42EW	A	zn	120	2	Gas	2
246	CM42EW	A	zn	120	8	Gas	2
247	CM42EW	A	zn	120	12	Gas	2
248	CM42EW	A	zn	315	2	Gas	2
249	CM42EW	A	zn	315	8	Gas	2
250	CM42EW	A	zn	315	12	Gas	2
251	CM42EW	A	zn	120	2	Gas	8
252	CM42EW	A	zn	120	8	Gas	8
253	CM42EW	A	zn	120	12	Gas	8
254	CM42EW	A	zn	315	2	Gas	8
255	CM42EW	A	zn	315	8	Gas	8
256	CM42EW	A	zn	315	12	Gas	8
257	CM42EW	A	zn	120	2	Gas	32
258	CM42EW	A	zn	120	8	Gas	32
259	CM42EW	A	zn	120	12	Gas	32
260	CM42EW	A	zn	315	2	Gas	32
261	CM42EW	A	zn	315	8	Gas	32
262	CM42EW	A	zn	315	12	Gas	32
263	CM42EW	A	zn	120	2	Gas	128
264	CM42EW	A	zn	120	8	Gas	128
265	CM42EW	A	zn	120	12	Gas	128
266	CM42EW	A	zn	315	2	Gas	128
267	CM42EW	A	zn	315	8	Gas	128
268	CM42EW	A	zn	315	12	Gas	128
269	CM42EW	A	zn	120	2	Gas	512
270	CM42EW	A	zn	120	8	Gas	512
271	CM42EW	A	zn	120	12	Gas	512
272	CM42EW	A	zn	315	2	Gas	512
273	CM42EW	A	zn	315	8	Gas	512
274	CM42EW	A	zn	315	12	Gas	512
275	CM42EW	A	zn	120	2	Gas	0.5
276	CM42EW	A	zn	315	8	Gas	0.5
277	CM42EW	A	zn	120	12	Gas	512
278	CM42EW	A	zn	315	2	Gas	512

Table 10.10: Module with delayed gas detection due to human intervention and with grid resolution 125000 and Courant number Max

Appendix D - Scripts to enable submitting simulations to the cluster

```
#! /usr/bin/python

import os
import sys

def main(directory):

    print 'Looking in directory: %s' % directory

    # List of the files we have found
    myfiles = list()

    # Suffix of the files we are looking for
    suffix = '.fsc'

    # Find them all
    for root, dirs, files in os.walk(directory):
        for f in files:
            if (f.endswith(suffix)) and (not f.startswith('_')):
                myfiles.append(os.path.join(root, f))
    sFile = ['universe = vanilla',
                        'executable = /usr/local/bin/runkfx_rbm',
              '',
              'transfer_executable = False',
              '',
              'requirements = HAS_KFXRBM == True',
              '',
              'error = kfx.error',
              'log = kfx.log',
              'output = kfx.out',
              '',
              'environment = \"KAM3ROOT=/opt/computit/kfx_pakke_test\"',
              '',
              'Concurrency_Limits = FURCIFER',
              '']

    for f in myfiles:
        fp = os.path.abspath(f)
        head, tail = os.path.split(fp)

        sFile.append('Initialdir = %s' % head)
        sFile.append('arguments = %s' %  tail.split('.')[0])
        sFile.append('Queue\n')



    with open('kfx_rbm.sub', 'w') as ofile:
        for f in sFile:
            ofile.write('%s\n' % f)


if __name__ == '__main__':
    main(sys.argv[1])
```

Figure 10.3: Python scripts to submit the simulations to the cluster.

```
universe = vanilla
executable = /usr/local/bin/runkfx_rbm

transfer_executable = False

requirements = HAS_KFXRBM == True

error = kfx.error
log = kfx.log
output = kfx.out

environment = "KAM3ROOT=/opt/computit/kfx_pakke_test"

Concurrency_Limits = FURCIFER

Initialdir = /data/proj/P10475_RA/STUDENTS/2019/sgo/Thesis/RBM/PrvntRls/CM42EW/BaseCase/LS_1_Pipe_GR125/CM42EW_ls1_gr2_q02_ws12_wd120
arguments = Pipefailure
Queue

Initialdir = /data/proj/P10475_RA/STUDENTS/2019/sgo/Thesis/RBM/PrvntRls/CM42EW/BaseCase/LS_1_Pipe_GR125/CM42EW_ls1_gr2_q32_ws12_wd315
arguments = Pipefailure
Queue

Initialdir = /data/proj/P10475_RA/STUDENTS/2019/sgo/Thesis/RBM/PrvntRls/CM42EW/BaseCase/LS_1_Pipe_GR125/CM42EW_ls1_gr2_q08_ws08_wd315
arguments = Pipefailure
Queue


Initialdir = /data/proj/P10475_RA/STUDENTS/2019/sgo/Thesis/RBM/PrvntRls/CM42EW/BaseCase/LS_1_Pipe_GR125/CM42EW_ls1_gr2_q08_ws02_wd315
arguments = Pipefailure
Queue

Initialdir = /data/proj/P10475_RA/STUDENTS/2019/sgo/Thesis/RBM/PrvntRls/CM42EW/BaseCase/LS_1_Pipe_GR125/CM42EW_ls1_gr2_q32_ws08_wd120
arguments = Pipefailure
Queue

Initialdir = /data/proj/P10475_RA/STUDENTS/2019/sgo/Thesis/RBM/PrvntRls/CM42EW/BaseCase/LS_1_Pipe_GR125/CM42EW_ls1_gr2_q512_ws02_wd120
arguments = Pipefailure
Queue
```

Figure 10.4: KFX-submit script - Part 1

```
Initialdir = /data/proj/P10475_RA/STUDENTS/2019/sgo/Thesis/RBM/PrvntRls/CM42EW/BaseCase/LS_1_Pipe_GR125/CM42EW_ls1_gr2_q128_ws16_wd315
arguments = Pipefailure
Queue

Initialdir = /data/proj/P10475_RA/STUDENTS/2019/sgo/Thesis/RBM/PrvntRls/CM42EW/BaseCase/LS_1_Pipe_GR125/CM42EW_ls1_gr2_q02_ws12_wd315
arguments = Pipefailure
Queue

Initialdir = /data/proj/P10475_RA/STUDENTS/2019/sgo/Thesis/RBM/PrvntRls/CM42EW/BaseCase/LS_1_Pipe_GR125/CM42EW_ls1_gr2_q512_ws18_wd120
arguments = Pipefailure
Queue

Initialdir = /data/proj/P10475_RA/STUDENTS/2019/sgo/Thesis/RBM/PrvntRls/CM42EW/BaseCase/LS_1_Pipe_GR125/CM42EW_ls1_gr2_q128_ws08_wd120
arguments = Pipefailure
Queue

Initialdir = /data/proj/P10475_RA/STUDENTS/2019/sgo/Thesis/RBM/PrvntRls/CM42EW/BaseCase/LS_1_Pipe_GR125/CM42EW_ls1_gr2_q02_ws02_wd315
arguments = Pipefailure
Queue

Initialdir = /data/proj/P10475_RA/STUDENTS/2019/sgo/Thesis/RBM/PrvntRls/CM42EW/BaseCase/LS_1_Pipe_GR125/CM42EW_ls1_gr2_q0.5_ws18_wd120
arguments = Pipefailure
Queue

Initialdir = /data/proj/P10475_RA/STUDENTS/2019/sgo/Thesis/RBM/PrvntRls/CM42EW/BaseCase/LS_1_Pipe_GR125/CM42EW_ls1_gr2_q128_ws02_wd120
arguments = Pipefailure
Queue

Initialdir = /data/proj/P10475_RA/STUDENTS/2019/sgo/Thesis/RBM/PrvntRls/CM42EW/BaseCase/LS_1_Pipe_GR125/CM42EW_ls1_gr2_q08_ws02_wd120
arguments = Pipefailure
Queue

Initialdir = /data/proj/P10475_RA/STUDENTS/2019/sgo/Thesis/RBM/PrvntRls/CM42EW/BaseCase/LS_1_Pipe_GR125/CM42EW_ls1_gr2_q08_ws12_wd120
arguments = Pipefailure
Queue


Initialdir = /data/proj/P10475_RA/STUDENTS/2019/sgo/Thesis/RBM/PrvntRls/CM42EW/BaseCase/LS_1_Pipe_GR125/CM42EW_ls1_gr2_q32_ws12_wd120
arguments = Pipefailure
Queue
```

Figure 10.5: KFX-submit script - Part 2

```
Initialdir = /data/proj/P10475_RA/STUDENTS/2019/sgo/Thesis/RBM/PrvntRls/CM42EW/BaseCase/LS_1_Pipe_GR125/CM42EW_ls1_gr2_q512_ws08_wd120
arguments = Pipefailure
Queue

Initialdir = /data/proj/P10475_RA/STUDENTS/2019/sgo/Thesis/RBM/PrvntRls/CM42EW/BaseCase/LS_1_Pipe_GR125/CM42EW_ls1_gr2_q32_ws02_wd120
arguments = Pipefailure
Queue

Initialdir = /data/proj/P10475_RA/STUDENTS/2019/sgo/Thesis/RBM/PrvntRls/CM42EW/BaseCase/LS_1_Pipe_GR125/CM42EW_ls1_gr2_q02_ws02_wd120
arguments = Pipefailure
Queue


Initialdir = /data/proj/P10475_RA/STUDENTS/2019/sgo/Thesis/RBM/PrvntRls/CM42EW/BaseCase/LS_1_Pipe_GR125/CM42EW_ls1_gr2_q128_ws08_wd315
arguments = Pipefailure
Queue


Initialdir = /data/proj/P10475_RA/STUDENTS/2019/sgo/Thesis/RBM/PrvntRls/CM42EW/BaseCase/LS_1_Pipe_GR125/CM42EW_ls1_gr2_q512_ws12_wd120
arguments = Pipefailure
Queue

Initialdir = /data/proj/P10475_RA/STUDENTS/2019/sgo/Thesis/RBM/PrvntRls/CM42EW/BaseCase/LS_1_Pipe_GR125/CM42EW_ls1_gr2_q128_ws12_wd120
arguments = Pipefailure
Queue

Initialdir = /data/proj/P10475_RA/STUDENTS/2019/sgo/Thesis/RBM/PrvntRls/CM42EW/BaseCase/LS_1_Pipe_GR125/CM42EW_ls1_gr2_q32_ws02_wd315
arguments = Pipefailure
Queue

Initialdir = /data/proj/P10475_RA/STUDENTS/2019/sgo/Thesis/RBM/PrvntRls/CM42EW/BaseCase/LS_1_Pipe_GR125/CM42EW_ls1_gr2_q02_ws08_wd120
arguments = Pipefailure
Queue

Initialdir = /data/proj/P10475_RA/STUDENTS/2019/sgo/Thesis/RBM/PrvntRls/CM42EW/BaseCase/LS_1_Pipe_GR125/CM42EW_ls1_gr2_q128_ws02_wd315
arguments = Pipefailure
Queue

Initialdir = /data/proj/P10475_RA/STUDENTS/2019/sgo/Thesis/RBM/PrvntRls/CM42EW/BaseCase/LS_1_Pipe_GR125/CM42EW_ls1_gr2_q0.5_ws18_wd315
arguments = Pipefailure
Queue
```

Figure 10.6: KFX-submit script - Part 3

```
Initialdir = /data/proj/P10475_RA/STUDENTS/2019/sgo/Thesis/RBM/PrvntRls/CM42EW/BaseCase/LS_1_Pipe_GR125/CM42EW_ls1_gr2_q08_ws08_wd120
arguments = Pipefailure
Queue

Initialdir = /data/proj/P10475_RA/STUDENTS/2019/sgo/Thesis/RBM/PrvntRls/CM42EW/BaseCase/LS_1_Pipe_GR125/CM42EW_ls1_gr2_q02_ws08_wd315
arguments = Pipefailure
Queue


Initialdir = /data/proj/P10475_RA/STUDENTS/2019/sgo/Thesis/RBM/PrvntRls/CM42EW/BaseCase/LS_1_Pipe_GR125/CM42EW_ls1_gr2_q32_ws08_wd315
arguments = Pipefailure
Queue

Initialdir = /data/proj/P10475_RA/STUDENTS/2019/sgo/Thesis/RBM/PrvntRls/CM42EW/BaseCase/LS_1_Pipe_GR125/CM42EW_ls1_gr2_q08_ws12_wd315
arguments = Pipefailure
Queue

Initialdir = /data/proj/P10475_RA/STUDENTS/2019/sgo/Thesis/RBM/PrvntRls/CM42EW/BaseCase/LS_1_Pipe_GR125/CM42EW_ls1_gr2_q512_ws18_wd315
arguments = Pipefailure
Queue

Initialdir = /data/proj/P10475_RA/STUDENTS/2019/sgo/Thesis/RBM/PrvntRls/CM42EW/BaseCase/LS_1_Pipe_GR125/CM42EW_ls1_gr2_q512_ws02_wd315
arguments = Pipefailure
Queue


Initialdir = /data/proj/P10475_RA/STUDENTS/2019/sgo/Thesis/RBM/PrvntRls/CM42EW/BaseCase/LS_1_Pipe_GR125/CM42EW_ls1_gr2_q512_ws08_wd315
arguments = Pipefailure
Queue


Initialdir = /data/proj/P10475_RA/STUDENTS/2019/sgo/Thesis/RBM/PrvntRls/CM42EW/BaseCase/LS_1_Pipe_GR125/CM42EW_ls1_gr2_q512_ws12_wd315
arguments = Pipefailure
Queue
```

Figure 10.7: KFX-submit script - Part 4

```
#! /usr/bin/python

import sys

def main(directory):

    print 'Looking in directory: %s' % directory

    # List of the files we have found
    myfiles = list()

    # Suffix of the files we are looking for
    suffix = '.fsc'

    # Find them all
    for root, dirs, files in os.walk(directory):
        for f in files:
            if f.endswith(suffix):
                myfiles.append(os.path.join(root, file))

    for f in




if __name__ == '__main__':
    main(sys.argv[0])
```

Figure 10.8: Python scripts to submit the simulations to the cluster.

Appendix E - Scenario file (.scn)

#Case_name	data_type	tmax
’./CM42EW_ls1_gr125_q02_ws02_wd120/Pipefailure’	’Jet_release_data:’	1,00E+30
’./CM42EW_ls1_gr125_q02_ws08_wd120/Pipefailure’	’Jet_release_data:’	1,00E+30
’./CM42EW_ls1_gr125_q02_ws12_wd120/Pipefailure’	’Jet_release_data:’	1,00E+30
’./CM42EW_ls1_gr125_q02_ws02_wd315/Pipefailure’	’Jet_release_data:’	1,00E+30
’./CM42EW_ls1_gr125_q02_ws08_wd315/Pipefailure’	’Jet_release_data:’	1,00E+30
’./CM42EW_ls1_gr125_q02_ws12_wd315/Pipefailure’	’Jet_release_data:’	1,00E+30
’./CM42EW_ls1_gr125_q08_ws02_wd120/Pipefailure’	’Jet_release_data:’	1,00E+30
’./CM42EW_ls1_gr125_q08_ws08_wd120/Pipefailure’	’Jet_release_data:’	1,00E+30
’./CM42EW_ls1_gr125_q08_ws12_wd120/Pipefailure’	’Jet_release_data:’	1,00E+30
’./CM42EW_ls1_gr125_q08_ws02_wd315/Pipefailure’	’Jet_release_data:’	1,00E+30
’./CM42EW_ls1_gr125_q08_ws08_wd315/Pipefailure’	’Jet_release_data:’	1,00E+30
’./CM42EW_ls1_gr125_q08_ws12_wd315/Pipefailure’	’Jet_release_data:’	1,00E+30
’./CM42EW_ls1_gr125_q32_ws02_wd120/Pipefailure’	’Jet_release_data:’	1,00E+30
’./CM42EW_ls1_gr125_q32_ws08_wd120/Pipefailure’	’Jet_release_data:’	1,00E+30
’./CM42EW_ls1_gr125_q32_ws12_wd120/Pipefailure’	’Jet_release_data:’	1,00E+30
’./CM42EW_ls1_gr125_q32_ws02_wd315/Pipefailure’	’Jet_release_data:’	1,00E+30
’./CM42EW_ls1_gr125_q32_ws08_wd315/Pipefailure’	’Jet_release_data:’	1,00E+30
’./CM42EW_ls1_gr125_q32_ws12_wd315/Pipefailure’	’Jet_release_data:’	1,00E+30
’./CM42EW_ls1_gr125_q128_ws02_wd120/Pipefailure’	’Jet_release_data:’	1,00E+30
’./CM42EW_ls1_gr125_q128_ws08_wd120/Pipefailure’	’Jet_release_data:’	1,00E+30
’./CM42EW_ls1_gr125_q128_ws12_wd120/Pipefailure’	’Jet_release_data:’	1,00E+30
’./CM42EW_ls1_gr125_q128_ws02_wd315/Pipefailure’	’Jet_release_data:’	1,00E+30
’./CM42EW_ls1_gr125_q128_ws08_wd315/Pipefailure’	’Jet_release_data:’	1,00E+30
’./CM42EW_ls1_gr125_q128_ws16_wd315/Pipefailure’	’Jet_release_data:’	1,00E+30
’./CM42EW_ls1_gr125_q512_ws02_wd120/Pipefailure’	’Jet_release_data:’	1,00E+30
’./CM42EW_ls1_gr125_q512_ws08_wd120/Pipefailure’	’Jet_release_data:’	1,00E+30
’./CM42EW_ls1_gr125_q512_ws12_wd120/Pipefailure’	’Jet_release_data:’	1,00E+30
’./CM42EW_ls1_gr125_q512_ws02_wd315/Pipefailure’	’Jet_release_data:’	1,00E+30
’./CM42EW_ls1_gr125_q512_ws08_wd315/Pipefailure’	’Jet_release_data:’	1,00E+30
’./CM42EW_ls1_gr125_q512_ws12_wd315/Pipefailure’	’Jet_release_data:’	1,00E+30
’./CM42EW_ls1_gr125_q0.5_ws18_wd120/Pipefailure’	’Jet_release_data:’	1,00E+30
’./CM42EW_ls1_gr125_q0.5_ws18_wd315/Pipefailure’	’Jet_release_data:’	1,00E+30
’./CM42EW_ls1_gr125_q512_ws18_wd120/Pipefailure’	’Jet_release_data:’	1,00E+30
’./CM42EW_ls1_gr125_q512_ws18_wd315/Pipefailure’	’Jet_release_data:’	1,00E+30

Table 10.11: Pipefailure.scn - Part 1

jet_position	jet_direction	res_temperature	jet_pressure	jet_flowrate
(15.502,7.9996,4.6937)	(0,0,-1)	50	50	2
(15.502,7.9996,4.6937)	(0,0,-1)	50	50	2
(15.502,7.9996,4.6937)	(0,0,-1)	50	50	2
(15.502,7.9996,4.6937)	(0,0,-1)	50	50	2
(15.502,7.9996,4.6937)	(0,0,-1)	50	50	2
(15.502,7.9996,4.6937)	(0,0,-1)	50	50	2
(15.502,7.9996,4.6937)	(0,0,-1)	50	50	8
(15.502,7.9996,4.6937)	(0,0,-1)	50	50	8
(15.502,7.9996,4.6937)	(0,0,-1)	50	50	8
(15.502,7.9996,4.6937)	(0,0,-1)	50	50	8
(15.502,7.9996,4.6937)	(0,0,-1)	50	50	8
(15.502,7.9996,4.6937)	(0,0,-1)	50	50	8
(15.502,7.9996,4.6937)	(0,0,-1)	50	50	32
(15.502,7.9996,4.6937)	(0,0,-1)	50	50	32
(15.502,7.9996,4.6937)	(0,0,-1)	50	50	32
(15.502,7.9996,4.6937)	(0,0,-1)	50	50	32
(15.502,7.9996,4.6937)	(0,0,-1)	50	50	32
(15.502,7.9996,4.6937)	(0,0,-1)	50	50	32
(15.502,7.9996,4.6937)	(0,0,-1)	50	50	128
(15.502,7.9996,4.6937)	(0,0,-1)	50	50	128
(15.502,7.9996,4.6937)	(0,0,-1)	50	50	128
(15.502,7.9996,4.6937)	(0,0,-1)	50	50	128
(15.502,7.9996,4.6937)	(0,0,-1)	50	50	128
(15.502,7.9996,4.6937)	(0,0,-1)	50	50	128
(15.502,7.9996,4.6937)	(0,0,-1)	50	50	512
(15.502,7.9996,4.6937)	(0,0,-1)	50	50	512
(15.502,7.9996,4.6937)	(0,0,-1)	50	50	512
(15.502,7.9996,4.6937)	(0,0,-1)	50	50	512
(15.502,7.9996,4.6937)	(0,0,-1)	50	50	512
(15.502,7.9996,4.6937)	(0,0,-1)	50	50	512
(15.502,7.9996,4.6937)	(0,0,-1)	50	50	0.5
(15.502,7.9996,4.6937)	(0,0,-1)	50	50	0.5
(15.502,7.9996,4.6937)	(0,0,-1)	50	50	512
(15.502,7.9996,4.6937)	(0,0,-1)	50	50	512

Table 10.12: Pipefailure.scn - Part 2

jet_diameter	transient_jet	jet_gas_components	jet_gas_composition	gas_cloud_sim
0	’N/A’	(’C1’)	-100	1
0	’N/A’	(’C1’)	-100	1
0	’N/A’	(’C1’)	-100	1
0	’N/A’	(’C1’)	-100	1
0	’N/A’	(’C1’)	-100	1
0	’N/A’	(’C1’)	-100	1
0	’N/A’	(’C1’)	-100	1
0	’N/A’	(’C1’)	-100	1
0	’N/A’	(’C1’)	-100	1
0	’N/A’	(’C1’)	-100	1
0	’N/A’	(’C1’)	-100	1
0	’N/A’	(’C1’)	-100	1
0	’N/A’	(’C1’)	-100	1
0	’N/A’	(’C1’)	-100	1
0	’N/A’	(’C1’)	-100	1
0	’N/A’	(’C1’)	-100	1
0	’N/A’	(’C1’)	-100	1
0	’N/A’	(’C1’)	-100	1
0	’N/A’	(’C1’)	-100	1
0	’N/A’	(’C1’)	-100	1
0	’N/A’	(’C1’)	-100	1
0	’N/A’	(’C1’)	-100	1
0	’N/A’	(’C1’)	-100	1
0	’N/A’	(’C1’)	-100	1
0	’N/A’	(’C1’)	-100	1
0	’N/A’	(’C1’)	-100	1
0	’N/A’	(’C1’)	-100	1
0	’N/A’	(’C1’)	-100	1
0	’N/A’	(’C1’)	-100	1
0	’N/A’	(’C1’)	-100	1
0	’N/A’	(’C1’)	-100	1
0	’N/A’	(’C1’)	-100	1
0	’N/A’	(’C1’)	-100	1
0	’N/A’	(’C1’)	-100	1

Table 10.13: Pipefailure.scn - Part 3

wind_angle	wind_10	wind_stability	wind_Z0	ambient_T	wind_roughness
120	2	'Neutral'	0	11	0.0002
120	8	'Neutral'	0	11	0.0002
120	12	'Neutral'	0	11	0.0002
315	2	'Neutral'	0	11	0.0002
315	8	'Neutral'	0	11	0.0002
315	12	'Neutral'	0	11	0.0002
120	2	'Neutral'	0	11	0.0002
120	8	'Neutral'	0	11	0.0002
120	12	'Neutral'	0	11	0.0002
315	2	'Neutral'	0	11	0.0002
315	8	'Neutral'	0	11	0.0002
315	12	'Neutral'	0	11	0.0002
120	2	'Neutral'	0	11	0.0002
120	8	'Neutral'	0	11	0.0002
120	12	'Neutral'	0	11	0.0002
315	2	'Neutral'	0	11	0.0002
315	8	'Neutral'	0	11	0.0002
315	12	'Neutral'	0	11	0.0002
120	2	'Neutral'	0	11	0.0002
120	8	'Neutral'	0	11	0.0002
120	12	'Neutral'	0	11	0.0002
315	2	'Neutral'	0	11	0.0002
315	8	'Neutral'	0	11	0.0002
315	12	'Neutral'	0	11	0.0002
120	2	'Neutral'	0	11	0.0002
120	8	'Neutral'	0	11	0.0002
120	12	'Neutral'	0	11	0.0002
315	2	'Neutral'	0	11	0.0002
315	8	'Neutral'	0	11	0.0002
315	12	'Neutral'	0	11	0.0002
120	18	'Neutral'	0	11	0.0002
315	18	'Neutral'	0	11	0.0002
120	18	'Neutral'	0	11	0.0002
315	18	'Neutral'	0	11	0.0002

Table 10.14: Pipefailure.scn - Part 4

geometry_file	geometry_min	geometry_max	vol_box_min	vol_box_max	stoppro
/CM42EW_01.kfx’	(-26,-25,0)	(54,50,50)	(-1,-0.3,0)	(29,15.7,8)	1
/CM42EW_01.kfx’	(-26,-25,0)	(54,50,50)	(-1,-0.3,0)	(29,15.7,8)	1
/CM42EW_01.kfx’	(-26,-25,0)	(54,50,50)	(-1,-0.3,0)	(29,15.7,8)	1
/CM42EW_01.kfx’	(-26,-25,0)	(54,50,50)	(-1,-0.3,0)	(29,15.7,8)	1
/CM42EW_01.kfx’	(-26,-25,0)	(54,50,50)	(-1,-0.3,0)	(29,15.7,8)	1
/CM42EW_01.kfx’	(-26,-25,0)	(54,50,50)	(-1,-0.3,0)	(29,15.7,8)	1
/CM42EW_01.kfx’	(-26,-25,0)	(54,50,50)	(-1,-0.3,0)	(29,15.7,8)	1
/CM42EW_01.kfx’	(-26,-25,0)	(54,50,50)	(-1,-0.3,0)	(29,15.7,8)	1
/CM42EW_01.kfx’	(-26,-25,0)	(54,50,50)	(-1,-0.3,0)	(29,15.7,8)	1
/CM42EW_01.kfx’	(-26,-25,0)	(54,50,50)	(-1,-0.3,0)	(29,15.7,8)	1
/CM42EW_01.kfx’	(-26,-25,0)	(54,50,50)	(-1,-0.3,0)	(29,15.7,8)	1
/CM42EW_01.kfx’	(-26,-25,0)	(54,50,50)	(-1,-0.3,0)	(29,15.7,8)	1
/CM42EW_01.kfx’	(-26,-25,0)	(54,50,50)	(-1,-0.3,0)	(29,15.7,8)	1
/CM42EW_01.kfx’	(-26,-25,0)	(54,50,50)	(-1,-0.3,0)	(29,15.7,8)	1
/CM42EW_01.kfx’	(-26,-25,0)	(54,50,50)	(-1,-0.3,0)	(29,15.7,8)	1
/CM42EW_01.kfx’	(-26,-25,0)	(54,50,50)	(-1,-0.3,0)	(29,15.7,8)	1
/CM42EW_01.kfx’	(-26,-25,0)	(54,50,50)	(-1,-0.3,0)	(29,15.7,8)	1
/CM42EW_01.kfx’	(-26,-25,0)	(54,50,50)	(-1,-0.3,0)	(29,15.7,8)	1
/CM42EW_01.kfx’	(-26,-25,0)	(54,50,50)	(-1,-0.3,0)	(29,15.7,8)	1
/CM42EW_01.kfx’	(-26,-25,0)	(54,50,50)	(-1,-0.3,0)	(29,15.7,8)	1
/CM42EW_01.kfx’	(-26,-25,0)	(54,50,50)	(-1,-0.3,0)	(29,15.7,8)	1
/CM42EW_01.kfx’	(-26,-25,0)	(54,50,50)	(-1,-0.3,0)	(29,15.7,8)	1
/CM42EW_01.kfx’	(-26,-25,0)	(54,50,50)	(-1,-0.3,0)	(29,15.7,8)	1
/CM42EW_01.kfx’	(-26,-25,0)	(54,50,50)	(-1,-0.3,0)	(29,15.7,8)	1
/CM42EW_01.kfx’	(-26,-25,0)	(54,50,50)	(-1,-0.3,0)	(29,15.7,8)	1
/CM42EW_01.kfx’	(-26,-25,0)	(54,50,50)	(-1,-0.3,0)	(29,15.7,8)	1
/CM42EW_01.kfx’	(-26,-25,0)	(54,50,50)	(-1,-0.3,0)	(29,15.7,8)	1
/CM42EW_01.kfx’	(-26,-25,0)	(54,50,50)	(-1,-0.3,0)	(29,15.7,8)	1
/CM42EW_01.kfx’	(-26,-25,0)	(54,50,50)	(-1,-0.3,0)	(29,15.7,8)	1
/CM42EW_01.kfx’	(-26,-25,0)	(54,50,50)	(-1,-0.3,0)	(29,15.7,8)	1
/CM42EW_01.kfx’	(-26,-25,0)	(54,50,50)	(-1,-0.3,0)	(29,15.7,8)	1
/CM42EW_01.kfx’	(-26,-25,0)	(54,50,50)	(-1,-0.3,0)	(29,15.7,8)	1
/CM42EW_01.kfx’	(-26,-25,0)	(54,50,50)	(-1,-0.3,0)	(29,15.7,8)	1
/CM42EW_01.kfx’	(-26,-25,0)	(54,50,50)	(-1,-0.3,0)	(29,15.7,8)	1

Table 10.15: Pipefailure.scn - Part 5

dt_rowcum	dt_volstop	gridpoints	lockedplanes	spray_file	grid_parameters
0.1	10000	125000	2	’N/A’	(’Grow’,’N/A’,0,1,0,0)
0.1	10000	125000	2	’N/A’	(’Grow’,’N/A’,0,1,0,0)
0.1	10000	125000	2	’N/A’	(’Grow’,’N/A’,0,1,0,0)
0.1	10000	125000	2	’N/A’	(’Grow’,’N/A’,0,1,0,0)
0.1	10000	125000	2	’N/A’	(’Grow’,’N/A’,0,1,0,0)
0.1	10000	125000	2	’N/A’	(’Grow’,’N/A’,0,1,0,0)
0.1	10000	125000	2	’N/A’	(’Grow’,’N/A’,0,1,0,0)
0.1	10000	125000	2	’N/A’	(’Grow’,’N/A’,0,1,0,0)
0.1	10000	125000	2	’N/A’	(’Grow’,’N/A’,0,1,0,0)
0.1	10000	125000	2	’N/A’	(’Grow’,’N/A’,0,1,0,0)
0.1	10000	125000	2	’N/A’	(’Grow’,’N/A’,0,1,0,0)
0.1	10000	125000	2	’N/A’	(’Grow’,’N/A’,0,1,0,0)
0.1	10000	125000	2	’N/A’	(’Grow’,’N/A’,0,1,0,0)
0.1	10000	125000	2	’N/A’	(’Grow’,’N/A’,0,1,0,0)
0.1	10000	125000	2	’N/A’	(’Grow’,’N/A’,0,1,0,0)
0.1	10000	125000	2	’N/A’	(’Grow’,’N/A’,0,1,0,0)
0.1	10000	125000	2	’N/A’	(’Grow’,’N/A’,0,1,0,0)
0.1	10000	125000	2	’N/A’	(’Grow’,’N/A’,0,1,0,0)
0.1	10000	125000	2	’N/A’	(’Grow’,’N/A’,0,1,0,0)
0.1	10000	125000	2	’N/A’	(’Grow’,’N/A’,0,1,0,0)
0.1	10000	125000	2	’N/A’	(’Grow’,’N/A’,0,1,0,0)
0.1	10000	125000	2	’N/A’	(’Grow’,’N/A’,0,1,0,0)
0.1	10000	125000	2	’N/A’	(’Grow’,’N/A’,0,1,0,0)
0.1	10000	125000	2	’N/A’	(’Grow’,’N/A’,0,1,0,0)
0.1	10000	125000	2	’N/A’	(’Grow’,’N/A’,0,1,0,0)
0.1	10000	125000	2	’N/A’	(’Grow’,’N/A’,0,1,0,0)
0.1	10000	125000	2	’N/A’	(’Grow’,’N/A’,0,1,0,0)
0.1	10000	125000	2	’N/A’	(’Grow’,’N/A’,0,1,0,0)
0.1	10000	125000	2	’N/A’	(’Grow’,’N/A’,0,1,0,0)
0.1	10000	125000	2	’N/A’	(’Grow’,’N/A’,0,1,0,0)
0.1	10000	125000	2	’N/A’	(’Grow’,’N/A’,0,1,0,0)
0.1	10000	125000	2	’N/A’	(’Grow’,’N/A’,0,1,0,0)
0.1	10000	125000	2	’N/A’	(’Grow’,’N/A’,0,1,0,0)
0.1	10000	125000	2	’N/A’	(’Grow’,’N/A’,0,1,0,0)

Table 10.16: Pipefailure.scn - Part 6

block_parameters	sub_block	pool_parameters
(10,10,10,9999,9999,9999)	(1,4000,1000)	('Rectangle',0.01,0,0.005,373,288,0,1)
(10,10,10,9999,9999,9999)	(1,4000,1000)	('Rectangle',0.01,0,0.005,373,288,0,1)
(10,10,10,9999,9999,9999)	(1,4000,1000)	('Rectangle',0.01,0,0.005,373,288,0,1)
(10,10,10,9999,9999,9999)	(1,4000,1000)	('Rectangle',0.01,0,0.005,373,288,0,1)
(10,10,10,9999,9999,9999)	(1,4000,1000)	('Rectangle',0.01,0,0.005,373,288,0,1)
(10,10,10,9999,9999,9999)	(1,4000,1000)	('Rectangle',0.01,0,0.005,373,288,0,1)
(10,10,10,9999,9999,9999)	(1,4000,1000)	('Rectangle',0.01,0,0.005,373,288,0,1)
(10,10,10,9999,9999,9999)	(1,4000,1000)	('Rectangle',0.01,0,0.005,373,288,0,1)
(10,10,10,9999,9999,9999)	(1,4000,1000)	('Rectangle',0.01,0,0.005,373,288,0,1)
(10,10,10,9999,9999,9999)	(1,4000,1000)	('Rectangle',0.01,0,0.005,373,288,0,1)
(10,10,10,9999,9999,9999)	(1,4000,1000)	('Rectangle',0.01,0,0.005,373,288,0,1)
(10,10,10,9999,9999,9999)	(1,4000,1000)	('Rectangle',0.01,0,0.005,373,288,0,1)
(10,10,10,9999,9999,9999)	(1,4000,1000)	('Rectangle',0.01,0,0.005,373,288,0,1)
(10,10,10,9999,9999,9999)	(1,4000,1000)	('Rectangle',0.01,0,0.005,373,288,0,1)
(10,10,10,9999,9999,9999)	(1,4000,1000)	('Rectangle',0.01,0,0.005,373,288,0,1)
(10,10,10,9999,9999,9999)	(1,4000,1000)	('Rectangle',0.01,0,0.005,373,288,0,1)
(10,10,10,9999,9999,9999)	(1,4000,1000)	('Rectangle',0.01,0,0.005,373,288,0,1)
(10,10,10,9999,9999,9999)	(1,4000,1000)	('Rectangle',0.01,0,0.005,373,288,0,1)
(10,10,10,9999,9999,9999)	(1,4000,1000)	('Rectangle',0.01,0,0.005,373,288,0,1)
(10,10,10,9999,9999,9999)	(1,4000,1000)	('Rectangle',0.01,0,0.005,373,288,0,1)
(10,10,10,9999,9999,9999)	(1,4000,1000)	('Rectangle',0.01,0,0.005,373,288,0,1)
(10,10,10,9999,9999,9999)	(1,4000,1000)	('Rectangle',0.01,0,0.005,373,288,0,1)
(10,10,10,9999,9999,9999)	(1,4000,1000)	('Rectangle',0.01,0,0.005,373,288,0,1)
(10,10,10,9999,9999,9999)	(1,4000,1000)	('Rectangle',0.01,0,0.005,373,288,0,1)
(10,10,10,9999,9999,9999)	(1,4000,1000)	('Rectangle',0.01,0,0.005,373,288,0,1)
(10,10,10,9999,9999,9999)	(1,4000,1000)	('Rectangle',0.01,0,0.005,373,288,0,1)
(10,10,10,9999,9999,9999)	(1,4000,1000)	('Rectangle',0.01,0,0.005,373,288,0,1)
(10,10,10,9999,9999,9999)	(1,4000,1000)	('Rectangle',0.01,0,0.005,373,288,0,1)
(10,10,10,9999,9999,9999)	(1,4000,1000)	('Rectangle',0.01,0,0.005,373,288,0,1)
(10,10,10,9999,9999,9999)	(1,4000,1000)	('Rectangle',0.01,0,0.005,373,288,0,1)
(10,10,10,9999,9999,9999)	(1,4000,1000)	('Rectangle',0.01,0,0.005,373,288,0,1)
(10,10,10,9999,9999,9999)	(1,4000,1000)	('Rectangle',0.01,0,0.005,373,288,0,1)
(10,10,10,9999,9999,9999)	(1,4000,1000)	('Rectangle',0.01,0,0.005,373,288,0,1)
(10,10,10,9999,9999,9999)	(1,4000,1000)	('Rectangle',0.01,0,0.005,373,288,0,1)

Table 10.17: Pipefailure.scn - Part 7

time_controls	subsea_parameters	rbm
(1,1e+30,10)	('Gauss',1,1.3)	('Segment_1',100,790000,900,2,2,20,1e-05,0.0023,5,0,1)
(1,1e+30,10)	('Gauss',1,1.3)	('Segment_1',100,790000,900,2,2,20,1e-05,0.0023,5,0,1)
(1,1e+30,10)	('Gauss',1,1.3)	('Segment_1',100,790000,900,2,2,20,1e-05,0.0023,5,0,1)
(1,1e+30,10)	('Gauss',1,1.3)	('Segment_1',100,790000,900,2,2,20,1e-05,0.0023,5,0,1)
(1,1e+30,10)	('Gauss',1,1.3)	('Segment_1',100,790000,900,2,2,20,1e-05,0.0023,5,0,1)
(1,1e+30,10)	('Gauss',1,1.3)	('Segment_1',100,790000,900,2,2,20,1e-05,0.0023,5,0,1)
(1,1e+30,10)	('Gauss',1,1.3)	('Segment_1',100,790000,900,2,2,20,1e-05,0.0023,5,0,1)
(1,1e+30,10)	('Gauss',1,1.3)	('Segment_1',100,790000,900,2,2,20,1e-05,0.0023,5,0,1)
(1,1e+30,10)	('Gauss',1,1.3)	('Segment_1',100,790000,900,2,2,20,1e-05,0.0023,5,0,1)
(1,1e+30,10)	('Gauss',1,1.3)	('Segment_1',100,790000,900,2,2,20,1e-05,0.0023,5,0,1)
(1,1e+30,10)	('Gauss',1,1.3)	('Segment_1',100,790000,900,2,2,20,1e-05,0.0023,5,0,1)
(1,1e+30,10)	('Gauss',1,1.3)	('Segment_1',100,790000,900,2,2,20,1e-05,0.0023,5,0,1)
(1,1e+30,10)	('Gauss',1,1.3)	('Segment_1',100,790000,900,2,2,20,1e-05,0.0023,5,0,1)
(1,1e+30,10)	('Gauss',1,1.3)	('Segment_1',100,790000,900,2,2,20,1e-05,0.0023,5,0,1)
(1,1e+30,10)	('Gauss',1,1.3)	('Segment_1',100,790000,900,2,2,20,1e-05,0.0023,5,0,1)
(1,1e+30,10)	('Gauss',1,1.3)	('Segment_1',100,790000,900,2,2,20,1e-05,0.0023,5,0,1)
(1,1e+30,10)	('Gauss',1,1.3)	('Segment_1',100,790000,900,2,2,20,1e-05,0.0023,5,0,1)
(1,1e+30,10)	('Gauss',1,1.3)	('Segment_1',100,790000,900,2,2,20,1e-05,0.0023,5,0,1)
(1,1e+30,10)	('Gauss',1,1.3)	('Segment_1',100,790000,900,2,2,20,1e-05,0.0023,5,0,1)
(1,1e+30,10)	('Gauss',1,1.3)	('Segment_1',100,790000,900,2,2,20,1e-05,0.0023,5,0,1)
(1,1e+30,10)	('Gauss',1,1.3)	('Segment_1',100,790000,900,2,2,20,1e-05,0.0023,5,0,1)
(1,1e+30,10)	('Gauss',1,1.3)	('Segment_1',100,790000,900,2,2,20,1e-05,0.0023,5,0,1)
(1,1e+30,10)	('Gauss',1,1.3)	('Segment_1',100,790000,900,2,2,20,1e-05,0.0023,5,0,1)
(1,1e+30,10)	('Gauss',1,1.3)	('Segment_1',100,790000,900,2,2,20,1e-05,0.0023,5,0,1)
(1,1e+30,10)	('Gauss',1,1.3)	('Segment_1',100,790000,900,2,2,20,1e-05,0.0023,5,0,1)
(1,1e+30,10)	('Gauss',1,1.3)	('Segment_1',100,790000,900,2,2,20,1e-05,0.0023,5,0,1)
(1,1e+30,10)	('Gauss',1,1.3)	('Segment_1',100,790000,900,2,2,20,1e-05,0.0023,5,0,1)
(1,1e+30,10)	('Gauss',1,1.3)	('Segment_1',100,790000,900,2,2,20,1e-05,0.0023,5,0,1)
(1,1e+30,10)	('Gauss',1,1.3)	('Segment_1',100,790000,900,2,2,20,1e-05,0.0023,5,0,1)
(1,1e+30,10)	('Gauss',1,1.3)	('Segment_1',100,790000,900,2,2,20,1e-05,0.0023,5,0,1)
(1,1e+30,10)	('Gauss',1,1.3)	('Segment_1',100,790000,900,2,2,20,1e-05,0.0023,5,0,1)
(1,1e+30,10)	('Gauss',1,1.3)	('Segment_1',100,790000,900,2,2,20,1e-05,0.0023,5,0,1)
(1,1e+30,10)	('Gauss',1,1.3)	('Segment_1',100,790000,900,2,2,20,1e-05,0.0023,5,0,1)
(1,1e+30,10)	('Gauss',1,1.3)	('Segment_1',100,790000,900,2,2,20,1e-05,0.0023,5,0,1)

Table 10.18: Pipefailure.scn - Part 8

Appendix F - Post processing calculations

Probability per m3	4,70E-06					
Module volume m3	3935,25					
Total Leak Frequency	0,0185					
Leak rates	**0.5**	**2**	**8**	**32**	**128**	**512**
	PLOFAM					100,000 %
Q	**C**	**K**	**A(Q)**	**F(Q)**	**Category**	**f(Q)**
0,1	0,3162	0,5	1	1,85E-02	0,1 - 0,2	5,42E-03
0,2	0,3162	0,5	0,707044694	1,31E-02	0,2 - 0,5	4,81E-03
0,5	0,3162	0,5	0,447174328	8,27E-03	0,5 - 1	2,42E-03
1	0,3162	0,7	0,3162	5,85E-03	1 - 4	3,63E-03
4	0,3162	0,7	0,119817395	2,22E-03	4 - 20	1,50E-03
20	0,3162	0,7	0,03883657	7,18E-04	20 - 80	4,46E-04
80	0,3162	0,7	0,014716308	2,72E-04	80 - 320	1,69E-04
320	0,3162	0,7	0,005576438	1,03E-04	320 - 512	2,89E-05
512	0,3162	0,7	0,004013034	7,42E-05	512 -	7,42E-05
				8,00E+01	320	
Range	**0.1-1 kg/s**	**1-4 kg/s**	**4-20 kg/s**	**20-80 kg/s**	**80-320 kg/s**	**>320**
Midpoint	0.5	2	8	32	128	512
Frequency	1,26E-02	3,63E-03	1,50E-03	4,46E-04	1,69E-04	1,03E-04

Only one leak point and leak direction					Total	Test
	Q= (2,8,32,128)	**Q=(0,5 & 512)**			1,85E-02	100 %
Wind speeds	3	4				
Wind directions	2	2				
Wind cases	6	8				
We assume uniform distribution of wind conditions						
Hence, our leak distribution becomes as follows						
Range	0.1-1 kg/s	1-4 kg/s	4-20 kg/s	20-80 kg/s	80-320 kg/s	>320
Midpoint	0.5	2	8	32	128	512
Frequency	1,58E-03	6,05E-04	2,50E-04	7,40E-05	2,80E-05	1,30E-05
	0,001581	0,000605	0,00025	0,000074	0,000028	0,000013
(* # of scenarios)	0,012648	0,00363	0,0015	0,000444	0,000168	0,000104
				Leak frequency per year		0,018494

Figure 10.9: Post processing calculation to extract total leak frequency per year.

Appendix G - Xml file containing detectors and ignitors

```
<?xml version = "1.0" encoding="UTF-8" standalone="no" ?>
<kfxScript>
<GUI protection="No" />
<!--
  This is a command shedule file automatically generated by [Quick run setup] in the
  "KFX Fire & gas cloud simulation wizard".
  You may want to edit this file in a text editor. To avoid unitentional overwrite
  from GUI after your own editing set:
      <GUI Protection="Yes" >
  in the third line of this .xml file
-->
   <atStartAndRestart>
       <runParameters TFIL="5 " TMAX="1500" />
      <xmlInclude xmlFile="blowdown.xml" />
        <RBM>
<Detector id="1" name="Detector_1" type="Infrared point sensor" x0="5" y0="4" z0="0.5" processing_time="1" response_time="1" trigger_matter="CH4"
trigger_point_low="0.01" trigger_point_high="0.02" angle="0." />
<Detector id="2" name="Detector_2" type="Infrared point sensor" x0="14" y0="4" z0="2" processing_time="1" response_time="1" trigger_matter="CH4"
trigger_point_low="0.01" trigger_point_high="0.02" angle="0." />
<Detector id="3" name="Detector_3" type="Infrared point sensor" x0="24" y0="4" z0="2" processing_time="1" response_time="1" trigger_matter="CH4"
trigger_point_low="0.01" trigger_point_high="0.02" angle="0." />
<Detector id="4" name="Detector_4" type="Infrared point sensor" x0="5" y0="12" z0="0.5" processing_time="1" response_time="1" trigger_matter="CH4"
trigger_point_low="0.01" trigger_point_high="0.02" angle="0." />
<Detector id="5" name="Detector_5" type="Infrared point sensor" x0="14" y0="12" z0="2" processing_time="1" response_time="1" trigger_matter="CH4"
trigger_point_low="0.01" trigger_point_high="0.02" angle="0." />
<Detector id="6" name="Detector_6" type="Infrared point sensor" x0="24" y0="12" z0="2" processing_time="1" response_time="1" trigger_matter="CH4"
trigger_point_low="0.01" trigger_point_high="0.02" angle="0." />
<Detector id="7" name="Detector_7" type="Infrared point sensor" x0="15" y0="6" z0="2" processing_time="1" response_time="1" trigger_matter="CH4"
trigger_point_low="0.01" trigger_point_high="0.02" angle="0." />
<Detector id="8" name="Detector_8" type="Infrared point sensor" x0="4" y0="4" z0="6" processing_time="1" response_time="1" trigger_matter="CH4"
trigger_point_low="0.01" trigger_point_high="0.02" angle="0." />
<Detector id="9" name="Detector_9" type="Infrared point sensor" x0="14" y0="4" z0="6" processing_time="1" response_time="1" trigger_matter="CH4"
trigger_point_low="0.01" trigger_point_high="0.02" angle="0." />
<Detector id="10" name="Detector_10" type="Infrared point sensor" x0="24" y0="4" z0="6" processing_time="1" response_time="1" trigger_matter="CH4"
trigger_point_low="0.01" trigger_point_high="0.02" angle="0." />
<Detector id="11" name="Detector_11" type="Infrared point sensor" x0="4" y0="12" z0="6" processing_time="1" response_time="1" trigger_matter="CH4"
trigger_point_low="0.01" trigger_point_high="0.02" angle="0." />
<Detector id="12" name="Detector_12" type="Infrared point sensor" x0="14" y0="12" z0="6" processing_time="1" response_time="1" trigger_matter="CH4"
trigger_point_low="0.01" trigger_point_high="0.02" angle="0." />
<Detector id="13" name="Detector_13" type="Infrared point sensor" x0="24" y0="12" z0="6" processing_time="1" response_time="1" trigger_matter="CH4"
trigger_point_low="0.01" trigger_point_high="0.02" angle="0." />
<Detector id="14" name="Detector_14" type="Infrared point sensor" x0="15" y0="8" z0="6" processing_time="1" response_time="1" trigger_matter="CH4"
trigger_point_low="0.01" trigger_point_high="0.02" angle="0." />
<Detector id="15" name="Detector_15" type="IR open path (Line)" x0="-1" y0="9.5" z0="4" x1="29" y1="9.5" z1="4" processing_time="1" response_time="1"
trigger_matter="CH4" trigger_point_low="0.01" trigger_point_high="0.02" angle="0." />
```

Figure 10.10: Details of gas detectors and ignitors in (.xml) file, Part 1.

```
<Detector id="16" name="Detector_16" type="IR open path (Line)" x0="-1" y0="14.5" z0="4.5" x1="29" y1="14.5" z1="4.5" processing_time="1" response_time="1"
trigger_matter="CH4" trigger_point_low="0.01" trigger_point_high="0.02" angle="0." />
<Detector id="17" name="Detector_17" type="IR open path (Line)" x0="-1.5" y0="0" z0="0.5" x1="-1.5" y1="16" z1="7.5" processing_time="1" response_time="1"
trigger_matter="CH4" trigger_point_low="0.01" trigger_point_high="0.02" angle="0." />
<Detector id="18" name="Detector_18" type="IR open path (Line)" x0="29.5" y0="0" z0="7.5" x1="29.5" y1="16" z1="0.5" processing_time="1" response_time="1"
trigger_matter="CH4" trigger_point_low="0.01" trigger_point_high="0.02" angle="0." />
<Detector id="19" name="Detector_19" type="Infrared point sensor" x0="1" y0="0" z0="7" processing_time="1" response_time="1" trigger_matter="CH4"
trigger_point_low="0.01" trigger_point_high="0.02" angle="0." />
<Ignitor id="1" name="IGS_1" type="Other generic [Ex]" x0="-1" y0="-0.3" z0="0" x1="29" y1="15.7" z1="8" cont_expec="6.0e-07" t_hot="20"
discr_expec="1.2e-08" piso="0.3" />
<Ignitor id="2" name="IGS_2" type="Electrical equipment, generic [Ex]" x0="-1" y0="-0.3" z0="0" x1="29" y1="15.7" z1="8" cont_expec="1.8e-06" t_hot="5"
discr_expec="1.5e-09" piso="0.25" />
<Ignitor id="3" name="Pump [ex] 112[ex]" type="Pump [Ex]" x0="23.6" y0="3.575" z0="0.1" x1="25.6" y1="4.625" z1="1.15" cont_expec="3.7e-03" t_hot="20"
discr_expec="1.5e-06" piso="1"/>
<Ignitor id="4" name="Pump [ex] 197[ex]" type="Pump [Ex]" x0="12.35" y0="3.7875" z0="0.0475" x1="13.35" y1="4.3125" z1="0.5725" cont_expec="3.7e-03"
t_hot="20" discr_expec="1.5e-06" piso="1"/>
<Ignitor id="5" name="Pump [ex] 204[ex]" type="Pump [Ex]" x0="13.05" y0="2.0375" z0="0.0725" x1="14.05" y1="2.5625" z1="0.5975" cont_expec="3.7e-03"
t_hot="20" discr_expec="1.5e-06" piso="1"/>
<Ignitor id="6" name="Pump [ex] 212[ex]" type="Pump [Ex]" x0="11.25" y0="13.1375" z0="0.0225" x1="12.25" y1="13.6625" z1="0.5475" cont_expec="3.7e-03"
t_hot="20" discr_expec="1.5e-06" piso="1"/>
</RBM>

   </atStartAndRestart>
   <atFixedTimeInterval dt="30" begin="0" end="1e+30">
      <save type="field" macro="s">
         <file name="$c_std_$t.r3d"  />
      </save>
      <save type="field" macro="VPROB_ACC">
         <file name="$c_iprob_$t.r3d"  />
      </save>
 </atFixedTimeInterval>

   <atExit>
      <save type="field" macro="s">
         <file name="$c_std_exit.r3d"  />
      </save>
      <save type="field" macro="VPROB_ACC">
         <file name="$c_iprob_$t.r3d"  />
      </save>
   </atExit>

</kfxScript>
```

Figure 10.11: Details of gas detectors and ignitors in (.xml) file, Part 2.

Appendix H - Details of ".xml" file used for simulation case with hot-working in one section of the module

```
<?xml version = "1.0" encoding="UTF-8" standalone="no" ?>
<kfxScript>
<GUI protection="No" /> <!--
  This is a command shedule file automatically generated by [Quick run setup] in the
  "KFX Fire & gas cloud simulation wizard".
  You may want to edit this file in a text editor. To avoid unitentional overwrite
  from GUI after your own editing set:
      <GUI Protection="Yes" >
  in the third line of this .xml file -->
   <atStartAndRestart>
       <runParameters TFIL="5 " TMAX="1500" />
      <xmlInclude xmlFile="blowdown.xml" /> <RBM>
<Detector id="1" name="Detector_1" type="Infrared point sensor" x0="5" y0="4" z0="0.5" processing_time="1" response_time="1" trigger_matter="CH4"
trigger_point_low="0.01" trigger_point_high="0.02" angle="0." />
<Detector id="2" name="Detector_2" type="Infrared point sensor" x0="14" y0="4" z0="2" processing_time="1" response_time="1" trigger_matter="CH4"
trigger_point_low="0.01" trigger_point_high="0.02" angle="0." />
<Detector id="3" name="Detector_3" type="Infrared point sensor" x0="24" y0="4" z0="2" processing_time="1" response_time="1" trigger_matter="CH4"
trigger_point_low="0.01" trigger_point_high="0.02" angle="0." />
<Detector id="4" name="Detector_4" type="Infrared point sensor" x0="5" y0="12" z0="0.5" processing_time="1" response_time="1" trigger_matter="CH4"
trigger_point_low="0.01" trigger_point_high="0.02" angle="0." />
<Detector id="5" name="Detector_5" type="Infrared point sensor" x0="14" y0="12" z0="2" processing_time="1" response_time="1" trigger_matter="CH4"
trigger_point_low="0.01" trigger_point_high="0.02" angle="0." />
<Detector id="6" name="Detector_6" type="Infrared point sensor" x0="24" y0="12" z0="2" processing_time="1" response_time="1" trigger_matter="CH4"
trigger_point_low="0.01" trigger_point_high="0.02" angle="0." />
<Detector id="7" name="Detector_7" type="Infrared point sensor" x0="15" y0="6" z0="2" processing_time="1" response_time="1" trigger_matter="CH4"
trigger_point_low="0.01" trigger_point_high="0.02" angle="0." />
<Detector id="8" name="Detector_8" type="Infrared point sensor" x0="4" y0="4" z0="6" processing_time="1" response_time="1" trigger_matter="CH4"
trigger_point_low="0.01" trigger_point_high="0.02" angle="0." />
<Detector id="9" name="Detector_9" type="Infrared point sensor" x0="14" y0="4" z0="6" processing_time="1" response_time="1" trigger_matter="CH4"
trigger_point_low="0.01" trigger_point_high="0.02" angle="0." />
<Detector id="10" name="Detector_10" type="Infrared point sensor" x0="24" y0="4" z0="6" processing_time="1" response_time="1" trigger_matter="CH4"
trigger_point_low="0.01" trigger_point_high="0.02" angle="0." />
<Detector id="11" name="Detector_11" type="Infrared point sensor" x0="4" y0="12" z0="6" processing_time="1" response_time="1" trigger_matter="CH4"
trigger_point_low="0.01" trigger_point_high="0.02" angle="0." />
<Detector id="12" name="Detector_12" type="Infrared point sensor" x0="14" y0="12" z0="6" processing_time="1" response_time="1" trigger_matter="CH4"
trigger_point_low="0.01" trigger_point_high="0.02" angle="0." />
<Detector id="13" name="Detector_13" type="Infrared point sensor" x0="24" y0="12" z0="6" processing_time="1" response_time="1" trigger_matter="CH4"
trigger_point_low="0.01" trigger_point_high="0.02" angle="0." />
<Detector id="14" name="Detector_14" type="Infrared point sensor" x0="15" y0="8" z0="6" processing_time="1" response_time="1" trigger_matter="CH4"
trigger_point_low="0.01" trigger_point_high="0.02" angle="0." />
<Detector id="15" name="Detector_15" type="IR open path (Line)" x0="-1" y0="9.5" z0="4" x1="29" y1="9.5" z1="4" processing_time="1" response_time="1"
trigger_matter="CH4" trigger_point_low="0.01" trigger_point_high="0.02" angle="0." />
<Detector id="16" name="Detector_16" type="IR open path (Line)" x0="-1" y0="14.5" z0="4.5" x1="29" y1="14.5" z1="4.5" processing_time="1" response_time="1"
trigger_matter="CH4" trigger_point_low="0.01" trigger_point_high="0.02" angle="0." />
```

Figure 10.12: Details of (.xml) file used for sensitivity 3, Part 1.

```
<Detector id="17" name="Detector_17" type="IR open path (Line)" x0="-1.5" y0="0" z0="0.5" x1="-1.5" y1="16" z1="7.5" processing_time="1" response_time="1"
trigger_matter="CH4" trigger_point_low="0.01" trigger_point_high="0.02" angle="0." />
<Detector id="18" name="Detector_18" type="IR open path (Line)" x0="29.5" y0="0" z0="7.5" x1="29.5" y1="16" z1="0.5" processing_time="1" response_time="1"
trigger_matter="CH4" trigger_point_low="0.01" trigger_point_high="0.02" angle="0." />
<Detector id="19" name="Detector_19" type="Infrared point sensor" x0="1" y0="0" z0="7" processing_time="1" response_time="1" trigger_matter="CH4"
trigger_point_low="0.01" trigger_point_high="0.02" angle="0." />
<Ignitor id="1" name="IGS_1" type="Other generic [Ex]" x0="-1" y0="-0.3" z0="0" x1="29" y1="15.7" z1="8" cont_expec="6.0e-07" t_hot="20"
discr_expec="1.2e-08" piso="0.3" />
<Ignitor id="2" name="IGS_2" type="Electrical equipment, generic [Ex]" x0="-1" y0="-0.3" z0="0" x1="29" y1="15.7" z1="8" cont_expec="1.8e-06" t_hot="5"
discr_expec="1.5e-09" piso="0.25" />
<Ignitor id="3" name="Pump [ex] 112[ex]" type="Pump [Ex]" x0="23.6" y0="3.575" z0="0.1" x1="25.6" y1="4.625" z1="1.15" cont_expec="3.7e-03" t_hot="20"
discr_expec="1.5e-06" piso="1"/>
<Ignitor id="4" name="Pump [ex] 197[ex]" type="Pump [Ex]" x0="12.35" y0="3.7875" z0="0.0475" x1="13.35" y1="4.3125" z1="0.5725" cont_expec="3.7e-03" t_hot="20"
discr_expec="1.5e-06" piso="1"/>
<Ignitor id="5" name="Pump [ex] 204[ex]" type="Pump [Ex]" x0="13.05" y0="2.0375" z0="0.0725" x1="14.05" y1="2.5625" z1="0.5975" cont_expec="3.7e-03" t_hot="20"
discr_expec="1.5e-06" piso="1"/>
<Ignitor id="6" name="Pump [ex] 212[ex]" type="Pump [Ex]" x0="11.25" y0="13.1375" z0="0.0225" x1="12.25" y1="13.6625" z1="0.5475" cont_expec="3.7e-03" t_hot="20"
discr_expec="1.5e-06" piso="1"/>
For leaks > 32 kg/s:
<Ignitor id="7" name="Habitat_30" type="Pump [Ex]" x0="22" y0="10" z0="3.3" x1="24" y1="12" z1="5.3" cont_expec="0.3" t_hot="30" discr_expec="0" piso="1" />
For leaks 8 kg/s - 32 kg/s
<Ignitor id="7" name="Habitat_10_30" type="Pump [Ex]" x0="22" y0="10" z0="3.3" x1="24" y1="12" z1="5.3" cont_expec="0.2" t_hot="20" discr_expec="0" piso="1" />
For leaks 1 kg/s - <=8 kg/s
<Ignitor id="7" name="Habitat_1_10" type="Pump [Ex]" x0="22" y0="10" z0="3.3" x1="24" y1="12" z1="5.3" cont_expec="0.1" t_hot="10" discr_expec="0" piso="1" />
For leaks <= 1 kg/s
<Ignitor id="7" name="Habitat_1" type="Pump [Ex]" x0="22" y0="10" z0="3.3" x1="24" y1="12" z1="5.3" cont_expec="0.05" t_hot="5" discr_expec="0" piso="1" /> </RBM>
   </atStartAndRestart>
   <atFixedTimeInterval dt="30" begin="0" end="1e+30">
      <save type="field" macro="s">
         <file name="$c_std_$t.r3d"  />
      </save>
      <save type="field" macro="VPROB_ACC">
         <file name="$c_iprob_$t.r3d"  />
      </save>
 </atFixedTimeInterval>
   <atExit>
      <save type="field" macro="s">
         <file name="$c_std_exit.r3d"  />
      </save>
      <save type="field" macro="VPROB_ACC">
         <file name="$c_iprob_$t.r3d"  />
      </save>
   </atExit>

</kfxScript>
```

Figure 10.13: Details of (.xml) file used for sensitivity 3, Part 2.

Appendix I - Result plots for leak rate of 8 kg/s.

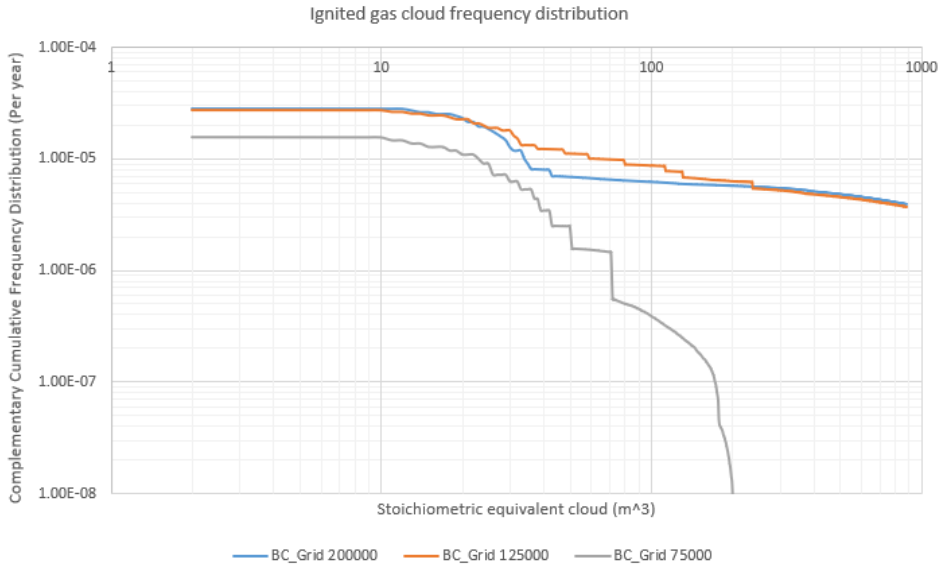

Figure 10.14: Stoichiometric cloud volume comparison for different grid resolutions.

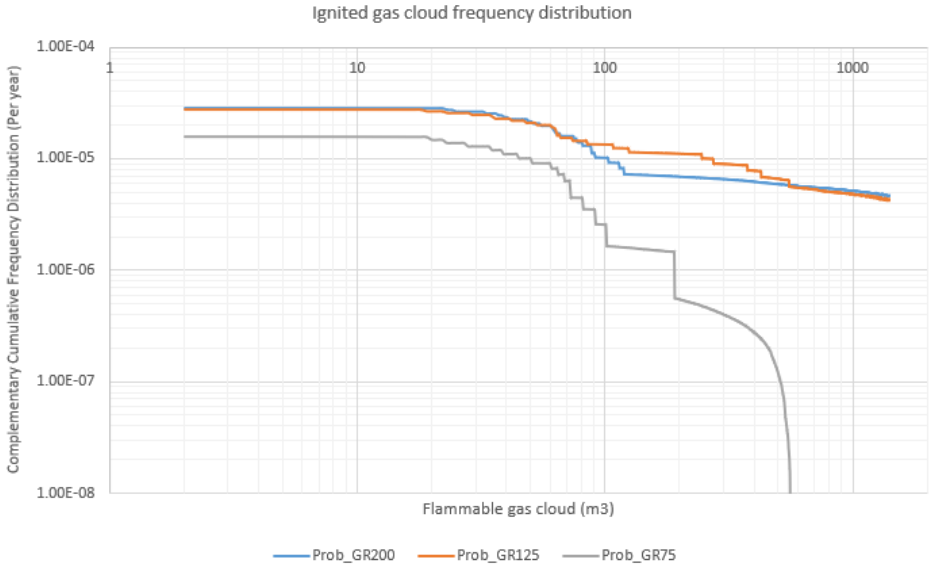

Figure 10.15: Comparison of flammable cloud volume for different grid resolutions.

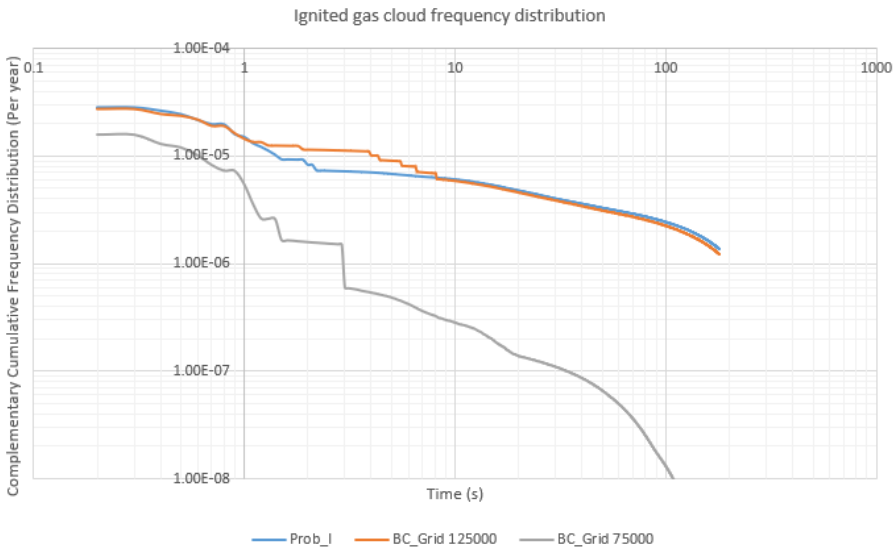

Figure 10.16: Transient cumulative frequency comparison for different grid resolutions.

Appendix J - Plots of contribution from various sources.

Sensitivity 2 - Partial isolation of gas detectors.

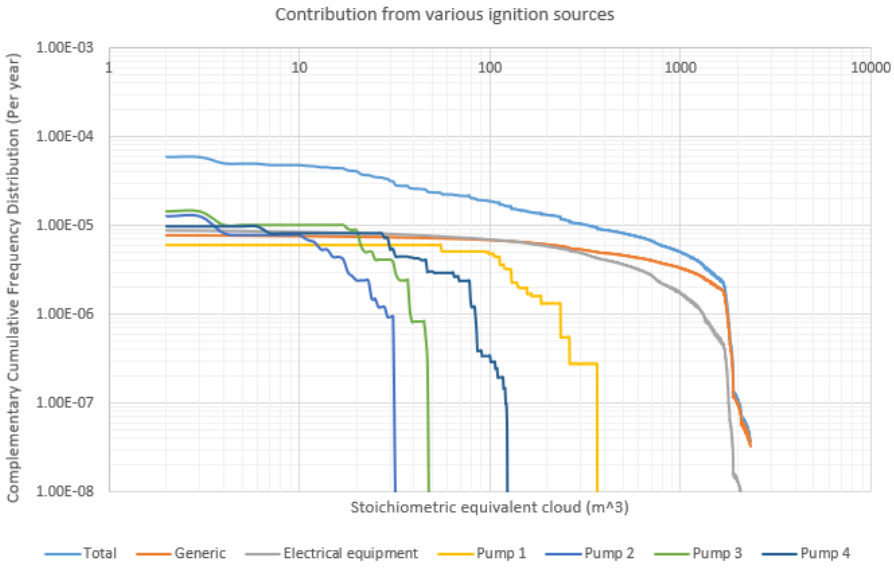

Figure 10.17: Cumulative frequency vs stoichiometric cloud contribution sources.

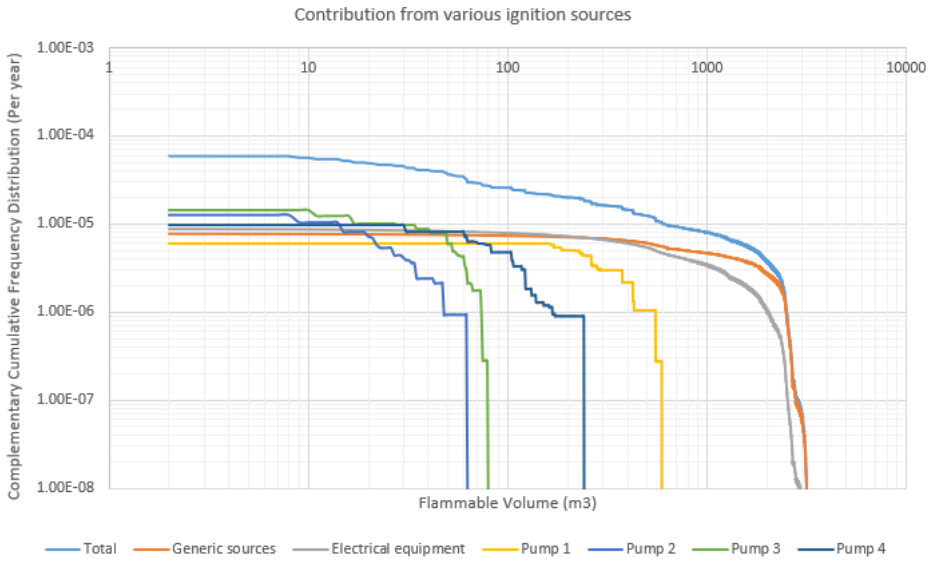

Figure 10.18: Cumulative frequency vs flammable cloud contribution sources.

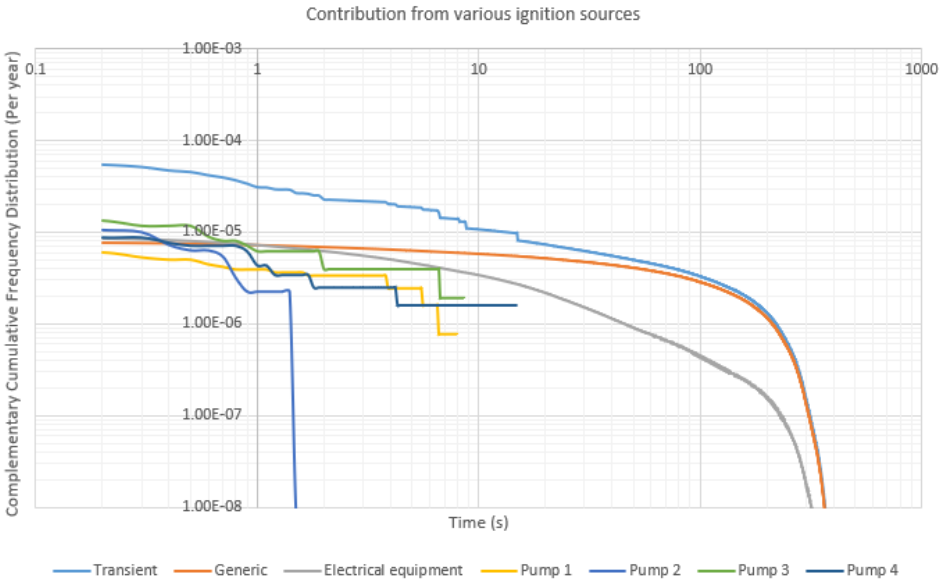

Figure 10.19: Transient cumulative frequency contribution sources.

Sensitivity 3 - Increased ignition sources the module.

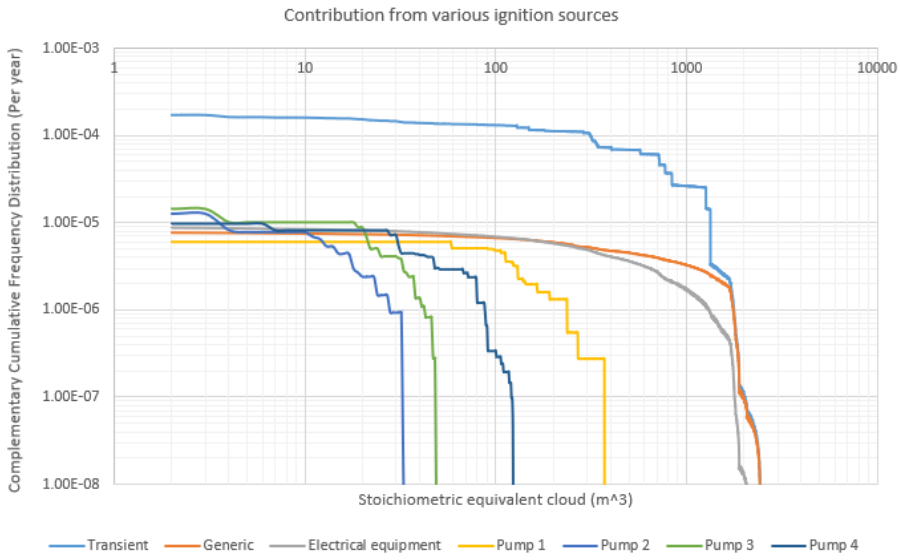

Figure 10.20: Cumulative frequency vs stoichiometric cloud contribution sources.

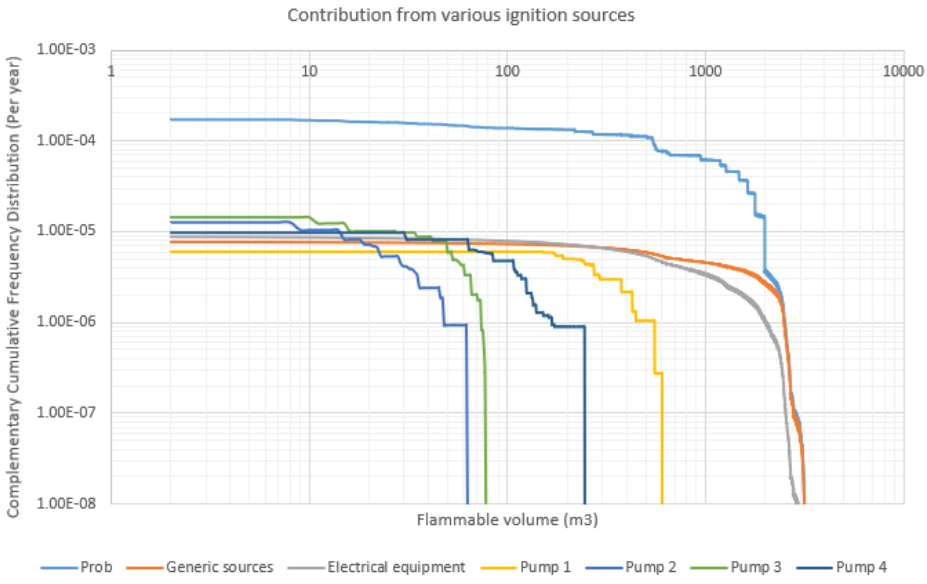

Figure 10.21: Cumulative frequency vs flammable cloud contribution sources.

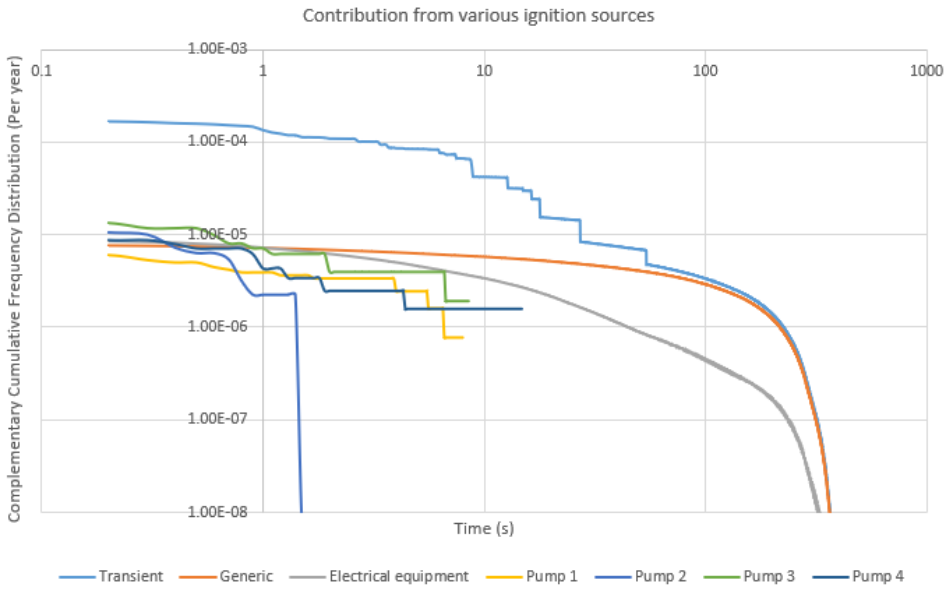

Figure 10.22: Transient cumulative frequency contribution sources.

Sensitivity 4 - Temporary weather cladding to prevent cold winds.

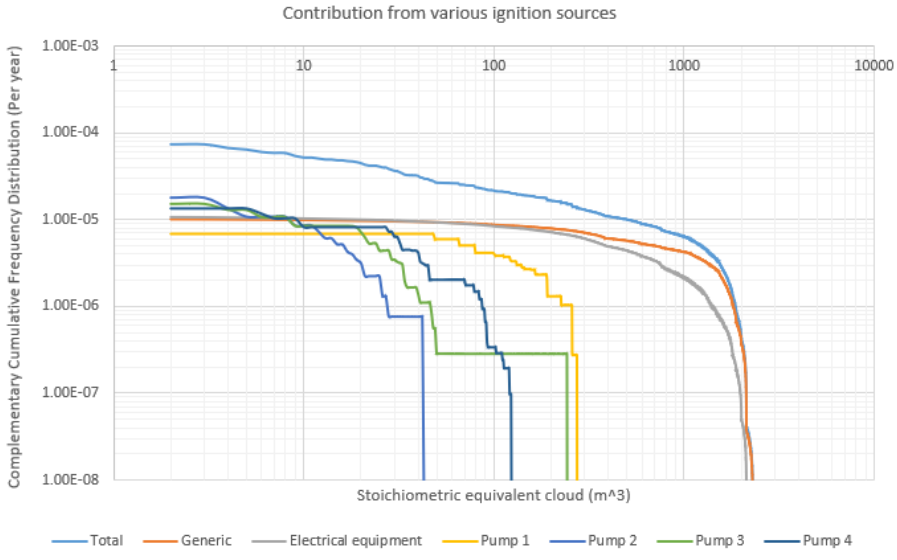

Figure 10.23: Cumulative frequency vs stoichiometric cloud contribution sources.

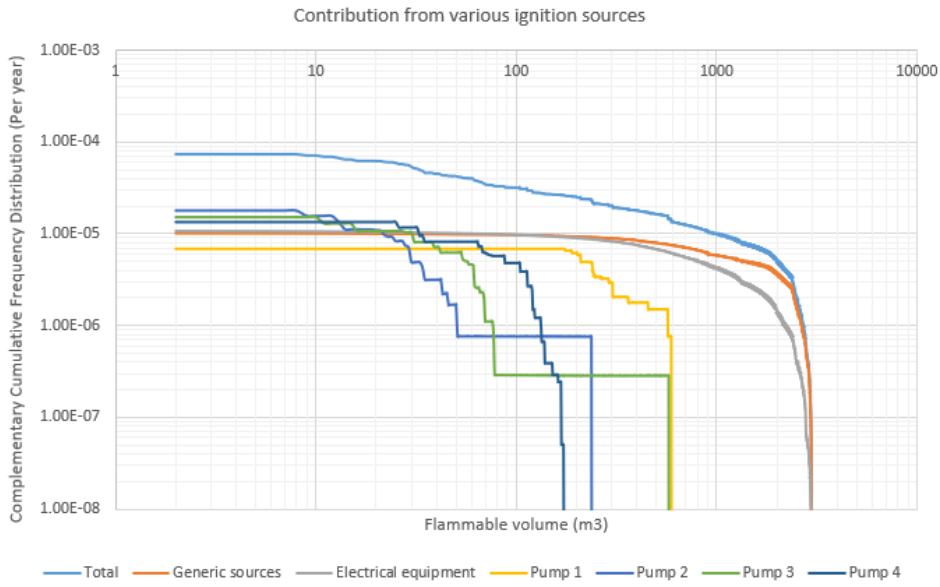

Figure 10.24: Cumulative frequency vs flammable cloud contribution sources.

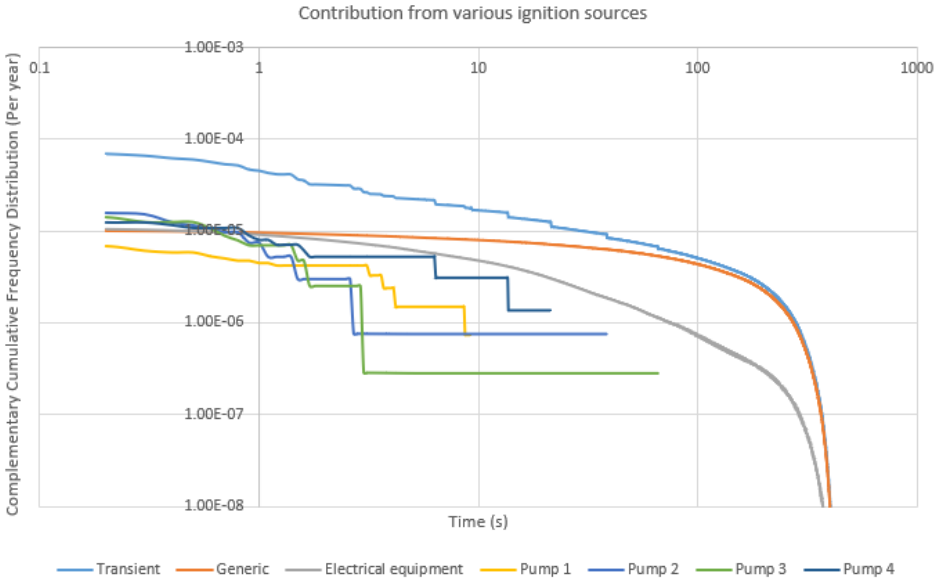

Figure 10.25: Transient cumulative frequency contribution sources.

Base case - Valve failure.

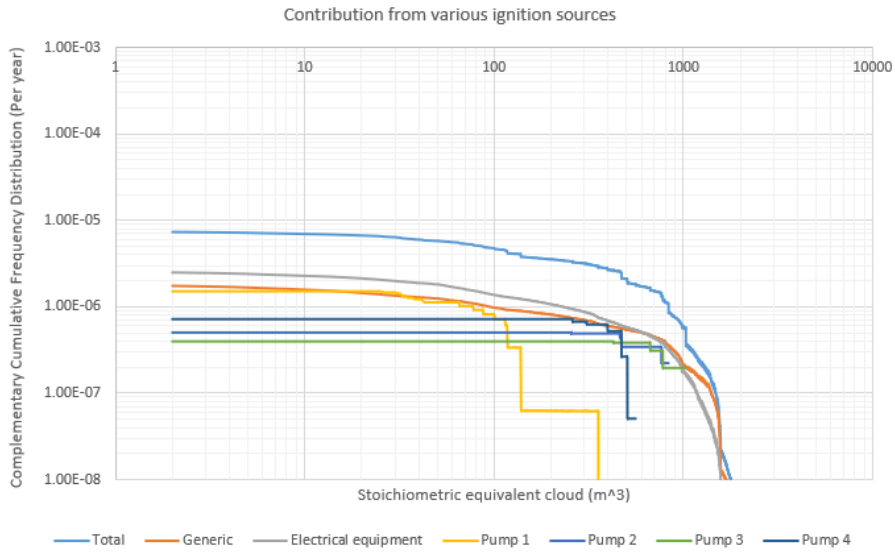

Figure 10.26: Cumulative frequency vs stoichiometric cloud contribution sources.

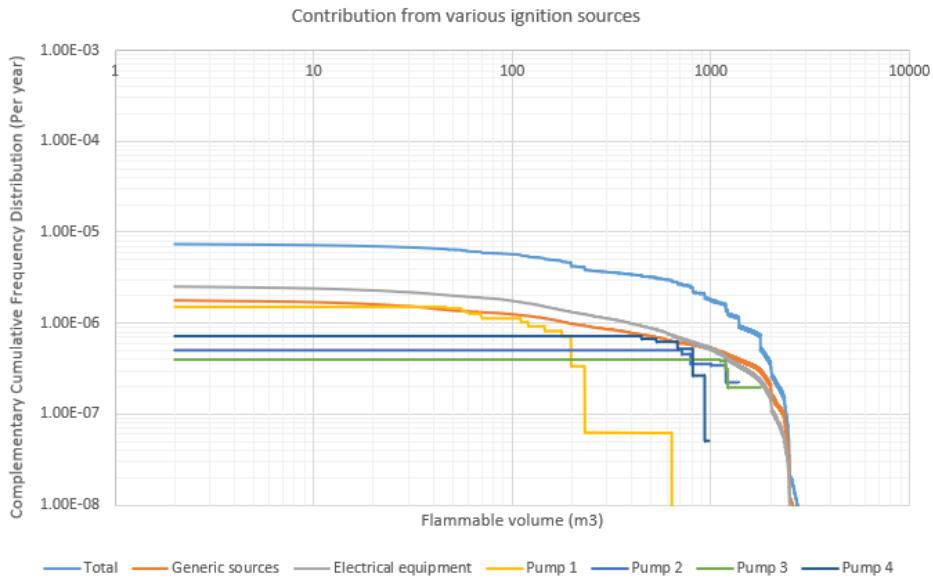

Figure 10.27: Cumulative frequency vs flammable cloud contribution sources.

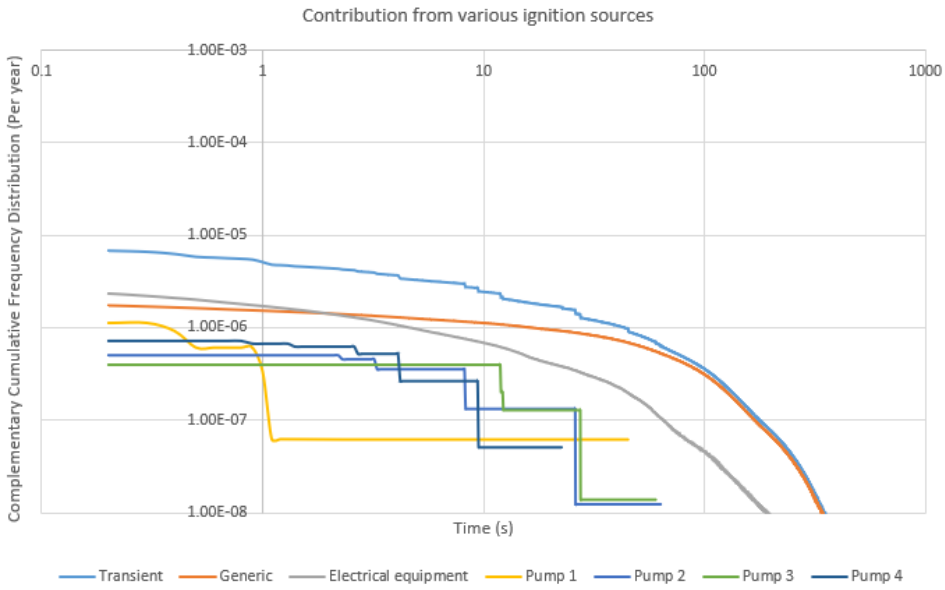

Figure 10.28: Transient cumulative frequency contribution sources.

Appendix K - Result files of base case with 125000 grids.

Due to enormous the size of the result files, the number of iterations presented in each of the file has been reduced to accommodate in the appendix.

Stoichiometric equivalent cloud volume result file

VolEqStCL	Prob	Prob_I	Prob_C	Prob_D	Prob_001	Prob_C_001
0	5.91E-05	4.25E-05	5.34E-05	5.73E-06	7.87E-06	2.84E-06
1	5.91E-05	0	5.34E-05	5.73E-06	7.85E-06	2.83E-06
10	4.79E-05	0	4.22E-05	5.63E-06	7.66E-06	2.71E-06
20	4.08E-05	0	3.52E-05	5.57E-06	7.52E-06	2.63E-06
40	2.65E-05	0	2.10E-05	5.48E-06	7.32E-06	2.49E-06
60	2.24E-05	0	1.70E-05	5.40E-06	7.13E-06	2.38E-06
80	2.02E-05	0	1.49E-05	5.32E-06	6.97E-06	2.29E-06
100	1.87E-05	0	1.34E-05	5.24E-06	6.82E-06	2.20E-06
200	1.31E-05	0	8.29E-06	4.81E-06	6.08E-06	1.84E-06
300	1.04E-05	0	6.13E-06	4.31E-06	5.35E-06	1.55E-06
400	8.88E-06	0	4.81E-06	4.08E-06	4.87E-06	1.28E-06
500	8.16E-06	0	4.22E-06	3.94E-06	4.60E-06	1.12E-06
600	7.42E-06	0	3.66E-06	3.77E-06	4.30E-06	9.73E-07
650	7.08E-06	0	3.38E-06	3.70E-06	4.17E-06	9.01E-07
700	6.71E-06	0	3.07E-06	3.64E-06	4.03E-06	8.21E-07
750	6.22E-06	0	2.65E-06	3.57E-06	3.86E-06	7.10E-07
800	5.89E-06	0	2.39E-06	3.50E-06	3.73E-06	6.42E-07
850	5.66E-06	0	2.23E-06	3.43E-06	3.62E-06	6.00E-07
900	5.44E-06	0	2.08E-06	3.35E-06	3.52E-06	5.59E-07
950	5.21E-06	0	1.94E-06	3.28E-06	3.41E-06	5.20E-07
1000	4.98E-06	0	1.78E-06	3.20E-06	3.30E-06	4.78E-07
1050	4.75E-06	0	1.63E-06	3.12E-06	3.19E-06	4.37E-07
1100	4.52E-06	0	1.49E-06	3.04E-06	3.08E-06	3.98E-07
1150	4.30E-06	0	1.35E-06	2.95E-06	2.96E-06	3.62E-07
1200	4.10E-06	0	1.23E-06	2.87E-06	2.86E-06	3.29E-07
1250	3.89E-06	0	1.10E-06	2.78E-06	2.75E-06	2.94E-07
1300	3.64E-06	0	9.52E-07	2.69E-06	2.63E-06	2.53E-07
1400	3.15E-06	0	6.59E-07	2.49E-06	2.37E-06	1.73E-07
1500	2.78E-06	0	4.78E-07	2.30E-06	2.16E-06	1.24E-07
1600	2.48E-06	0	3.62E-07	2.11E-06	1.96E-06	9.31E-08
1700	2.05E-06	0	2.57E-07	1.80E-06	1.65E-06	6.54E-08
1800	6.98E-07	0	3.50E-09	6.94E-07	6.14E-07	7.75E-10
1900	1.31E-07	0	0	1.31E-07	1.16E-07	0
2000	1.07E-07	0	0	1.07E-07	9.41E-08	0
2100	6.59E-08	0	0	6.59E-08	5.82E-08	0
2200	5.47E-08	0	0	5.47E-08	4.83E-08	0
2300	4.09E-08	0	0	4.09E-08	3.61E-08	0
2400	2.05E-08	0	0	2.05E-08	1.81E-08	0
2443	1.29E-09	0	0	1.30E-09	1.14E-09	0

Table 10.19: Stoichiometric equivalent cloud volume results - Part 1

Prob_D_001	Prob_002	Prob_C_002	Prob_D_002	Prob_003	Prob_C_003
5.03E-06	8.82E-06	8.15E-06	6.75E-07	6.01E-06	6.01E-06
5.03E-06	8.79E-06	8.12E-06	6.74E-07	6.01E-06	6.01E-06
4.95E-06	8.44E-06	7.78E-06	6.63E-07	6.01E-06	6.01E-06
4.89E-06	8.20E-06	7.54E-06	6.56E-07	6.01E-06	6.01E-06
4.82E-06	7.79E-06	7.15E-06	6.47E-07	6.01E-06	6.01E-06
4.75E-06	7.44E-06	6.80E-06	6.37E-07	5.09E-06	5.09E-06
4.68E-06	7.17E-06	6.54E-06	6.28E-07	5.09E-06	5.09E-06
4.62E-06	6.92E-06	6.30E-06	6.19E-07	4.78E-06	4.78E-06
4.24E-06	5.83E-06	5.26E-06	5.69E-07	1.32E-06	1.32E-06
3.79E-06	4.91E-06	4.41E-06	5.09E-07	2.75E-07	2.73E-07
3.59E-06	4.09E-06	3.61E-06	4.82E-07	9.45E-10	0
3.48E-06	3.63E-06	3.17E-06	4.66E-07	5.97E-10	0
3.32E-06	3.19E-06	2.74E-06	4.46E-07	2.68E-10	0
3.27E-06	2.97E-06	2.53E-06	4.38E-07	1.87E-10	0
3.21E-06	2.73E-06	2.30E-06	4.31E-07	1.12E-10	0
3.15E-06	2.40E-06	1.98E-06	4.23E-07	4.48E-11	0
3.09E-06	2.20E-06	1.79E-06	4.15E-07	0	0
3.02E-06	2.08E-06	1.67E-06	4.06E-07	0	0
2.96E-06	1.95E-06	1.56E-06	3.97E-07	0	0
2.89E-06	1.84E-06	1.45E-06	3.88E-07	0	0
2.82E-06	1.71E-06	1.33E-06	3.78E-07	0	0
2.75E-06	1.59E-06	1.22E-06	3.69E-07	0	0
2.68E-06	1.47E-06	1.11E-06	3.59E-07	0	0
2.60E-06	1.36E-06	1.01E-06	3.49E-07	0	0
2.53E-06	1.26E-06	9.23E-07	3.40E-07	0	0
2.46E-06	1.16E-06	8.26E-07	3.30E-07	0	0
2.37E-06	1.03E-06	7.15E-07	3.18E-07	0	0
2.19E-06	7.92E-07	4.97E-07	2.95E-07	0	0
2.03E-06	6.34E-07	3.62E-07	2.73E-07	0	0
1.87E-06	5.25E-07	2.75E-07	2.50E-07	0	0
1.59E-06	4.08E-07	1.95E-07	2.13E-07	0	0
6.13E-07	8.48E-08	2.53E-09	8.23E-08	0	0
1.15E-07	1.55E-08	0	1.55E-08	0	0
9.41E-08	1.26E-08	0	1.26E-08	0	0
5.81E-08	7.81E-09	0	7.80E-09	0	0
4.83E-08	6.49E-09	0	6.48E-09	0	0
3.61E-08	4.85E-09	0	4.84E-09	0	0
1.81E-08	2.43E-09	0	2.43E-09	0	0
1.14E-09	1.63E-10	0	1.53E-10	0	0

Table 10.20: Stoichiometric equivalent cloud volume results - Part 2

Prob_D_003	Prob_004	Prob_C_004	Prob_D_004	Prob_005	Prob_C_005
1.77E-09	1.27E-05	1.27E-05	1.21E-08	1.44E-05	1.44E-05
1.77E-09	1.27E-05	1.27E-05	1.21E-08	1.44E-05	1.44E-05
1.77E-09	7.81E-06	7.80E-06	8.17E-09	1.01E-05	1.01E-05
1.77E-09	2.40E-06	2.39E-06	7.88E-09	8.80E-06	8.79E-06
1.77E-09	5.18E-09	0	5.19E-09	1.37E-06	1.37E-06
1.75E-09	2.47E-09	0	2.48E-09	2.34E-09	0
1.67E-09	2.06E-09	0	2.06E-09	1.91E-09	0
1.66E-09	2.00E-09	0	2.00E-09	1.86E-09	0
1.51E-09	1.67E-09	0	1.67E-09	1.55E-09	0
1.24E-09	1.31E-09	0	1.32E-09	1.23E-09	0
9.41E-10	9.35E-10	0	9.43E-10	9.35E-10	0
5.95E-10	5.98E-10	0	5.95E-10	6.04E-10	0
2.66E-10	2.55E-10	0	2.66E-10	2.68E-10	0
1.80E-10	1.68E-10	0	1.80E-10	1.81E-10	0
1.10E-10	1.06E-10	0	1.10E-10	1.12E-10	0
4.08E-11	3.92E-11	0	4.08E-11	4.48E-11	0
0	0	0	0	0	0
0	0	0	0	0	0
0	0	0	0	0	0
0	0	0	0	0	0
0	0	0	0	0	0
0	0	0	0	0	0
0	0	0	0	0	0
0	0	0	0	0	0
0	0	0	0	0	0
0	0	0	0	0	0
0	0	0	0	0	0
0	0	0	0	0	0
0	0	0	0	0	0
0	0	0	0	0	0
0	0	0	0	0	0
0	0	0	0	0	0
0	0	0	0	0	0
0	0	0	0	0	0
0	0	0	0	0	0
0	0	0	0	0	0
0	0	0	0	0	0
0	0	0	0	0	0
0	0	0	0	0	0
0	0	0	0	0	0

Table 10.21: Stoichiometric equivalent cloud volume results - Part 3

Prob_D_005	Prob_006	Prob_C_006	Prob_D_006	ftf_vol	LeL_vol	LeakRate
7.54E-09	9.74E-06	9.73E-06	5.24E-09	-1.71E-08	0.109099	0.015679
7.54E-09	9.74E-06	9.73E-06	5.24E-09	0.000367	0.103485	-0.09736
7.48E-09	8.16E-06	8.15E-06	5.24E-09	-0.00507	0.307819	-0.09245
7.46E-09	8.16E-06	8.15E-06	5.24E-09	-0.009	0.367466	-0.09115
5.03E-09	4.25E-06	4.25E-06	3.55E-09	-0.01524	0.455918	-0.09001
2.32E-09	2.92E-06	2.91E-06	1.88E-09	-0.01553	0.478709	-0.08901
1.91E-09	1.21E-06	1.20E-06	1.60E-09	-0.01398	0.486132	-0.08312
1.85E-09	3.38E-07	3.36E-07	1.55E-09	-0.01894	0.494403	-0.07488
1.54E-09	1.24E-09	0	1.22E-09	-0.02374	0.481198	-0.04763
1.23E-09	9.18E-10	0	9.10E-10	-0.01947	0.396783	-0.03094
9.38E-10	6.17E-10	0	6.19E-10	-0.01247	0.280679	-0.0198
5.95E-10	3.07E-10	0	2.97E-10	-0.00877	0.268122	-0.01717
2.66E-10	4.44E-11	0	4.24E-11	-0.00759	0.224899	-0.01471
1.80E-10	7.41E-12	0	6.36E-12	-0.00731	0.180948	-0.01389
1.10E-10	0	0	0	-0.00694	0.121757	-0.013
4.08E-11	0	0	0	-0.00413	0.00453	-0.0117
0	0	0	0	-0.00387	-0.02844	-0.01082
0	0	0	0	-0.00277	-0.02969	-0.0101
0	0	0	0	-0.00302	-0.04031	-0.00953
0	0	0	0	-0.00344	-0.05478	-0.00904
0	0	0	0	-0.00247	-0.06754	-0.00854
0	0	0	0	-0.00228	-0.07713	-0.00809
0	0	0	0	-0.0019	-0.08781	-0.00754
0	0	0	0	-0.00203	-0.09296	-0.00681
0	0	0	0	-0.00105	-0.10305	-0.00632
0	0	0	0	-0.00149	-0.11001	-0.0058
0	0	0	0	-0.00121	-0.13374	-0.00515
0	0	0	0	-0.00055	-0.18246	-0.00367
0	0	0	0	-0.00064	-0.18531	-0.00276
0	0	0	0	-0.00026	-0.16601	-0.00227
0	0	0	0	-9.25E-05	-0.13967	-0.00183
0	0	0	0	0	-0.14028	-0.00058
0	0	0	0	0	-0.04755	-0.00013
0	0	0	0	0	-0.03777	-9.72E-05
0	0	0	0	0	-0.02267	-4.26E-05
0	0	0	0	0	-0.01854	-3.52E-05
0	0	0	0	0	-0.01363	-2.62E-05
0	0	0	0	0	-0.00684	-1.32E-05
0	0	0	0	0	-0.00036	-8.36E-07

Table 10.22: Stoichiometric equivalent cloud volume results - Part 4

Flammable cloud volume result file

VolUel2Lel	Prob	Prob_I	Prob_C	Prob_D	Prob_001	Prob_C_001
0	5.91E-05	4.25E-05	5.34E-05	5.73E-06	7.87E-06	2.84E-06
1	5.91E-05	0	5.34E-05	5.73E-06	7.86E-06	2.83E-06
10	5.67E-05	0	5.10E-05	5.71E-06	7.80E-06	2.79E-06
50	3.66E-05	0	3.10E-05	5.63E-06	7.60E-06	2.65E-06
100	2.59E-05	0	2.03E-05	5.59E-06	7.45E-06	2.53E-06
150	2.20E-05	0	1.64E-05	5.54E-06	7.30E-06	2.42E-06
200	2.01E-05	0	1.46E-05	5.48E-06	7.13E-06	2.30E-06
250	1.81E-05	0	1.27E-05	5.41E-06	6.97E-06	2.20E-06
300	1.63E-05	0	1.09E-05	5.34E-06	6.81E-06	2.10E-06
400	1.45E-05	0	9.35E-06	5.15E-06	6.45E-06	1.91E-06
500	1.24E-05	0	7.45E-06	4.94E-06	6.05E-06	1.70E-06
600	1.04E-05	0	5.79E-06	4.60E-06	5.52E-06	1.46E-06
700	9.31E-06	0	4.96E-06	4.34E-06	5.15E-06	1.32E-06
800	8.79E-06	0	4.55E-06	4.24E-06	4.95E-06	1.21E-06
900	8.38E-06	0	4.21E-06	4.16E-06	4.79E-06	1.12E-06
1000	7.99E-06	0	3.89E-06	4.10E-06	4.65E-06	1.04E-06
1100	7.59E-06	0	3.56E-06	4.03E-06	4.51E-06	9.51E-07
1200	7.17E-06	0	3.20E-06	3.97E-06	4.36E-06	8.57E-07
1300	6.57E-06	0	2.69E-06	3.89E-06	4.15E-06	7.23E-07
1400	6.26E-06	0	2.47E-06	3.80E-06	4.01E-06	6.64E-07
1500	5.93E-06	0	2.24E-06	3.69E-06	3.86E-06	6.03E-07
1600	5.54E-06	0	1.98E-06	3.56E-06	3.67E-06	5.33E-07
1700	5.16E-06	0	1.75E-06	3.42E-06	3.48E-06	4.70E-07
1800	4.77E-06	0	1.50E-06	3.28E-06	3.29E-06	4.02E-07
1900	4.21E-06	0	1.19E-06	3.02E-06	2.98E-06	3.19E-07
2000	3.72E-06	0	9.24E-07	2.80E-06	2.71E-06	2.45E-07
2100	3.32E-06	0	6.93E-07	2.63E-06	2.50E-06	1.82E-07
2200	2.95E-06	0	5.26E-07	2.42E-06	2.27E-06	1.37E-07
2300	2.57E-06	0	4.02E-07	2.17E-06	2.02E-06	1.04E-07
2400	2.02E-06	0	2.15E-07	1.80E-06	1.64E-06	5.45E-08
2500	1.10E-06	0	3.53E-08	1.06E-06	9.47E-07	8.65E-09
2600	4.85E-07	0	1.75E-09	4.83E-07	4.27E-07	4.25E-10
2700	1.64E-07	0	0	1.64E-07	1.45E-07	0
2800	1.07E-07	0	0	1.07E-07	9.40E-08	0
2900	8.69E-08	0	0	8.69E-08	7.66E-08	0
3000	6.31E-08	0	0	6.31E-08	5.57E-08	0
3050	4.76E-08	0	0	4.76E-08	4.20E-08	0
3100	3.09E-08	0	0	3.09E-08	2.72E-08	0
3179	6.51E-10	0	0	6.51E-10	5.62E-10	0

Table 10.23: Flammable cloud volume results - Part 1

Prob_D_001	Prob_002	Prob_C_002	Prob_D_002	Prob_003	Prob_C_003
5.03E-06	8.82E-06	8.15E-06	6.75E-07	6.01E-06	6.01E-06
5.03E-06	8.80E-06	8.12E-06	6.75E-07	6.01E-06	6.01E-06
5.01E-06	8.67E-06	8.00E-06	6.72E-07	6.01E-06	6.01E-06
4.95E-06	8.27E-06	7.60E-06	6.64E-07	6.01E-06	6.01E-06
4.92E-06	7.91E-06	7.25E-06	6.60E-07	6.01E-06	6.01E-06
4.88E-06	7.58E-06	6.92E-06	6.55E-07	6.01E-06	6.01E-06
4.83E-06	7.24E-06	6.59E-06	6.48E-07	5.01E-06	5.00E-06
4.77E-06	6.93E-06	6.29E-06	6.39E-07	4.38E-06	4.38E-06
4.71E-06	6.63E-06	6.00E-06	6.32E-07	2.99E-06	2.99E-06
4.54E-06	6.03E-06	5.42E-06	6.09E-07	2.17E-06	2.17E-06
4.35E-06	5.41E-06	4.82E-06	5.84E-07	1.05E-06	1.05E-06
4.06E-06	4.69E-06	4.14E-06	5.44E-07	2.74E-07	2.73E-07
3.83E-06	4.24E-06	3.72E-06	5.14E-07	8.54E-10	0
3.73E-06	3.92E-06	3.41E-06	5.01E-07	6.34E-10	0
3.67E-06	3.65E-06	3.16E-06	4.93E-07	4.35E-10	0
3.62E-06	3.40E-06	2.92E-06	4.85E-07	2.94E-10	0
3.56E-06	3.14E-06	2.67E-06	4.78E-07	1.87E-10	0
3.50E-06	2.87E-06	2.40E-06	4.70E-07	9.80E-11	0
3.43E-06	2.47E-06	2.01E-06	4.60E-07	2.80E-12	0
3.35E-06	2.29E-06	1.84E-06	4.50E-07	0	0
3.25E-06	2.11E-06	1.67E-06	4.37E-07	0	0
3.14E-06	1.90E-06	1.48E-06	4.21E-07	0	0
3.02E-06	1.71E-06	1.31E-06	4.05E-07	0	0
2.89E-06	1.51E-06	1.12E-06	3.88E-07	0	0
2.66E-06	1.25E-06	8.94E-07	3.57E-07	0	0
2.47E-06	1.02E-06	6.94E-07	3.31E-07	0	0
2.32E-06	8.33E-07	5.22E-07	3.11E-07	0	0
2.14E-06	6.84E-07	3.97E-07	2.87E-07	0	0
1.92E-06	5.62E-07	3.05E-07	2.57E-07	0	0
1.59E-06	3.77E-07	1.64E-07	2.13E-07	0	0
9.38E-07	1.53E-07	2.73E-08	1.26E-07	0	0
4.26E-07	5.87E-08	1.43E-09	5.72E-08	0	0
1.45E-07	1.94E-08	0	1.94E-08	0	0
9.40E-08	1.26E-08	0	1.26E-08	0	0
7.66E-08	1.03E-08	0	1.03E-08	0	0
5.57E-08	7.47E-09	0	7.47E-09	0	0
4.20E-08	5.64E-09	0	5.63E-09	0	0
2.72E-08	3.66E-09	0	3.65E-09	0	0
5.62E-10	8.14E-11	0	7.55E-11	0	0

Table 10.24: Flammable cloud volume results - Part 2

Prob_D_003	Prob_004	Prob_C_004	Prob_D_004	Prob_005	Prob_C_005
1.77E-09	1.27E-05	1.27E-05	1.21E-08	1.44E-05	1.44E-05
1.77E-09	1.27E-05	1.27E-05	1.21E-08	1.44E-05	1.44E-05
1.77E-09	1.04E-05	1.04E-05	9.74E-09	1.44E-05	1.44E-05
1.77E-09	9.31E-07	9.23E-07	7.72E-09	5.96E-06	5.95E-06
1.77E-09	5.91E-09	0	5.93E-09	5.83E-09	0
1.77E-09	3.67E-09	0	3.66E-09	3.51E-09	0
1.75E-09	2.37E-09	0	2.38E-09	2.25E-09	0
1.71E-09	2.03E-09	0	2.02E-09	1.88E-09	0
1.55E-09	1.71E-09	0	1.72E-09	1.59E-09	0
1.40E-09	1.51E-09	0	1.52E-09	1.42E-09	0
1.24E-09	1.32E-09	0	1.32E-09	1.24E-09	0
1.07E-09	1.08E-09	0	1.08E-09	1.06E-09	0
8.54E-10	8.59E-10	0	8.54E-10	8.67E-10	0
6.35E-10	6.36E-10	0	6.35E-10	6.31E-10	0
4.36E-10	4.30E-10	0	4.36E-10	4.38E-10	0
2.92E-10	2.89E-10	0	2.92E-10	2.92E-10	0
1.85E-10	1.81E-10	0	1.85E-10	1.89E-10	0
9.93E-11	9.24E-11	0	9.93E-11	1.01E-10	0
1.20E-12	2.80E-12	0	1.20E-12	2.80E-12	0
0	0	0	0	0	0
0	0	0	0	0	0
0	0	0	0	0	0
0	0	0	0	0	0
0	0	0	0	0	0
0	0	0	0	0	0
0	0	0	0	0	0
0	0	0	0	0	0
0	0	0	0	0	0
0	0	0	0	0	0
0	0	0	0	0	0
0	0	0	0	0	0
0	0	0	0	0	0
0	0	0	0	0	0
0	0	0	0	0	0
0	0	0	0	0	0
0	0	0	0	0	0
0	0	0	0	0	0
0	0	0	0	0	0
0	0	0	0	0	0

Table 10.25: Flammable cloud volume results - Part 3

Prob_D_005	Prob_006	Prob_C_006	Prob_D_006	ftf_vol	LeL_vol	LeakRate
7.54E-09	9.74E-06	9.73E-06	5.24E-09	-1.51E-09	0.107479	0.015678
7.54E-09	9.74E-06	9.73E-06	5.24E-09	0.001072	0.101551	-0.09799
7.54E-09	9.74E-06	9.73E-06	5.24E-09	-1.86E-03	0.087926	-0.09475
7.36E-09	8.16E-06	8.15E-06	5.24E-09	-0.01044	0.070584	-0.09184
5.78E-09	4.77E-06	4.76E-06	4.54E-09	-1.29E-02	0.045161	-0.09028
3.51E-09	1.28E-06	1.27E-06	2.91E-09	-0.01497	0.030262	-0.08189
2.22E-09	8.93E-07	8.91E-07	1.93E-09	-1.63E-02	-0.00333	-0.07129
1.86E-09	1.59E-09	0	1.56E-09	-1.87E-02	-0.02346	-0.06338
1.58E-09	1.28E-09	0	1.27E-09	-2.17E-02	-0.04122	-0.05595
1.40E-09	1.08E-09	0	1.08E-09	-2.15E-02	-0.06704	-0.04221
1.23E-09	9.26E-10	0	9.08E-10	-1.85E-02	-0.11381	-0.03301
1.05E-09	7.43E-10	0	7.30E-10	-1.00E-02	-0.22495	-0.02388
8.54E-10	5.45E-10	0	5.34E-10	-0.00953	-0.25231	-0.02017
6.35E-10	3.38E-10	0	3.23E-10	-0.00904	-0.24507	-0.01835
4.36E-10	1.63E-10	0	1.55E-10	-0.00807	-0.23746	-0.01692
2.92E-10	6.66E-11	0	5.94E-11	-0.00657	-0.22426	-0.01582
1.85E-10	1.48E-11	0	8.48E-12	-0.00662	-0.23703	-0.0147
9.93E-11	0	0	0	-0.00453	-0.26695	-0.01355
1.20E-12	0	0	0	-0.00322	-0.3535	-0.01172
0	0	0	0	-0.00289	-0.3234	-0.01088
0	0	0	0	-0.00305	-0.29032	-0.01011
0	0	0	0	-0.00207	-0.28176	-0.00904
0	0	0	0	-0.00225	-0.26299	-0.0082
0	0	0	0	-0.00174	-0.25907	-0.00749
0	0	0	0	-0.00164	-0.2318	-0.00534
0	0	0	0	-0.00061	-0.23194	-0.00397
0	0	0	0	-0.00065	-0.256	-0.00349
0	0	0	0	-0.00023	-0.2439	-0.00301
0	0	0	0	-5.39E-05	-0.20712	-0.00254
0	0	0	0	-7.41E-05	-0.18556	-0.00177
0	0	0	0	3.50E-05	-0.17651	-0.0009
0	0	0	0	0	-0.11235	-0.00039
0	0	0	0	0	-0.05631	-0.00016
0	0	0	0	0	-0.03598	-7.27E-05
0	0	0	0	0	-0.02808	-6.01E-05
0	0	0	0	0	-0.01958	-4.50E-05
0	0	0	0	0	-0.01474	-3.45E-05
0	0	0	0	0	-0.00949	-2.27E-05
0	0	0	0	0	-0.00021	-4.81E-07

Table 10.26: Flammable cloud volume results - Part 4

Transient result file

Time(s)	Prob	Prob_I	Prob_C	Prob_D	Prob_001	Prob_C_001
0	5.91E-05	4.25E-05	5.34E-05	5.73E-06	7.87E-06	2.84E-06
1	3.20E-05	0.00E+00	2.63E-05	5.73E-06	7.35E-06	2.32E-06
10	1.08E-05	0.00E+00	5.27E-06	5.58E-06	5.92E-06	9.97E-07
20	7.44E-06	0.00E+00	2.07E-06	5.38E-06	5.29E-06	5.47E-07
30	6.35E-06	0	1.21E-06	5.14E-06	4.84E-06	3.11E-07
40	5.63E-06	0	7.50E-07	4.88E-06	4.49E-06	1.89E-07
50	5.09E-06	0	4.86E-07	4.60E-06	4.18E-06	1.21E-07
60	4.68E-06	0	3.46E-07	4.34E-06	3.91E-06	8.51E-08
70	4.32E-06	0	2.45E-07	4.08E-06	3.66E-06	5.99E-08
80	4.01E-06	0	1.81E-07	3.83E-06	3.42E-06	4.40E-08
90	3.70E-06	0	1.24E-07	3.58E-06	3.19E-06	3.00E-08
100	3.42E-06	0	7.49E-08	3.34E-06	2.97E-06	1.81E-08
120	2.92E-06	0	2.53E-08	2.90E-06	2.56E-06	6.02E-09
140	2.51E-06	0	5.11E-09	2.50E-06	2.21E-06	1.19E-09
160	2.13E-06	0	2.00E-09	2.13E-06	1.88E-06	4.76E-10
180	1.77E-06	0	1.40E-09	1.77E-06	1.56E-06	3.55E-10
200	1.44E-06	0	1.40E-09	1.44E-06	1.27E-06	3.55E-10
220	1.12E-06	0	8.98E-10	1.12E-06	9.89E-07	2.05E-10
240	8.30E-07	0	6.48E-10	8.29E-07	7.32E-07	1.55E-10
260	5.80E-07	0	1.48E-10	5.80E-07	5.11E-07	2.96E-11
280	3.62E-07	0	1.48E-10	3.62E-07	3.20E-07	2.96E-11
300	1.96E-07	0	0	1.96E-07	1.73E-07	0
320	1.01E-07	0	0	1.01E-07	8.90E-08	0
340	4.78E-08	0	0	4.78E-08	4.22E-08	0
360	1.60E-08	0	0	1.60E-08	1.41E-08	0
380	5.22E-09	0	0	5.22E-09	4.57E-09	0
400	2.56E-09	0	0	2.56E-09	2.24E-09	0
420	1.11E-09	0	0	1.11E-09	9.73E-10	0
440	3.73E-10	0	0	3.73E-10	3.20E-10	0
460	1.75E-10	0	0	1.75E-10	1.52E-10	0
480	1.36E-10	0	0	1.36E-10	1.19E-10	0
525	7.38E-11	0	0	7.38E-11	6.29E-11	0
550	5.02E-11	0	0	5.02E-11	4.11E-11	0
575	3.15E-11	0	0	3.15E-11	2.72E-11	0
600	1.69E-11	0	0	1.69E-11	1.51E-11	0
625	1.15E-11	0	0	1.15E-11	1.03E-11	0
650	6.66E-12	0	0	6.66E-12	6.05E-12	0
675	3.02E-12	0	0	3.03E-12	3.03E-12	0
700	6.03E-13	0	0	6.05E-13	6.05E-13	0

Table 10.27: Transient results - Part 1

Prob_D_001	Prob_002	Prob_C_002	Prob_D_002	Prob_003	Prob_C_003
5.04E-06	8.82E-06	8.15E-06	6.75E-07	6.01E-06	6.01E-06
5.03E-06	7.26E-06	6.59E-06	6.75E-07	3.92E-06	3.91E-06
4.92E-06	3.42E-06	2.76E-06	6.60E-07	0	0
4.74E-06	2.19E-06	1.55E-06	6.37E-07	0	0
4.53E-06	1.52E-06	9.13E-07	6.08E-07	0	0
4.30E-06	1.15E-06	5.70E-07	5.77E-07	0	0
4.06E-06	9.16E-07	3.71E-07	5.45E-07	0	0
3.82E-06	7.78E-07	2.65E-07	5.13E-07	0	0
3.60E-06	6.71E-07	1.88E-07	4.83E-07	0	0
3.38E-06	5.92E-07	1.39E-07	4.53E-07	0	0
3.16E-06	5.19E-07	9.51E-08	4.24E-07	0	0
2.95E-06	4.53E-07	5.75E-08	3.96E-07	0	0
2.56E-06	3.63E-07	1.92E-08	3.44E-07	0	0
2.21E-06	3.00E-07	3.84E-09	2.97E-07	0	0
1.88E-06	2.54E-07	1.49E-09	2.53E-07	0	0
1.56E-06	2.11E-07	1.10E-09	2.10E-07	0	0
1.27E-06	1.72E-07	1.10E-09	1.71E-07	0	0
9.89E-07	1.33E-07	6.46E-10	1.33E-07	0	0
7.32E-07	9.88E-08	4.71E-10	9.84E-08	0	0
5.11E-07	6.88E-08	9.62E-11	6.88E-08	0	0
3.20E-07	4.31E-08	9.62E-11	4.30E-08	0	0
1.73E-07	2.33E-08	0	2.33E-08	0	0
8.91E-08	1.20E-08	0	1.20E-08	0	0
4.22E-08	5.62E-09	0	5.67E-09	0	0
1.41E-08	1.85E-09	0	1.90E-09	0	0
4.63E-09	5.92E-10	0	6.23E-10	0	0
2.27E-09	3.01E-10	0	3.03E-10	0	0
9.78E-10	1.09E-10	0	1.31E-10	0	0
3.48E-10	2.54E-11	0	4.65E-11	0	0
1.55E-10	2.30E-11	0	2.08E-11	0	0
1.20E-10	1.45E-11	0	1.62E-11	0	0
6.53E-11	5.45E-12	0	8.77E-12	0	0
4.54E-11	4.24E-12	0	5.99E-12	0	0
2.84E-11	3.03E-12	0	3.81E-12	0	0
1.57E-11	1.82E-12	0	2.12E-12	0	0
1.03E-11	1.21E-12	0	1.33E-12	0	0
6.05E-12	6.05E-13	0	7.87E-13	0	0
3.03E-12	6.05E-13	0	3.63E-13	0	0
6.05E-13	0	0	6.05E-14	0	0

Table 10.28: Transient results - Part 2

Prob_D_003	Prob_004	Prob_C_004	Prob_D_004	Prob_005	Prob_C_005
1.77E-09	1.27E-05	1.27E-05	1.21E-08	1.44E-05	1.44E-05
1.32E-09	2.24E-06	2.23E-06	9.75E-09	7.12E-06	7.12E-06
0	0	0	0	0	0
0	0	0	0	0	0
0	0	0	0	0	0
0	0	0	0	0	0
0	0	0	0	0	0
0	0	0	0	0	0
0	0	0	0	0	0
0	0	0	0	0	0
0	0	0	0	0	0
0	0	0	0	0	0
0	0	0	0	0	0
0	0	0	0	0	0
0	0	0	0	0	0
0	0	0	0	0	0
0	0	0	0	0	0
0	0	0	0	0	0
0	0	0	0	0	0
0	0	0	0	0	0
0	0	0	0	0	0
0	0	0	0	0	0
0	0	0	0	0	0
0	0	0	0	0	0
0	0	0	0	0	0
0	0	0	0	0	0
0	0	0	0	0	0
0	0	0	0	0	0
0	0	0	0	0	0
0	0	0	0	0	0
0	0	0	0	0	0
0	0	0	0	0	0
0	0	0	0	0	0
0	0	0	0	0	0
0	0	0	0	0	0
0	0	0	0	0	0
0	0	0	0	0	0
0	0	0	0	0	0
0	0	0	0	0	0
0	0	0	0	0	0

Table 10.29: Transient results - Part 3

Prob_D_005	Prob_006	Prob_C_006	Prob_D_006	ftf_vol	LeL_vol	LeakRate
7.54E-09	9.74E-06	9.73E-06	5.24E-09	-7.92E-09	0.107168	0.015678
6.11E-09	4.32E-06	4.32E-06	4.51E-09	-0.02665	-0.66083	-0.09057
0	1.58E-06	1.58E-06	0.00E+00	-0.00243	-2.70025	-0.04773
0	0	0	0	-0.00132	-3.31894	-0.03169
0	0	0	0	-0.00062	-3.5169	-0.02407
0	0	0	0	-0.00025	-3.55779	-0.02007
0	0	0	0	-0.00013	-3.47641	-0.0171
0	0	0	0	8.73E-11	-3.31903	-0.01475
0	0	0	0	-0.0002	-3.16123	-0.01295
0	0	0	0	-3.52E-05	-3.02894	-0.01151
0	0	0	0	-3.42E-05	-2.91658	-0.0102
0	0	0	0	-4.37E-11	-2.78729	-0.00906
0	0	0	0	0	-2.51104	-0.00725
0	0	0	0	0	-2.20712	-0.00573
0	0	0	0	0	-2.05408	-0.00464
0	0	0	0	0	-1.90841	-0.00373
0	0	0	0	0	-1.75194	-0.00297
0	0	0	0	0	-1.58282	-0.00248
0	0	0	0	0	-1.34087	-0.00212
0	0	0	0	0	-1.17983	-0.00181
0	0	0	0	0	-0.99111	-0.00152
0	0	0	0	0	-0.63103	-0.00126
0	0	0	0	0	-0.35414	-0.00101
0	0	0	0	0	-0.24292	-0.00084
0	0	0	0	0	-0.12231	-0.0007
0	0	0	0	0	-0.0179	-0.00058
0	0	0	0	0	-0.00986	-0.00046
0	0	0	0	0	-0.00394	-0.00038
0	0	0	0	0	-0.00123	-0.00032
0	0	0	0	0	-0.00027	-0.00027
0	0	0	0	0	-0.00022	-0.00024
0	0	0	0	0	-0.00012	-0.00016
0	0	0	0	0	-8.48E-05	-0.00013
0	0	0	0	0	-5.86E-05	-9.12E-05
0	0	0	0	0	-2.85E-05	-5.87E-05
0	0	0	0	0	-2.85E-05	-4.29E-05
0	0	0	0	0	-1.69E-05	-2.87E-05
0	0	0	0	0	-6.99E-06	-1.53E-05
0	0	0	0	0	-6.99E-06	-2.79E-06

Table 10.30: Transient results - Part 4